22

NMR CHARACTERIZATION OF INTERSTITIAL MYOCARDIAL SODIUM

by

Brent D. Foy

B.S. Physics, Massachusetts Institute of Technology (1985)

SUBMITTED TO THE HARVARD-MASSACHUSETTS INSTITUTE OF TECHNOLOGY
DIVISION OF HEALTH SCIENCES AND TECHNOLOGY
IN PARTIAL FULFILLMENT OF THE REQUIREMENTS FOR THE DEGREE OF
DOCTOR OF PHILOSOPHY

at the

Massachusetts Institute of Technology

April, 1991

Signature of Author_____
Harvard-Massachusetts Institute of Technology
Division of Health Sciences and Technology
April, 1991

Certified by_____
Deborah Burstein
Thesis Supervisor

Accepted by_____
Roger G. Mark
Chairman, Graduate Committee

NMR CHARACTERIZATION OF INTERSTITIAL MYOCARDIAL SODIUM

by
Brent D. Foy

Submitted to the Harvard-Massachusetts Institute of Technology
Division of Health Sciences and Technology on April 11, 1991
in partial fulfillment of the requirements for the Degree of
Doctor of Philosophy in Medical Physics

ABSTRACT

Sodium nuclear magnetic resonance (NMR) has the potential to non-invasively monitor electrophysiologic processes. However, the ability to separate the intracellular and interstitial sodium NMR signals is essential. One method proposed to do this, other than the use of toxic contrast agents, involves exploiting possible differences in the NMR relaxation times (T1 and T2) of sodium in these compartments. Relaxation time differences are also an important source of contrast on sodium NMR images which have recently been shown to delineate regions of pathology such as brain infarctions, tumors, and edema. Therefore, in order to fully realize the applications of sodium NMR, a greater understanding of the NMR relaxation times of sodium in tissue is needed. While previous work has succeeded in characterizing T1 and T2 for the intracellular sodium of some systems, these time constants have not previously been determined for the interstitial sodium. The objective of this work was to characterize the interstitial sodium relaxation times under control and pathologic conditions.

Spectroscopic studies of interstitial sodium relaxation times of perfused frog and rat hearts under control conditions revealed that the interstitium has relaxation times similar to those of the intracellular space. The finding that a fraction of both the intracellular and interstitial sodium signal have a fast T2 time constant of approximately 2 ms is significant since this fast T2 had been proposed as a means of identifying the intracellular sodium signal. Results from perfused rat heart studies of interstitial edema revealed that the amount of interstitial sodium signal with a fast component of T2 decay can increase significantly. Therefore, increases in the amount of signal with a fast T2 cannot be ascribed to a particular compartment, since they occur with both intracellular and interstitial pathologic increases in sodium content. Sodium images at two echo times were obtained of several pathologic states revealing a high contrast between normal and pathologic tissue. However, the image contrast appeared to be non-specific for the different pathologic states. The interstitial sodium relaxation time information found in this study has important implications for the interpretation of relaxation based sodium NMR studies of electrophysiologic and pathologic events.

Thesis Supervisor: Deborah Burstein, Ph.D.
Title: Assistant Professor of Radiology,
Beth Israel Hospital
Harvard Medical School

ACKNOWLEDGEMENTS

I feel fortunate to have been given the opportunity to pursue and complete this thesis and doctoral degree. The largest part of my fortune is the people I have been associated with who have supported and encouraged me in every facet of this endeavor. I would like to thank everyone I have met during my graduate studies for their friendship and assistance. I would especially like to thank the following individuals:

Deborah Burstein, my thesis supervisor, for educating me in the many aspects of NMR research. Her kindness and honesty at all times, and her willingness to spend extra time discussing experiments, reading my documents, or aiding in preparation of presentations has been greatly appreciated.

Bruce Rosen and Toyoichi Tanaka, members of my thesis committee, for providing me with many tools necessary for this thesis. Bruce's NMR course was an extremely solid starting point for further work in NMR. Toyo's lab introduced me to many phases of biologic and physics research.

Joyce Peetermans, post-doctoral associate in Toyo's lab, for working with me on my first graduate research project. Her patience and enthusiasm succeeded in teaching me the basics of scientific, logical thinking. She also encouraged me in my desire to study NMR, so that a physics background could be applied to medical problems.

Roger Mark, co-director of HST, for helping to mold and organize the MEMP program at MIT. His efforts toward promoting student contact with other students, thouroughly examining and clarifying the requirements for graduation, and keeping students informed of happenings at HST have directly enhanced my graduate experience.

My experience at the Radiology Research lab at Beth Israel Hospital has been made enjoyable and rewarding due to the presence of the following individuals, whom I would like to thank:

Steve Gladstone, for his assistance with perfusing rat hearts, for many technical details, and for many enjoyable conversations.

John Lewin, David Powell, Leann Lesperance, Kathleen Donahue, Rob Gipe, Harold Litt, Elena Tarratuta, and Luke Cheung, my fellow students in the laboratory, for friendship and fruitful discussions as we experienced the ups and downs of our research projects.

Ivan Jemelka, Jacqui Tan, Christine Zanella, Kathleen Hui, Paul Shamlian, Colin Cook, and Kei Hanafusa, co-workers in the laboratory, for being there to talk with on those "rare" occasions when I was less than 100% motivated to work.

Jackie Solberg, Christine Holbrook, and Yvette Alphonse, for much assistance with administrative details and document preparation.

Eric Fossel, head of the laboratory, for helping to gather such a truly great group of people into one place, and for lending his experience and suggestions regarding a research career.

Many fellow MEMP students have been both colleagues and friends. Their friendship and fellowship, along with the personal and scientific discussions we have had, have enriched my life and have made the MEMP experience a special one.

I would also like to thank my family for supporting me at every stage of my life and career. Much of who and what I am is a result of their love and wise guidance. I thank them for giving me the freedom to chose my path in life, and for making it possible to pursue my choices.

Finally, I would like to thank my wife Susan. I realized early on in graduate school that I needed her in my life, so I didn't waste too much time in marrying her. Without her consistent love and support throughout graduate school, this thesis would not have been possible. Her capacity for giving of herself and caring for others continually amazes me. I am truly a lucky person to have her as my friend and companion for life.

Table of Contents

1. Introduction

The sodium ion is involved in numerous physiologic and pathologic events. Cell death, edema formation, tumor growth, electrophysiologic processes, and ion transport all involve alterations in intracellular and extracellular sodium levels. By observing intracellular sodium, the state of the Na-K ATPase pump, ion transport, mitogenesis, and other cellular activity can be monitored. By observing extracellular sodium, one is able to monitor extracellular volume, since the sodium concentration in the extracellular space remains constant. In this way, the presence of extracellular edema can be detected. Nuclear magnetic resonance (NMR) provides a nondestructive method of observing sodium; however, it is difficult to separate the intracellular sodium signal from the extracellular sodium signal. This difficulty limits the use of sodium NMR both for basic electrophysiologic research and for identifying pathologic lesions on sodium NMR images.

Two primary NMR methods have been proposed to obtain this compartmental sodium information. These methods are (1), the use of shift reagents and (2), exploiting differences between the NMR relaxation times of sodium in the two compartments. Shift reagents are large, negatively charged molecules which are added to a system of biological interest and which penetrate only the extracellular spaces (Gupta and Gupta, 1982; Pike et. al., 1985). The shift reagent alters the NMR resonant frequency of the extracellular cations; therefore the intracellular and extracellular signals have different resonant frequencies, enabling the signal from the two compartments to be separated. However, problems exist with the use of

shift reagents. Shift reagents chelate calcium and thus may be toxic to functioning organs (Pike et. al., 1985; Gullans et. al., 1985; Anderson et. al., 1988), and shift reagents may not be distributed uniformly throughout the body, such as through the blood-brain barrier, in necrotic centers of tumors, or in underperfused tissue.

Differences in the NMR relaxation times (T_1 and T_2) between intra- and extracellular sodium have also been proposed as a means of obtaining compartmental sodium information (Hilal et. al., 1988). The intracellular relaxation times have been measured with shift reagents and have in general been found to short (about 20 ms for T_1 and 2 and 15 ms for a biexponential T_2) (Burstein and Fossel, 1987a; Shinar and Navon, 1991). The relaxation times of body fluids have also been measured *in vitro* and were found to be significantly longer than the intracellular relaxation times (Shinar and Navon, 1986). With this information in mind, techniques have been devised which detect or emphasize only signal with fast T_2 decay, such as the 2 ms T_2 component of intracellular sodium. If the intracellular compartment is the only compartment with such fast T_2 decay, then these techniques would enable the selective monitoring of intracellular sodium. However, the relaxation characteristics of sodium present between the cells, the interstitial sodium, have not been previously determined. Thus one is not sure whether techniques which emphasize fast components of T_2 decay are selectively detecting intracellular sodium, or whether contributions from both intracellular and interstitial sodium are present.

Another method which depends indirectly on differences in sodium relaxation times to separate the sodium signal from the intracellular and extracellular compartments is to utilize multiple quantum spectroscopy (MQS) (Pekar et. al., 1987). This technique can selectively yield signal from compartments which exhibit biexponential T_2 decay as a result of quadrupolar relaxation (see Theory). However, since the characteristics of interstitial sodium have not been determined, it is unknown whether interstitial sodium contributes to the multiple quantum signal. Recently, the combination of MQS and paramagnetic relaxation reagents to "quench" any contribution of extracellular sodium has been proposed (Jelicks and Gupta, 1989a). This approach is still under investigation for its use in perfused organs or *in vivo* applications. It does still require the use of an exogenous agent whose distribution in the body may not be uniform.

Clearly one difficulty in interpreting data obtained by the compartmental discrimination techniques discussed above is the lack of NMR information concerning interstitial sodium. The main goal of this work was to characterize the NMR relaxation times of interstitial sodium in perfused hearts under control and pathologic conditions. Spectroscopic techniques were used to characterize the interstitial sodium relaxation times under control conditions for both perfused frog and rat hearts. Spectroscopic techniques were also used to quantify the fast component of T_2 decay due to the sodium in the interstitial space during pathologic conditions in perfused rat hearts. Sodium images of perfused rat hearts under control and pathologic conditions were then obtained utilizing relaxation-based contrast.

2. THEORY

2.1. General spectroscopy

The discussion that follows is a brief outline of the theory of NMR, with an emphasis given to those aspects which are most relevant to the methods used in this thesis. A more complete description can be found in several textbooks (Abragam, 1961; Farrar and Becker, 1971; Slichter, 1980; Fukishima and Roeder, 1981; Morris, 1986; Farrar, 1989).

The nuclei of many elements have a magnetic moment μ, meaning they are magnetic dipoles with associated magnetic fields. In the absence of external magnetic fields, these moments are randomly oriented. However, in the presence of a static magnetic field B_0, these moments become oriented along the direction of B_0 with some pointing parallel to B_0 and some pointing antiparallel. Because the parallel state is the state of lower energy, slightly more moments reside in the parallel configuration. A collection of nuclei in field B_0 will thus have a net magnetization M (the vector sum of all nuclear moments) pointing along B_0, whereas without B_0 the net magnetization is zero. This vector M describes the state of magnetization of a given sample.

Additionally, in the presence of B_0, each magnetic moment μ will precess about the direction of B_0 (Fig. 2-1) with a frequency given by

$$\omega_0 = \gamma B_0 \qquad (2\text{-}1)$$

where ω_0 is called the Larmor frequency, γ is the gyromagnetic ratio intrinsic to each nucleus, and B_0 is the magnitude of B_0. For sodium $\gamma/2\pi$

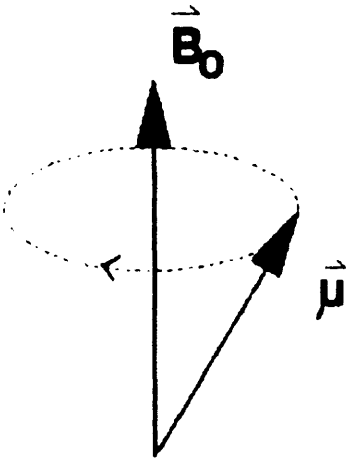

Figure 2-1 Magnetic moment μ of a single nucleus precessing about the static magnetic field B_0.

is 11.26 MHz/Tesla where Tesla is a unit of magnetic field. In the equilibrium state, the precessing moments are randomly phased with respect to each other and thus no net magnetization in the plane perpendicular to B_0 exists.

To observe these nuclei, a radiofrequency (RF) magnetic field (B_1) must be applied in the plane perpendicular to B_0. This field is oscillating at frequency ω_0 which enables it to "resonate" with the precessing nuclear magnetic moments. Application of this RF field induces a redistribution of the parallel and anti-parallel spins, changing the net magnetization aligned along B_0. It also induces a phase coherence in the precessing magnetic moments, and thus a net magnetization in the plane perpendicular to B_0 is produced. This process can be equivalently described by the effects of B_1 on M. The RF field tips the net magnetization M of the sample so that it no longer points along B_0. The angle through which M is tipped depends on the strength and the duration

of B_1 and is given by

$$\theta = \gamma B_1 t \qquad (2\text{-}2)$$

where γ is the same gyromagnetic ratio, t is the duration of B_1, and B_1 is the magnitude of vector B_1. Pulses of B_1 are typically designed to flip M either 90^o or 180^o by varying the duration or magnitude of B_1 (Fig. 2-2).

The reason a B_1 pulse enables one to observe the nuclei is that the phase coherence of the precessing magnetic moments results in a net M which precesses in the transverse plane (the plane perpendicular to B_0). (Before the RF pulse, the moments were phase incoherent and M was stationary along B_0). This precessing magnetization is observable by placing a coil about the sample. Faraday's law states that an electromotive force is generated in the coil when magnetic flux changes

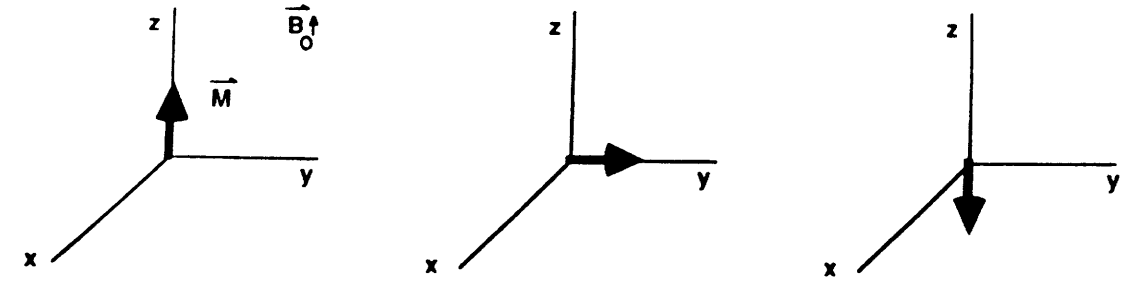

Equilibrium | Following 90° Pulse | Following 180° Pulse

Figure 2-2 The net magnetization of a sample at equilibrium before the radiofrequency pulse B_1, following a 90^o B_1 pulse, and following a 180^o B_1 pulse.

with time, such as occurs with the precessing **M**, and thus a detectable current is generated.

After being tipped out of alignment with $\mathbf{B}_0$, **M** is not in its thermodynamically stable position, and thus starts to relax back to its original position. There are two relaxation processes which must be described. One is the loss of phase coherence of the spins, or equivalently the loss of net transverse magnetization, and is described by the time constant T_2. The other is the reestablishment of equilibrium populations of parallel and anti-parallel spins, or equivalently the recovery of longitudinal (or along $\mathbf{B}_0$) magnetization, and is described by the time constant T_1. Different interactions between a nucleus and its environment contribute to each relaxation process, and thus in many samples T_1 and T_2 are different, with T_2 always being equal to or less than T_1. We assume the relaxation processes to be exponential, and thus T_1 and T_2 are exponential time constants.

Specialized RF pulse sequences have been developed to measure the NMR properties of the nuclei, such as Mo (the magnitude of **M** at equilibrium), T_1, and T_2. The most basic pulse sequence is (90^o - AQ) where 90^o means apply an RF pulse which flips **M** 90^o (thus into the transverse plane) and AQ represents "acquire signal". Following the 90^o pulse, the induced signal oscillates at frequency ω_0 and in the ideal case, the envelope of these oscillations exponentially decays with time constant T_2. This most basic signal is called the free induction decay (FID). In reality, inhomogeneity of the static magnetic field $\mathbf{B}_0$ causes the FID to decay

faster than T_2 due to dephasing of the spins precessing in slightly different fields and thus at slightly different frequencies (Eq. (2-1)). The time constant which describes the actual decay of the FID is called T_2^* (Fig. 2-3).

To measure the actual T_2 value, a pulse sequence called a Hahn spin-echo (SE) sequence is used (Hahn, 1950). This sequence is written

$$90^\circ - \frac{TE}{2} - 180^\circ - \frac{TE}{2} - AQ \qquad (2\text{-}3)$$

where TE is a time delay which stands for the echo time. The purpose of this sequence is to create an "echo" of the original FID signal at time TE following the initial 90° pulse. This occurs because the 180° pulse inverts the system of spins so that spins which were dephasing due to B_0 inhomogeneity converge after the 180° pulse and refocus at time TE. The magnitude of this echo will thus minimize the effects of B_0 inhomogeneity

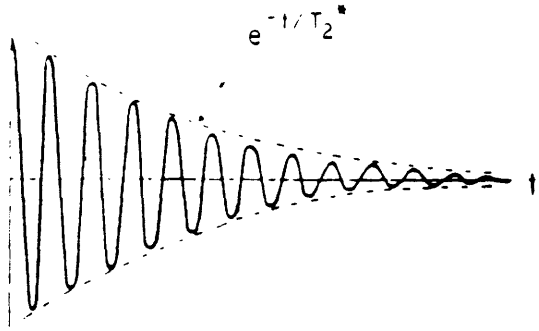

Figure 2-3 Schematic of a free induction decay (FID) observed in an NMR experiment.

and will reflect the correct magnitude for an exponential decay of time constant T_2 measured at time TE. A single experiment measures one point on the exponential decay curve (at time TE) and to determine T_2 several experiments are needed, each at a different value of TE (Fig. 2-4).

A slight modification of this pulse sequence is the Carr-Purcell-Meiboom-Gill (CPMG) sequence (Carr and Purcell, 1954; Meiboom and Gill, 1958). This sequence is

$$90^\circ - \frac{TE}{2} - [180^\circ - TE - 180^\circ - TE - 180^\circ - \ldots] \qquad (2\text{-}4)$$

This pulse sequence generates an echo at intervals of TE and thus acquisitions (not shown above) are made halfway between each pair of 180° pulses. The advantages of this pulse sequence are that a complete T_2 measurement can be made with a single experiment, and that the effects of diffusion of the nuclei within B_0 inhomogeneity are reduced.

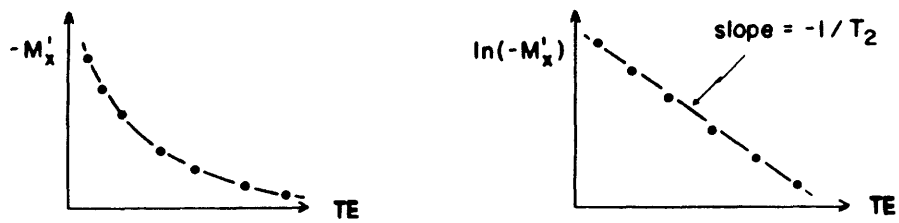

Figure 2-4 Schematic of the T_2 decay curve obtained in a Hahn spin-echo experiment. Each point represents the magnitude of the FID obtained at a given echo time (TE).

Another pulse sequence, designed to measure T_1, is called an inversion-recovery (IR) pulse sequence and is written

$$180° - ID - 90° - AQ \qquad (2\text{-}5)$$

where ID is a time delay and stands for inversion delay. The first 180° pulse is called the inverting pulse because it takes magnetization M pointing along positive z direction (along B_0) and flips it to the negative z direction. After being flipped, M begins to relax back to its original orientation with time constant T_1. The final 90° pulse takes the longitudinal magnetization (along +z or -z axis) and flips it into the transverse plane, so that a signal is induced in the coil. The magnitude and sign of the signal acquired depends on the magnitude and sign of the longitudinal magnetization just prior to the 90° pulse. By varying ID, one can measure the amount of signal at different stages of relaxation. A T_1 experiment thus results in the graph shown in Fig. 2-5.

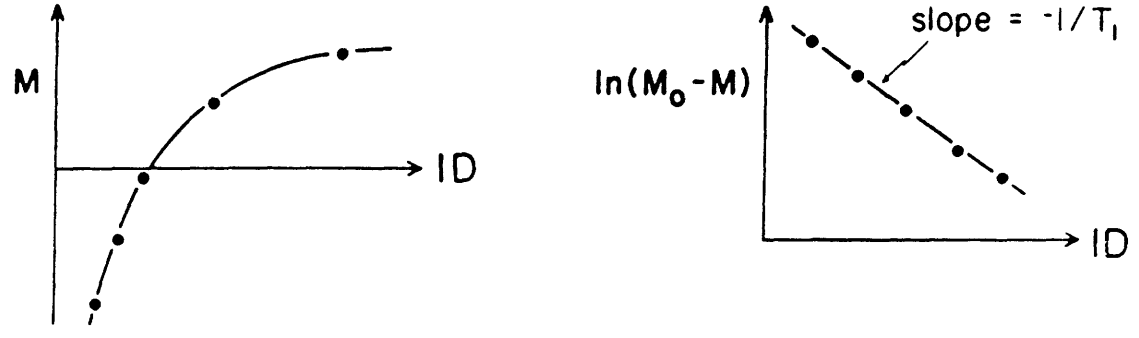

Figure 2-5 Schematic of the T_1 recovery curve obtained in an inversion-recovery experiment. Each point represents the magnitude of signal after a given inversion delay (ID).

An additional point to consider is that for sodium studies these pulse sequences generally need to be repeated many times in order to acquire enough signal-to-noise (S/N) (see next paragraph). However, one wants the sample's magnetization to be fully recovered to its equilibrium state before starting a pulse sequence. This is to insure that the magnitude and direction of the magnetization at the start of a pulse sequence is the same each time, which simplifies analysis of the data. It also minimizes potential residual effects of previous pulse sequences, such as generation of unanticipated echoes. Therefore, one usually has to wait a certain amount of time, typically 3 to 5 T_1, before repeating the pulse sequence. The time between initiation of successive pulse sequences is called TR or the repetition time.

By acquiring a signal many times and summing the signals together, the S/N is enhanced. If NA represents the number of averages or the number of times which the pulse sequence is repeated, then the signal is increased linearly by a factor of NA. However, the noise is incoherent and increases only by a factor of the square root of NA. Therefore, S/N is proportional to the square root of NA.

2.2. Quadrupolar effects

Thus far the theory of NMR has been presented in terms of magnetic moments being parallel or anti-parallel to B_0. However, the sodium nucleus can be in one of four states relative to B_0. While the classical vector picture described above is also valid for sodium in many situations, some aspects of sodium NMR need a quantum mechanical

description to be complete.

Each NMR visible nucleus has a spin number I. For protons I=1/2 and for sodium I=3/2. In the presence of a magnetic field, these nuclei are split into 2I+1 different energy states corresponding in protons to the up or down spin state (Fig. 2-6). These energy levels are separated by an energy difference ΔE which can be associated with a frequency ω_0 through the quantum theory of radiation. The equation is

$$\Delta E=\hbar\omega_0. \tag{2-6}$$

This frequency ω_0 is the same as the Larmor frequency for precessing

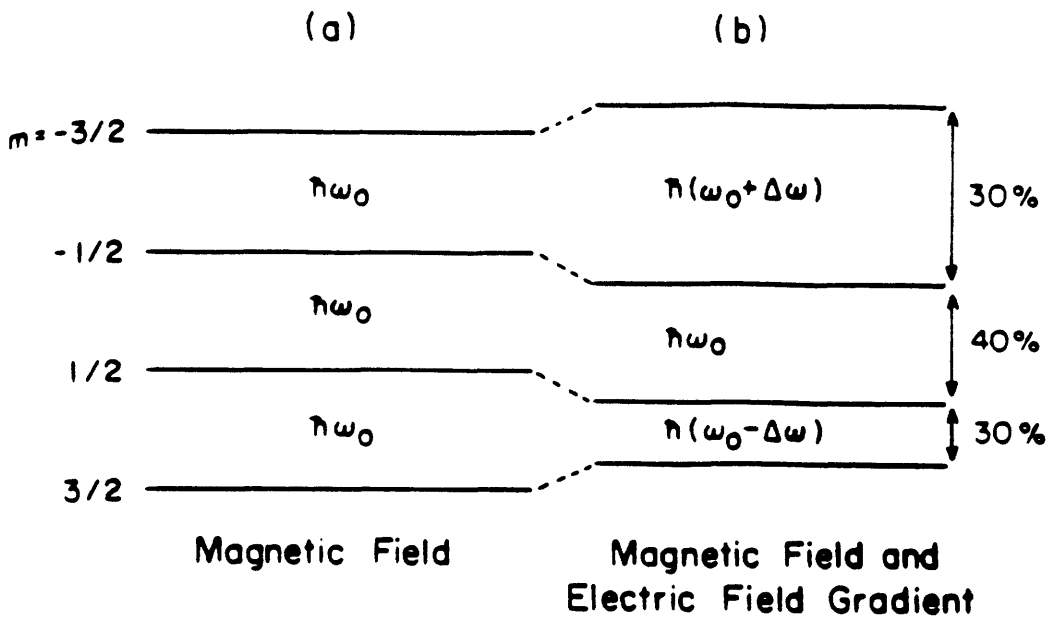

Figure 2-6 Energy diagram for a spin 3/2 nucleus such as the sodium nucleus; (a) in the presence of a static magnetic field, and (b) in the presence of both a magnetic field and an electric field gradient. The percentages on the right refer to the transition probabilities between the adjacent levels.

magnetic moments and is the frequency at which the NMR signal is detected. In the equilibrium state, slightly more nuclei exist in the lower energy states than in the higher energy states due to the Boltzman energy distribution. When a RF field of frequency ω_0 is applied to a group of these nuclei, transitions of nuclei between states are excited. After this RF "pulse", the system begins to relax back to its equilibrium configuration by further transitions between the states. The relaxation process occurs through several mechanisms, the most important of which are dipole-dipole interactions (each nuclear magnetic moment is a dipole) and quadrupole-electric field gradient interactions. Protons have no quadrupolar moment and therefore dipolar interactions are the predominant mechanism of relaxation for protons.

Sodium, with spin 3/2, does have a quadrupolar moment (as do all nuclei with spin > 1/2). There are four energy levels for sodium which are equally spaced in the presence of a magnetic field. However, if electric field gradients are present these levels are perturbed slightly so that they are not equally spaced (Fig. 2-6). This might be expected to lead to a sodium spectrum with signal present at 3 frequencies $\omega_0+\Delta\omega$, ω_0, $\omega_0-\Delta\omega$, and in some specially oriented samples this can be seen. However, in biologic samples only one resonant frequency has been detected (Joseph and Summers, 1987). This may be explained by the fact that the sodium nuclei are in fast isotropic motion such that the mean electric field gradient experienced at the nucleus over the course of a measurement is zero. Consequently the frequency of the detected signal is the frequency which occurs in the absence of an electric field gradient, or ω_0. Another

possibility is that the techniques used are not sensitive enough to detect signal which occurs at the other resonances.

The presence of multiple energy levels and thus multiple transitions between energy levels also leads to the possibility of multiexponential relaxation behavior, even if all of the nuclei are in the same environment or "pool". This differs from the situation that exists for nuclei which have only a single transition, such as protons and other spin 1/2 nuclei, where the presence of multiexponential decay indicates multiple pools of nuclei. For a single homogeneous pool of sodium ions with a single resonant frequency, theory predicts that both T_1 and T_2 relaxation behavior will be biexponential with a ratio of fast to slow components of 0.2 to 0.8 for T_1 and 0.6 to 0.4 for T_2 (Hubbard, 1970; Berendsen and Edzes, 1973). The two relaxation time constants for T_1, called T_{1f} (fast component) and T_{1s} (slow component), are difficult to separate experimentally, due both to the small fraction of the fast component and to the small difference predicted for the two T_1 values. Thus a single T_1 time constant is usually determined, which is approximated by the expression

$$\frac{1}{T_1} = \frac{0.2}{T_{1f}} + \frac{0.8}{T_{1s}} \qquad (2\text{-}7)$$

For T_2 data, multiexponential relaxation behavior is more obvious, and two relaxation time constants, called T_{2f} and T_{2s}, are frequently necessary to characterize the relaxation decay.

Quadrupolar relaxation, due to an interaction of the quadrupolar moment of the sodium nucleus with electric field gradients, has been shown to be the predominant relaxation mechanism for sodium (Berendsen and Edzes, 1973). Quadrupolar relaxation is quite effective, leading to fast T_1 and T_2 values. Fast T_1 values are helpful in that they allow a short repetition time (TR) of a given pulse sequence and thus more signal averaging can be performed in a given amount of time. A fast T_2 however means that the signal decays very quickly. Necessary hardware delays between excitation of the nuclei and acquisition of the signal, called the dead time of the receiver, may lead to an inability to detect the entire magnitude of the signal. That magnitude of the signal which is not detected is called "invisible". The possibility exists that the fast (60%) component of T_2 may be NMR invisible if the sodium ions are in an environment that leads to unusually fast relaxation.

The above analysis is for a single homogeneous pool of sodium ions. If two or more pools of ions are present, then the rate of exchange of ions between the pools becomes a factor in determining the overall relaxation behavior. A fast exchange will produce a weighted average of the relaxation times, while a slow exchange will produce a superposition of each compartment's relaxation behavior. With this additional complexity, many T_1 and T_2 time constants can be present in a physiologic system which has multiple compartments and environments with unknown exchange rates between these pools of sodium ions. This also indicates that the percent of the total signal which may decay with a given time constant or which may be invisible is not possible to predict.

2.3. Sodium imaging

In addition to quantifying the amount of signal within the sensitive volume of a coil and measuring T_1 and T_2, images of the spatial distribution of nuclei within the coil can be produced. In order to spatially encode the position of the observed nuclei within a sample, a magnetic field gradient given by $B = B_0 + Gx$ is imposed on the sample. G is the gradient applied to the system, and x is a spatial coordinate such that G times x produces different magnetic fields for different x values. Therefore from Eq. (2-1), the resonant frequency of each nucleus is proportional to its location. A Fourier transform of the signal yields a spatial map of the location of the nuclei.

NMR imaging of sodium has two unique aspects compared to the more common NMR imaging of protons. These aspects are the low sensitivity of the sodium nucleus relative to protons and the quadrupolar relaxation effects.

The product of several factors determine the overall sensitivity of the technique of NMR for a given nucleus -- relative sensitivity per nucleus at a given field, the natural abundance of the NMR detectable isotope, and the physiologic concentration of the element. Compared to biologically useful NMR detectable nuclei other than protons -- such as ^{31}P, ^{39}K, ^{17}O, ^{14}N and others -- ^{23}Na has a high relative sensitivity per nucleus (13% as sensitive as protons versus 8%, 0.1%, 0.002%, and 0.2% respectively for the above mentioned nuclei). It also has 100% natural abundance, and a high physiologic concentration (when the average of both

intra- and extracellular sodium is considered) making it the second best nucleus to image after protons (Kramer, 1981). However, the lower concentration and lower relative sensitivity of sodium nuclei when compared with protons make the overall imaging sensitivity of sodium 5,000 to 10,000 times less than that for protons.

Several techniques can be used to partially compensate for this lack of sensitivity. One method is to decrease the image resolution (increase the volume contained in each voxel). Since S/N depends on the third order of spatial resolution, a voxel size of 1 cm^3 instead of 1 mm^3 can partially compensate for the decreased sensitivity. However, a voxel size of $1cm^3$ is unacceptable in many applications, and therefore other approaches are necessary to enhance the S/N of the sodium image. Another approach is to employ signal averaging. Due to the short T_1 of sodium, a pulse sequence can be repeated quickly making this method relatively effective. However, the fact that S/N increases only as the square root of the number of averages limits the extent to which this can be used, since it is usually necessary in biologic applications to keep the imaging time to a reasonable value. Another technique which can be employed to improve S/N is optimization of the filling factor. This means choosing or designing a RF coil which is nearly the same size as the object to be imaged, or equivalently, choosing a model system which nearly fills the RF coil. In addition, if multiple slices are to be obtained, then acquiring the data using a 3-D technique instead of a 2-D multislice technique should provide better S/N for a given total acquisition time (Brunner and Ernst, 1979). A further advantage of using the 3-D technique is that the

RF pulses can be non-selective which means they are shorter in duration. This can shorten the echo time obtainable which, as will be discussed below, is important for sodium imaging.

Another approach to optimizing the S/N is to use a fast gradient echo sequence instead of an imaging sequence based on a Hahn spin echo (Granot, 1986). This sequence enables a short TR to be utilized in conjunction with an excitation pulse less than 90^{o}. This can improve the S/N but provides less flexibility in choosing T_1 or T_2 weighting.

A smaller receiver bandwidth can also improve S/N on an image. Since the noise amplitude is proportional to the square root of the bandwidth, a reduction in the bandwidth can lead to a dramatic improvement in the overall S/N. However, a lower receiver bandwidth necessitates the use of smaller gradients to maintain the same field of view in the image, and this leads to a lower limit which one can use for the receiver bandwidth. The gradients determine the frequency separation of adjacent pixels in an image according to

$$\Delta\omega = \gamma G \Delta x \qquad (2\text{-}8)$$

where $\Delta\omega$ is the frequency separation of adjacent pixels, γ is the gyromagnetic ratio, G is the gradient strength, and Δx is the distance separation of two adjacent pixels. However, the nuclei which give rise to the signal in each pixel have an intrinsic linewidth due to a combination of natural T_2 decay and B_0 inhomogeneity. This linewidth is

$$\Delta\omega_{fwhm} = \frac{2}{T_{2(pix)}^{*}} \qquad (2\text{-}9)$$

where $\Delta\omega_{fwhm}$ is the full width at half-maximal amplitude of the spectral lineshape, and $T_2{}^*_{(pix)}$ is the exponential time constant which describes the rate of decay of signal in that pixel. Note that only B_0 inhomogeneity over the region of pixel itself produces broadening of the linewidth. In order for each pixel to be resolved from adjacent pixels, the frequency separation due to the gradients (Eq. (2-8)) must be larger than the linewidth of the pixels (Eq. (2-9)). This sets a lower limit on the gradient value and hence the receiver bandwidth which can be used.

The echo time used to acquire a sodium image is very important in determining the information obtained and the S/N level. Imaging sequences require a longer echo time than spectroscopy sequences in order to allow sufficient time for the gradients to ramp up to the desired level and then ramp down at the appropriate time. This results in a loss of some signal, similar to the discussion of "invisible" signal above. The shorter the T_2 of the sample, the more signal will be lost, and since sodium can have very short T_2 values, the amount of signal lost can be significant. As will be described in the chapter on previous work, several researchers have developed imaging sequences which utilize a shorter echo time.

Finally, one point which refers to the characterization of the relaxation behavior of a system using sodium imaging should be mentioned.

The quadrupolar moment of the sodium nucleus, as described above, leads to a biexponential T_2 decay. In order to accurately characterize the T_2 behavior of a system, data points at many echo times are required. With sodium imaging, the time required to obtain an image or the necessity of using specialized sequences which obtain a very short echo time tend to limit the number of echo times at which data is acquired. This means that an accurate characterization of the T_2 decay is difficult when working with sodium imaging sequences. The limitations of using only two or three data points to characterize T_2 decay, while necessary in some circumstances, should be kept in mind.

2.4. Compartmental information in spectroscopy versus imaging

The distinction between the signal intensity in a sodium spectrocopy experiment and the image intensity in a sodium imaging experiment should be emphasized. The signal intensity in a spectroscopic measurement is due to all of the "visible" signal from all of the nuclei in the sample within the RF coil. Image intensity, on the other hand, represents the number of nuclei within a given voxel in the sample, weighted by the loss of some signal due to a fast T_2 decay.

Therefore, the spectroscopy experiment is very sensitive to changes in the overall volume of the sample, as well as concentration changes within the sample. On the other hand, the imaging experiment is sensitive to concentration changes within a voxel, or relative volume changes between two compartments with different concentrations within a voxel.

For example, interstitial edema increases the interstitial volume of the heart tissue and thus increases the total volume of the heart tissue. The magnitude of the signal from a spectroscopy experiment will increase substantially due to the increased total number of sodium nuclei in the sample. The signal intensity in an imaging experiment will also increase due to the relative increase of the interstitial space (with a high sodium concentration) at the expense of the intracellular space (with a low sodium concentration) within a voxel. However, this increase will not be as dramatic as the increased spectroscopic magnitude. On the other hand, any change in the sodium concentration in either compartment will lead to an equal percent change in the spectroscopy and imaging experiment. These features are important when comparing signals of pathologic tissue obtained from spectroscopic and imaging techniques.

3. PREVIOUS WORK

The methods proposed to distinguish compartmental sodium signals, or to interpret image contrast, depend on previously obtained data on the sodium NMR signal in biologic tissue. In this section, the early interpretation of the sodium signal from tissue, the separation of the compartmental sodium signals using shift reagents or multiple quantum signals, and the previous measurements of sodium relaxation times in biologic tissue will be presented. Previous imaging results of short echo time imaging and sodium imaging of normal and pathologic tissue are also described, as well as imaging techniques proposed for obtaining compartmental sodium signals.

3.1 Spectroscopy

3.1.1 Relaxation theory

The early sodium NMR studies of physiologic systems focussed on determining if all of the sodium in tissue was visible (i.e. able to be detected by NMR) and the first reports (Cope, 1967) found in fact that 20-70% was "invisible". The conclusion drawn from this was that two pools of sodium were present in biologic tissue, bound and free, with the bound portion being invisible due to broadening of the lineshape (i.e. due to rapid T2 decay). Later it was suggested that the invisible fraction could be explained on the basis of quadrupolar effects (Shporer and Civan, 1972) which would result in two T2 decay rates even if only a single pool of sodium is present, with 60% of the total sodium having a short T2 and possibly being invisible. A theory for quadrupolar ions in tissue was presented and biexponential T2 decay was detected in muscle, as predicted

by the theory (Berendsen and Edzes, 1973). Another possibility considered was that several pools of sodium may be present in tissue, and these pools may be in fast, slow, or intermediate rates of exchange with each other. The rate of exchange as well as the characteristics of each pool--whether totally free or in some degree associated with larger molecules ("bound") and experiencing quadrupolar effects--could affect the observed relaxation behavior of a system. This complexity results in a wide range of interpretations possible for any given relaxation data, and work has been done to attempt to sort out these possibilities (Monoi, 1974a,b; Goldberg and Gilboa, 1978a,b), but no clear interpretation has yet been achieved.

3.1.2 Shift reagents and relaxation reagents

Much of the recent work done with sodium NMR in biological systems has involved the use of shift reagents. Shift reagents are compounds which are able to shift the resonant frequency of cationic nuclei. This is useful if the shift reagent penetrates only certain areas of a given system, thus separating what was a single resonance into two resonances -- one resonance at the new shifted resonance frequency indicating the presence of shift reagent among those nuclei, and another resonance at the original frequency which includes nuclei not affected by shift reagent. For sodium, two principle shift reagents are utilized -- dysprosium triethylenetetramine hexaacetic acid ($Dy(TTHA)^{-3}$) (Pike et. al., 1985) and dysprosium tripolyphosphate ($Dy(PPP)_2^{-7}$) (Gupta and Gupta, 1982). The principle utility of these shift reagents arises from the fact that these highly anionic compounds will not enter biological cells, thereby

resulting in a signal which resolves intracellular and extracellular sodium resonances. For the purpose of monitoring intracellular sodium levels and measuring intracellular sodium relaxation rates, this approach has been applied to several biological systems including red blood cells (Shinar and Navon, 1984; Pettegrew et. al., 1984; Burstein and Fossel, 1987b; Shinar and Navon, 1991), perfused hearts (Burstein and Fossel, 1987a,c; Pike et. al., 1985), kidney tubules (Boulanger et. al., 1987; Ammann et. al., 1990), and microvilli (Barac-Nieto et. al., 1988), neoplastic tissue (Liebling and Gupta, 1986), epithelia (Civan et. al., 1983), skeletal muscle (Gupta and Gupta, 1982; Balschi et. al., 1990), and exocrine glands (Seo et. al., 1987). One group has correlated the extracellular sodium compartments with the complex extracellular lineshape of an isolated heart perfused with a shift reagent buffer (Kohler et. al., 1991).

Certain difficulties are associated with the use of shift reagents. $Dy(PPP)_2^{-7}$ results in the best separation of intra- and extracellular resonances, but is a strong calcium chelator making its use undesirable in the presence of a functioning heart or gland (Seo et. al., 1987) (Pike et. al., 1985). In such cases $Dy(TTHA)^{-3}$ is preferred, but this compound yields less separation of the intracellular resonance from the extracellular resonance such that the intracellular resonance is obscured by the large extracellular resonance under normal conditions. If the intracellular sodium concentration is increased by means such as ouabain in a heart, then two resonances are observable with $Dy(TTHA)^{-3}$ (Pike et. al., 1985). Work is being done to overcome these difficulties by

quantifying the amount of shift reagent which can be added without causing cytotoxicity and by devising methods to increase the concentration of free calcium in the $Dy(PPP)_2^{-7}$ buffer solution (Anderson et. al., 1988). It is likely, though, that certain sensitive systems, such as mammalian hearts, will present difficulties when studies are performed using the current selection of shift reagents. This toxicity makes their future use in human studies doubtful.

A further difficulty arises when considering their use in live animal preparations. In this case the shift reagent is injected intravenously or intraperitoneal and one then performs imaging or spectroscopy. Preliminary work has been restricted to $Dy(TTHA)^{-3}$ due to the *in vivo* toxicity of $Dy(PPP)_2^{-7}$. $Dy(TTHA)^{-3}$ enters the extracellular space, but it is unclear if the entire extracellular space will be penetrated and if an even distribution of shift reagent will be maintained *in vivo*. Specifically, it is possible that the shift reagent will not penetrate an intact blood-brain barrier (Albert et. al., 1990) or the necrotic center of tumors, and it is possible that the concentration of shift reagent will not remain stable in all organs and spaces throughout the course of an experiment (Boulanger and Vinay, 1989; Ammann et. al., 1990).

A relaxation reagent, dextran magnetite, has been proposed (Renshaw et. al., 1986) which will remain only in the intravascular space. This would be useful for determining the NMR sodium signal magnitude and relaxation times of the fraction of the interstitial space excluding vessels. This could be accomplished, for instance, by comparing the

intracellular signal obtained by using $Dy(PPP)_2^{-7}$ with the intracellular plus interstitial signal obtained by using this intravascular agent. However, the strong magnetic character of magnetite makes it possible that long-range susceptibility effects will alter the relaxation times of interstitial ions outside the vessel. Estimates of the magnitude of the interstitial sodium signal (minus vascular sodium) may still be possible with this reagent.

It is certainly possible that new shift reagents will be developed over the next several years. For example thulium$(DOTP)^{-5}$ is currently being investigated by several labs as a shift reagent which overcomes some of these difficulties (Kohler et. al., 1990). However, the current selection of compounds does not present a viable option for *in vivo* studies.

3.1.3 Multiple quantum spectroscopy

Another technique which has been proposed for compartmental discrimination of the sodium signal is multiple quantum spectroscopy (Pekar and Leigh, 1986; Pekar et. al., 1987). This technique investigates the $\Delta M=2$ or $\Delta M=3$ transitions of the spin 3/2 sodium nucleus. These double and triple quantum signals are detected by using a pulse sequence which passes the system of spins through a multiple quantum filter, selectively exciting and detecting a double or triple quantum coherence. Only nuclei which have a correlation time short enough to lead to biexponential T_2 relaxation will be visible with multiple quantum techniques. Thus no signal will be seen for the sodium in saline, which exhibits mono-

exponential T_2 decay, whereas intracellular sodium, which exhibits biexponential decay, may yield a detectable signal. Therefore, the technique was proposed as a non-invasive method to detect only the biexponential relaxing components of the sodium signal.

Two principle difficulties arise with the use of multiple-quantum spectroscopy. The first is a loss of sensitivity incurred by passing the nuclei through a double or triple quantum coherence. For example, if the fast and slow T_2 relaxation times have a ratio of 1:10 and arise from a single pool, then the magnitude of the signal from a double quantum pulse sequence is reduced to about 25% of what it would be with a 90^{o}-AQ (one pulse) sequence (Pekar, 1988). In this example, multiple quantum spectroscopy would require 16 times as much total acquisition time to obtain S/N equivalent to that of a one pulse sequence. The fact that the magnitude of the multiple quantum signal depends on the ratio of the two T_2 components also makes it difficult to quantify the amount of sodium present when using a multiple quantum pulse sequence, since the T_2 values may not be known. The other difficulty arises with identifying the source of biexponential relaxation. In cell suspensions it has been proposed that the multiple quantum signal is due to sodium inside the cells (Pekar et. al., 1987), but in tissue or *in vivo* animal preparations, biexponential T_2 and hence multiple quantum signal will not only come from inside the cells but also possibly from the interstitium.

To resolve the question of the origin of the multiple quantum signal, two investigators have combined the use of shift reagent with multiple

quantum spectroscopy to determine if the total multiple quantum signal (obtained without shift reagent) matches the intracellular multiple quantum signal (obtained with shift reagent). This procedure has been performed on plasma and intact blood (Jelicks and Gupta, 1989a,b). The result was that a significant double quantum signal was attributed to extracellular sodium. This procedure was also performed on a perfused, rat heart (Payne et. al., 1990; Jelicks and Gupta, 1989c) with the result that double and triple quantum sodium signal was present at the shifted (extracellular) frequency in a normal heart. Since multiple quantum spectroscopy doesn't appear to provide compartmental information by itself, one possibility proposed to achieve this goal was to use a relaxation reagent such as gadolinium tripolyphosphate to "quench" the multiple quantum signal from the extracellular space (Jelicks and Gupta, 1989a).

3.1.4 Sodium relaxation times in tissue

Intracellular relaxation times have been obtained with the use of shift reagents. For perfused frog hearts, intracellular T_1 was 23 ms and intracellular T_2 relaxation was biexponential with times of approximately 2 and 16 msec (Burstein and Fossel, 1987a). Similar relaxation times were found for intracellular sodium of chicken erythrocytes (Shinar and Navon, 1991). In both of the above studies, the intracellular relaxation times were found to be relatively stable despite 5 to 7 fold increases in intracellular sodium concentration. Other studies of intracellular sodium relaxation in dog and human red blood cells found T_1 values between 18 and 30 ms and shorter T_2 values of 14 ms (Pettegrew et. al., 1984) or

biexponential T_2 values of about 6 and 16 ms (Shinar and Navon, 1984). Intracellular sodium T_1 values for proximal tubules of the rabbit kidney were found to be about 10 ms (Gullans et.al., 1985). Intracellular sodium T_1 values for the perfused rat heart with ouabain in the buffer were found to be about 25 ms (Pike et. al., 1985).

Previous studies of *in vitro* body fluids revealed that cerebrospinal fluid had T_1 and T_2 values of around 53 ms (Shinar and Navon, 1986). For human plasma, T_1 was 30 to 40 ms while evidence was found to indicate that T_2 was biexponential, although only monoexponential T_2 values of 17 to 26 ms were experimentally determined (Pettegrew et. al., 1984; Shinar and Navon, 1986). One study found biexponential T_2 decay of blood serum with T_2 values of 12 and 49.5 ms (Perman et. al., 1986).

Studies of excised tissue have usually found T_1 values in the range of 11 to 32 ms and a biexponential T_2 with a fast component of 0.7 to 5 ms (rat skeletal muscle--Berendsen and Edzes, 1973; Chang and Woessner, 1978; frog muscle--Shporer and Civan, 1974; human colon and breast--Cheung et. al., 1988; myelinated nerve of rabbit and rat brain--Cope, 1970; cat head--Hilal et. al., 1985).

Concerning studies of sodium NMR relaxation in solutions of biologic macromolecules, protein solutions have been found to produce fast T_2 components of around 3 ms for some proteins (hemocyanin--Norne et. al., 1979) and not for others (serum globulins--Shinar and Navon, 1986). Solutions of proteoglycans (Gustavsson et.al., 1978; Lerner and Torchia,

1986), and heparin (Lerner and Torchia, 1986) have been found to have T_1 and T_2 values that are shorter than T_1 and T_2 of sodium in dilute saline solution, but these studies have not indicated the presence of a biexponential T_2. T_1 and T_2 of the more concentrated solutions in these studies were less than 5 ms.

3.2 Imaging

Due to the fast T_2 decay of sodium in tissue, a short echo time is helpful in maximizing the S/N of a sodium image, and the techniques developed by previous researchers to obtain a short echo time are presented in this section. Results of early sodium imaging experiments on biologic tissue which characterized the normal appearance of major organs on a sodium image are then described. Many studies have also examined pathologic states using sodium imaging, with an emphasis on ischemia, tumors, and interstitial edema since these pathologies are expected to produce large changes in the observed sodium signal. The results of these studies are outlined in this section. Also described are attempts by several researchers to utilize relaxation time information in sodium images to improve diagnostic specificity and/or to derive information concerning intracellular and interstitial sodium compartmentation. When available, data from these previous studies which compares contrast on sodium MRI with contrast from other diagnostic modalities, mainly proton MRI, is presented since this information is important in determining the future role of sodium imaging in medicine.

3.2.1 Development of short echo times

Early sodium images were obtained with echo times of 10 to 20 ms as this was the shortest echo time obtainable using conventional hardware and pulse sequences. This is much longer than the fast component of T_2 relaxation of many tissues (see Section 3.1.4) and therefore will detect only the slower components of sodium T_2 decay in tissue, as well as sodium present in saline, CSF, and plasma, fluids which have T_2 time constants greater than 10 ms.

Several approaches have been developed to shorten the echo time with a Hahn spin echo experiment. Two groups used nonselective 90^o and 180^o pulses to shorten the echo time. The spatial information was obtained through a projection-reconstruction algorithm (Ra et. al., 1986) or through slice selection prior to the 90^o excitation pulse (Perman et. al., 1989) in order to obtain echo times of 3.6 ms and 2.5 ms respectively. Another group used specialized gradient coils which enabled fast ramping of the gradient current, thereby allowing an echo time of 2.6 ms to be obtained using conventional imaging sequences (Burstein and Mattingly, 1989).

Another approach to produce a short echo time is to use a gradient echo instead of a Hahn spin echo (Moseley et. al., 1985; Granot, 1986). A gradient echo is produced by reversing the sign of a gradient midway through a sequence instead of producing an echo with a 180^o refocussing pulse as is used in a Hahn spin echo. The gradient echo can produce a shorter echo time because the time required to execute the 180^o pulse,

which can be several ms for a selective 180^{o} pulse, is not necessary. It also produces a shorter echo time because the readout gradient need only be switched in sign instead of having to be switched off for the 180^{o} pulse and then switched on after the pulse. Using gradient echoes, echo times of 2.8 ms (Moseley et. al., 1985) and 6.4 ms (Granot, 1986) were obtained in early sodium imaging studies. A gradient echo sequence also improves signal-to-noise for a given imaging time by enabling a faster repetition rate to be utilized. This is because the excitation flip angle can be substantially less than 90^{o}, allowing a much shorter TR to be utilized for recovery of magnetization before the next excitation pulse.

A drawback of gradient echo imaging sequences is that the signal is affected by inhomogeneities of B_0 since these inhomogeneities are not refocussed by a 180^{o} pulse. This means that relaxation time information is lost due to the fact that the signal decays with time constant T_2^* instead of at the more fundamental time constant of T_2.

Finally, since some tissues possess T_2 values of 2 ms or less, even echo times on the order of 2 ms, such as those discussed above, will still miss an appreciable amount of signal. Therefore, one group developed a method of imaging the FID signal directly (Hilal et. al., 1988; Ra et. al., 1989). Although it involves significant post-acquisition processing, it does produce an imaging signal 0.2 ms after excitation, which can lead to improved S/N and improved detection of sodium components missed by other techniques.

3.2.2 Sodium imaging of normal tissue

The very first biologic application of sodium imaging was of a perfused rat heart (Delayre et. al., 1981). The image revealed a bright signal from the bathing solution surrounding the heart and low signal from heart tissue itself. The majority of the other early sodium imaging experiments on normal tissue involved the brain (Hilal et. al., 1983; Maudsley and Hilal, 1984; Feinberg et. al., 1985). The findings from all of them were that CSF and the aqueous and vitreous of the eye had a high intensity signal, while brain parenchyma was considerably less intense, or not visualized at all under normal conditions. It should be noted that most of these early studies used echo times of greater than 10 ms. Another early study of normal tissue was performed on canine kidney where it was found that the medulla produced a greater sodium intensity than the cortex (Hilal et. al., 1984).

More recent studies have been able to improve their detection of normal brain parenchyma. One used a surface coil and a gradient echo time of 2.8 ms (Moseley et. al., 1985), and another optimized the image acquisition parameters (but still utilized a 12 ms echo time) to deduce that grey matter had a slightly higher intensity than white matter on sodium images (Hilal et. al., 1985). In other studies, the ratio of brain parenchyma intensity to ventricle intensity was found to be 50% higher using a Hahn spin echo time of 3.6 ms instead of a Hahn spin echo time of 14 ms (Ra et. al., 1986).

Using 8 echoes with times between 3.2 ms and 25.6 ms, the T_2

characteristics of the normal human brain were determined. The data was found to follow a monoexponential decay with the following values: white matter, 17.6 ms; gray matter, 16.8 ms; and vitreous, 56.8 ms (Perman et. al., 1989). A similar study using 4 echo times between 3 ms and 12 ms found the following relaxation times: white matter, 12.4 ms; gray matter, 11.2 ms; CSF, 47.5 ms; Blood in the superior sagittal sinus, 20.9 ms; and vitreous, 58.0 ms (Winkler et. al., 1989). This study (Winkler et. al., 1989) also attempted to quantify the sodium concentration in various parts of the brain by back extrapolating image intensities at the various echo times to an intensity at time zero. Certain difficulties were encountered as the concentration estimates from the sodium images were 30 to 50% higher than predicted for brain tissue. Using the FID image described above, detection of signal from brain parenchyma was greatly improved. This enabled the authors to deduce that normal brain parenchyma possesses a short and long component of T_2 decay, although the actual relaxation times were not obtained in the study (Ra et. al., 1989).

Other recent studies have obtained sodium images of various other non-pathologic organs in the body. Using an FID image and a 14 ms Hahn spin echo time (Ra et. al., 1988) or a 6.4 ms gradient echo time (Granot, 1988), *in vivo* images of the human heart, kidneys, mid-thoracic spine region, liver, eye, feet, and knee were acquired. Categorizing the sodium signal from both studies into roughly high intensity and low intensity sources, it was found that high intensity signals were obtained from blood, the kidneys, intervertebral disks, CSF, gallbladder, aqueous and vitreous fluids, synovial fluid, bursae, and possibly ligaments and

cartilage of the knee. Low intensity signals were obtained from heart tissue, bone, liver, and lens.

3.2.3. Sodium imaging of pathology

Ischemia

The appearance of ischemia, tumors, and interstitial edema on sodium images is of considerable interest, since a large contrast is expected between normal tissue and these pathologies. The first study of ischemic tissue observed a cat brain 9 hours after a stroke was induced in one hemisphere (Hilal et. al., 1983). A bright sodium signal was found from the affected hemisphere (echo time not given) which they attributed to both increased sodium concentration and increased sodium visibility. The proton image of the same lesion taken at 24 hours after the stroke revealed a slight loss of gray/white matter contrast and a minimal increase in proton density.

Later studies found a similar high intensity sodium signal for ischemic tissue in cat, rat, and human brains using acquisition parameters which ranged from an echo time of 12 ms to an FID acquisition at an effective post-excitation time of 0.2 ms (Maudsley and Hilal, 1984; Hilal et. al., 1984; Hilal et. al., 1985; Moseley et. al., 1985; Hilal et. al., 1988; Grodd and Klose, 1988; Perman and Turski, 1988). Most of these studies were performed 6 to 24 hours after the stroke occurred, but similar images were also obtained of strokes 2 hours old, and of "old" strokes (Hilal et. al., 1985). The magnitude of the sodium intensity of the ischemic tissue was found to be 4 times greater than uninjured brain

tissue (Hilal et. al., 1985; Moseley et. al., 1985). One group of authors (Hilal et. al., 1985) reasoned that if the fraction

$$\frac{\text{image intensity at echo time of 12 ms}}{\text{image intensity at echo time of 0 ms, (maximum possible)}}$$

were the same for both uninjured and ischemic brain tissue, the observed increase in image intensity by a factor of 4 would indicate ischemic brain tissue sodium concentrations greater than plasma sodium concentrations, since plasma sodium concentrations are only 3 times greater than normal brain tissue sodium concentrations. Since this is unlikely, they concluded that a greater fraction of the total sodium was detected in ischemic tissue than in normal brain parenchyma, indicating that a prolongation of sodium T_2 values occurred in the ischemic case. Proton magnetic resonance images corresponding to sodium images of ischemic tissue were obtained only in two isolated cases, revealing that the lesion was also visualized on the proton image (Hilal et. al., 1988; Grodd and Klose, 1988).

An additional study of ischemic tissue examined perfused dog hearts following a one hour occlusion of a coronary artery and one hour of reperfusion (Cannon et. al., 1986). Sodium images, obtained on the excised hearts using an echo time of 12 ms, revealed that the sodium signal was 2.2 to 2.6 times larger in the affected region than in the normal region, which correlated with increases in sodium content as measured by flame photometry. Another study examined the guinea pig kidney following occlusion of the renal artery, vein, and ureter (Maeda et. al., 1990). The sodium image used an echo time of 19 ms and revealed

that the affected kidney had a decreased intensity of 55% of its pre-occlusion intensity. The corresponding proton images revealed minimal intensity changes.

Tumors

Several studies have obtained sodium images of brain tumors. One early study examined a treated malignant glioma and an anaplastic astrocytoma in humans and found an increased sodium signal intensity from the tumor region, but found it difficult to distinguish tumor from CSF or edema (Feinberg et. al., 1985). Three studies by one group examined a variety of brain tumors in humans including astrocytomas, brainstem gliomas, a glioblastoma multiforme, a benign pituitary tumor, and a nasopharyngeal carcinoma (Perman et. al., 1986; Turski et. al., 1987; Perman and Turski, 1988). These studies acquired signal at multiple echo times ranging from 13 to 52 ms. The finding was that tumors of higher grade tended to have a greatly increased sodium signal intensity over normal brain parenchyma, while more benign tumors produced a slight or no increase in sodium signal intensity. It was believed that this was due to the fact that malignant tumors have a greater intracellular sodium concentration as well as greater expansion of the interstitial space than benign tumors. Again the difficulty of distinguishing the tumor from nearby cerebrospinal fluid and edema was mentioned. Proton magnetic resonance T_2-weighted images of these lesions tended to reveal an increased signal intensity on all types of tumors, both malignant and benign. Sodium T_2 measurements of these tumors and of experimentally induced gliosarcomas in dog brain (Turski et. al., 1987) revealed that the

T_2 of the tumor was 42 to 47 ms, which compares to a T_2 of 54 to 58 ms for cerebrospinal fluid. The T_2 of normal brain tissue was not determined in these studies due to the low level of sodium signal from normal brain parenchyma at these echo times.

Two later sodium imaging studies of tumors again found that the tumor had an increased sodium signal intensity, although these studies used an FID image at 0.2 ms post-excitation (Hilal et. al., 1988), and a 4.5 ms gradient echo (Grodd and Klose, 1988). Compared to surrounding edema, the tumor sodium intensity was either equivalent, or slightly reduced. These studies also compared the sodium images to proton images. One study found that three low grade gliomas were detected by sodium imaging which could not be visualized on T_2-weighted proton images (Hilal et. al., 1988). The other study found that the proton signal from the tumor had prolonged T_1 and T_2 values in the region of the tumor, making it easily visible on T_1 and T_2 weighted images (Grodd and Klose, 1988). Additionally, while the authors concluded that the sodium image provided more contrast between vital tumor (high intensity) and central necrosis (lower intensity) than normal proton images, the proton images obtained using a contrast agent were felt to provide the best visualization of the central necrosis (Grodd and Klose, 1988). The contrast agent gadolinium-diethylenetriaminepentaacetate shortens the relaxation times of vascular tissues, enabling contrast to be achieved between vascular structures such as tumors and less vascularized structures, such as necrotic tissue. Contrast is also enhanced if the contrast passes through the blood-brain barrier in some regions of tissue, such as tumors, and not in others, such

as normal brain.

Edema

Studies of interstitial edema have also been conducted using sodium imaging. One study examined two forms of edema, vasogenic edema in the dog brain induced by injection of hypertonic mannitol and chronic edema surrounding a meningioma in the human brain (Turski et. al., 1986). The sodium images revealed that both forms of edema had an increased sodium intensity at echo times of 13 ms and 52 ms compared to normal brain tissue. Corresponding proton images had a decreased signal intensity on T_1-weighted images and an increased signal intensity on T_2-weighted images. Sodium T_2 values of the edematous region were slightly shorter than T_2 values for CSF (approximately 46 ms for edema versus approximately 55 ms for CSF). T_2 values for normal brain parenchyma were not obtained due to low signal-to-noise. Another study of interstitial edema in the brain, this time due to herpes simplex enchephalitis, found that the sodium intensity was increased but that the T_2-weighted proton images demonstrated the lesion with similar or superior contrast (Grodd and Klose, 1988).

Another sodium imaging study focussed on edema induced in the rat lung (Kundel et. al., 1988). Using a gradient echo time of 3.3 ms, the sodium imaging intensity was found to increase by a factor of approximately 2 due to edema caused either by a drug induced increase in vascular permeability (and thus increased protein content in the edema fluid) or for edema caused by an infusion of saline (resulting in

increased vascular pressure and little protein in the edema fluid). The sodium intensity was found to be correlated with the water fraction for both types of edema. Sodium T_2 values for normal lung and edematous lung were found to be similar at about 24 ms using data from a gradient echo at 3.3 ms and 4 spin echos at 15 ms to 58 ms.

Other pathologies

Several studies of specific pathologies other than the general types described above have been performed. Sodium imaging of the rabbit kidney has been performed (Wolff et. al., 1988; Wolff et. al., 1990). These studies used a surface coil positioned over the surgically exposed rabbit kidney and used a gradient echo time of 7 to 11 ms. Normally, the renal medulla has a greater sodium intensity than the cortex, but it was demonstrated that sodium imaging was capable of detecting a decrease in the medullary sodium imaging intensity during saline infusion. Since the relaxation times were relatively unchanged by the saline infusion as determined by spectroscopic techniques, the decreased intensity was attributed to a decrease in medullary sodium concentration.

A study of heterotopic heart transplants in dogs found that the sodium image intensity was correlated with the rejection score. The proton T_1 and T_2 were also found to be correlated with the rejection score (Nishimura et. al., 1989). A study of cytotoxic edema induced in the rat liver by injection of carbon tetrachloride (CCl_4) found that the sodium imaging intensity increased 3 fold compared to normal liver. Proton imaging of the pathologic liver found an increased signal intensity also,

largely due to increased proton T_2. Spectroscopic sodium T_2 measurements on the excised liver tissue found no differences between the normal and CCl_4 damaged liver (Brauer et. al., 1990). Sodium imaging of intraocular lesions found that the hemorrhages and melanomas were hypointense relative to normal aqueous and vitreous. Using a gradient echo time of 3.5 ms, the same authors found that the sodium was only 80% visible in the normal vitreous, but was 100% visible after collagenase treatment (Kohler et. al., 1989; Kolodny et. al., 1989). Other pathologic lesions which have been found to produce an increased sodium image intensity include arteriovenous malformations, multiple sclerosis plaques, and brain abscesses (Perman and Turski, 1988; Hilal et. al., 1988).

3.2.4. Sodium imaging of compartmental sodium distribution

The above studies have demonstrated that sodium imaging is capable of visualizing various pathologies, but the benefit of using sodium MRI over other diagnostic modalities has yet to be clearly demonstrated. The ability to discriminate intracellular and extracellular sodium signals would greatly enhance the usefulness of sodium imaging for identifying pathologic states and for electrophysiologic studies. Several investigators have attempted to separate the compartmental sodium signals in an imaging application using the spectroscopic methods described above, namely shift reagents and multiple quantum spectroscopy. A technique which utilizes possible differences in relaxation times between the compartments has also been explored for this purpose.

Using the shift reagent $Dy(PPP)_2^{-7}$ in a perfused frog heart

preparation, one study demonstrated the feasibility of performing sodium imaging of the intracellular sodium. By comparing spectra and images using a conventional pulse sequence with spectra and images using a pulse sequence designed to eliminate signal from the shifted, extracellular resonance, it was demonstrated that the sodium image contained signal from only the unshifted, intracellular resonance (Burstein and Mattingly, 1989).

The multiple quantum pulse sequence described above has also been applied to imaging. The capability of performing double-quantum sodium imaging was demonstrated on agarose gels (Cockman et. al., 1990). Another study compared conventional sodium images with triple quantum coherence (TQC) images of normal rats and rats with gliomas. The conventional sodium image presented with elevated signal in the heart (blood in chambers), kidneys, bladder, and tumor when present. The TQC image showed a relatively homogeneous intensity throughout the body, except for the tumor which presented with an elevated signal intensity (Griffey et. al., 1990). The ability of this TQC pulse sequence to selectively detect intracellular sodium was not studied in these experiments on tumors in rats, although the authors did not find any extracellular TQC signal from cell suspensions or perfused hearts, in contradiction to the double and triple quantum coherence findings presented in the spectroscopy section above.

Another method proposed to obtain compartmental information on sodium images is to use possible differences in relaxation times between

the compartments (Hilal et. al., 1988; Ra et. al., 1989). As mentioned above, relaxation times for the intracellular space of some systems have been found to possess a component of T_2 decay of approximately 2 ms, while certain *in vitro* extracellular fluids (CSF, plasma) do not have this fast component of T_2 decay. Based on this data, the proposal was to obtain an image which emphasized the fast component of T_2 decay.

The specific technique (Hilal et. al., 1988; Ra et. al., 1989) was to acquire a sodium image at a short echo time and one at a long echo time and then to subtract the image at the long echo time from the image at the short echo time. Since an image at a long echo time will be primarily due to the slower T2 components, while an image at a short echo time will have contributions from both slow and fast T2 components, the effect of the subtraction will be to emphasize the fast T2 components. Since the fast T_2 components which the authors wished to emphasize were the intracellular fractions with T_2 values of about 2 ms, an imaging technique which was capable of detecting these components was used, namely the FID image described above (Ra et. al., 1989).

These subtraction images revealed 1) a uniform gray signal in the brain parenchyma of a normal individual; 2) the non-cystic character of a malignant glioma (bright on subtraction image) and the corresponding region of edema surrounding it (dark on the image); 3) the low grade of a glioma (dark on the subtraction image); and 4) the presence of a glioma in a field of radiation necrosis which was not detected by other diagnostic means. Each of these results was obtained from a single case (Hilal et.

al., 1988), although additional work in the area of tumor grading with this technique has been presented (Hilal et. al., 1989).

A difficulty with this method is that the technique emphasizes the fast T_2 components of the tissue under study, but the source of the fast T_2 signal is not easily identified. Although the intracellular compartment of some systems has been demonstrated to have a fast T_2 component of around 2 ms, while certain *in vitro* extracellular fluids do not have this fast T_2 component, the T_2 behavior of interstitial sodium had not previously been characterized in any organ. Thus the interstitial sodium may contribute to the signal on a subtraction image. In addition, the T_2 behavior of both intracellular and extracellular sodium present in pathologic lesions has not been thoroughly studied and may further complicate interpretation of the subtraction image.

The presence of a biexponential T_2 decay in blood serum, the presence of fast T_2 components (about 3 ms) in sodium-protein solutions (Norne et.al., 1979), and the fact that some forms of edema fluid contain proteins are interpreted by some investigators as evidence that compartmental discrimination can not be achieved by exploiting differences in relaxation times (Perman et. al., 1986; Perman et. al., 1989). Therefore the capability to discriminate between intracellular and extracellular sodium using relaxation times has not been proven. Regardless of its ability to obtain compartmental sodium information, the technique of emphasizing the fast component of T_2 decay on an image does provide an extension of the conventional sodium imaging sequences and may

provide useful diagnostic information.

4. PHYSIOLOGY

In this section, the gross anatomy of both frog and rat hearts is presented. Of more relevance to the experiments in this work are the sodium concentrations and relative volumes of the intracellular and interstitial compartments. The subcompartmentalization of the interstitial compartment will also be presented for each type of heart. Differences between the perfused heart preparations employed in these studies and the *in vivo* characteristics of frog and rat hearts are pointed out when necessary. Finally, theories about the chemical and physical nature of the interstitial matrix and its response to edema are presented.

Several terms used to refer to various compartments of tissue and perfused heart preparations may be unclear. A definition of terms as they are used in this thesis will aid in clarifying the specific compartments referred to by each term. The following terms are used throughout this thesis:

interstitial - refers to the spaces between cells and includes connective tissue, connective tissue cells, blood vessels, and endothelial cells of vessels. Does not include major fluid compartments exterior to tissue such as cerebrospinal fluid or heart atrial and ventricular cavities. Also does not include bathing solution in a perfused heart preparation.

extracellular - refers to all spaces exterior to cells. Thus it includes all of the interstitial space, as well as major fluid compartments

both *in vivo* and in perfused heart preparations.

interstitial matrix - refers to the interstitial space minus connective tissue cells, blood vessels, and endothelial cells lining vessels. Thus it includes collagen, proteoglycans, and fluid associated with this matrix of connective tissue macromolecules.

cardiac or myocardial - refers to the combination of intracellular and interstitial spaces in a heart.

bath or bathing solution - refers to the fluid in a perfused heart preparation which is exterior to heart tissue or inside the atrial or ventricular cavities. Thus it is equivalent to all spaces in a perfused heart preparation which are not cardiac.

perfusate or buffer - does not refer to a specific space. It refers to the solution which flows into a perfused heart preparation to supply the heart with nutrients. Both Ringer's solution and Krebs Henseleit solution are referred to as perfusate or buffer interchangeably.

Two additional terms used in this chapter need to be defined:

total volume fraction - the ratio of the total volume occupied by a compartment over the total volume of the organ. Note that the total volume occupied by a compartment or organ includes volume occupied

by solid (non-water) material and water.

water volume fraction - the ratio of the water volume of a compartment over the water volume of the entire organ.

4.1. Frog heart

4.1.1. Anatomy

The frog heart consists of two atria and one ventricle. Blood from the body flows into the right atrium, while oxygenated blood from the lungs flows into the left atrium. From both atria, blood enters the ventricle where it is pumped out through the bulbus cordis to the body and lungs. It is unclear whether some separation of oxygenated and deoxygenated blood is maintained by the flow patterns in the heart (Robb, 1965). Frog hearts do not possess coronary arteries, and exchange of substances between cells and the heart cavities occurs by diffusion.

4.1.2. Tissue compartmentation

Muscle cells of the frog heart are arranged in bundles or trabeculae which branch and interconnect in a complex network to form the wall of the ventricle. The trabeculae are covered by a layer of endothelial cells which divides the interstitial space into an extra-trabecular space and a subendothelial space. The term subendothelial space refers to the large space between the endothelial cells and the fiber bundle and occasional large spaces between muscle fibers. A small additional interstitial space exists between muscle fibers in close apposition to each other, termed the interfiber space (Page and Niedergerke, 1972). The total volume fractions

of these interstitial compartments and the intracellular compartment as determined with histologic stereological methods are: interfiber space, 1%; subendothelial space, 10%; extra-trabecular space, 15%; and intracellular space, 74% (Cohen and Kline, 1982; Page and Niedergerke, 1972).

In order to calculate the relative amounts of sodium signal expected from the intracellular and interstitial compartments, it is necessary to know the sodium concentrations and the water volume fractions of each compartment. The sodium concentration of frog serum is 114 mM (Armstrong et. al., 1969). The sodium concentration of Ringers buffer used in this work was 120 mM, and thus the interstitial sodium concentration of perfused frog hearts is estimated to be 120 mM. The sodium concentration in the intracellular space is estimated to be between 5 and 10 mM (Keenan and Niedergerke, 1967).

The water volume fractions of the intracellular and interstitial compartments will differ from the total volume fractions given above due to differing amounts of solid material in each compartment. From chemical tracer studies, the water volume fraction of the interstitial space is found to be 31%. (This figure is derived from measurements of the water volume of each compartment per wet weight of the whole heart for the interstitial (24.5 ml water per 100 g heart wet weight) and the intracellular (55 ml water per 100 g heart wet weight) compartments.) These studies were performed on frog hearts which had been perfused for at least two hours (Keenan and Niedergerke, 1967).

Using 7.5 mM as the estimate of intracellular sodium concentration and assuming the interstitial water volume fraction described above, the relative magnitudes of sodium signal expected from the intracellular and interstitial compartments of the perfused frog heart can be estimated to be 12% and 88% respectively.

4.2. Rat heart

4.2.1. Anatomy

The gross anatomy of the rat heart is similar to other mammals, consisting of 2 atria and 2 ventricles and no normal communications between right and left halves of the heart. The major arteries and veins entering and leaving the heart are also similar to other mammals, with the aorta and pulmonary artery originating from the left and right ventricles, respectively. The systemic venous flow returns via 3 major veins to the right atrium--the inferior, right superior, and left superior venae cavae. The presence of two superior venae cavae is normal in rats and differs from humans. The pulmonary veins enter the left atrium (Bishop, 1980).

The left and right coronary arteries originate at left and right coronary ostia at the root of the ascending aorta. The coronary arteries supply all of the blood for the ventricular tissue, and also supply some blood to the atrial tissue. The majority of the atrial blood supply is provided by cardiacomediastinal branches of the internal mammary arteries (Bishop, 1980).

4.2.2. Tissue compartmentation

The muscle cells of the rat heart are organized into parallel bundles. The orientation of the bundles is generally vertical (along base to apex) in the subendocardium, and becomes transverse towards the subepicardium. The cells are connected to each other at intercalated disks at the ends and sides of the cells (Bishop, 1980).

Using histologic stereological methods and chemical tracer studies, the total volume fraction for the interstitial space of *in vivo* rat hearts was found to be 19% (Polimeni, 1974). Note that the interstitial space of rat hearts includes an extensive transverse tubular system, which is estimated to comprise 1% of total tissue volume and which is included in the above value.

The total volume fractions of subcompartments of the interstitial space can be quantified using histologic stereological techniques. Data for rat hearts on this topic was not available. In a study of perfused rabbit heart interventricular septum, the interstitium was divided into the following volume fractions, expressed as total volume (solids plus water) of the subcompartment over total volume of the interstitium: blood vessels including both lumen and endothelial cells lining lumen--59%, ground substance--23%, connective tissue cells--7%, collagen--4%, and "empty" space--6%. The ground substance was distributed in homogeneous mats throughout the interstitium and transverse tubules, and was demonstrated to contain anionic polysaccharides. The "empty" space is believed to be an artifact of tissue preparation (Frank and Langer, 1974).

In order to estimate the relative fractions of sodium signal magnitude arising from the intracellular and interstitial compartments, it is necessary to know the sodium concentrations and water volume fractions of each compartment. The sodium concentration of plasma for the rat is 144 mmoles/kg plasma (Polimeni, 1974). The sodium concentration of Krebs Henseleit is also 144 mM. An upper estimate for the intracellular sodium concentration of rat hearts is 16 mM, although if the sarcoplasmic reticulum has a sodium concentration similar to that of the interstitium, then the upper estimate for intracellular sodium concentration is 7 to 9 mM (Polimeni, 1974).

The water volume fractions of the intracellular and interstitial compartments will differ from the total volume fractions given above due to differing amounts of solid material in each compartment. The water volume fraction of the interstitial space was found to be 25% for *in vivo* rat hearts (Polemini, 1974). See perfusion section below for possible changes in this value which occur upon perfusion of rat hearts.

Using 10 mM and 144 mM as estimates of intracellular and interstitial sodium concentrations respectively, and assuming the water volume fractions noted above, the relative magnitudes of sodium signal expected from the intracellular and interstitial compartments of the *in vivo* rat heart can be calculated to be 17% and 83%, respectively.

4.2.3. Perfused rat hearts

Certain structural and functional differences exist between perfused

rat hearts and *in vivo* rat hearts. One important difference upon perfusion is that the capillaries of the isolated, perfused rat heart are much more permeable than those of the *in vivo* heart, such that the capillaries are freely permeable to bovine plasma albumin (Sutherland and Young, 1966). This change is suggested to be due to release of a permeability factor from nerve endings upon resection of the heart.

Another major change upon perfusion is the onset of interstitial edema. In a survey of interstitial water volume fraction measurements (Polimeni, 1974), it was found that for perfused rat hearts, the interstitial water volume fraction was frequently greater than 40%. This compares with the interstitial water volume fraction of 25% noted above for *in vivo* rat hearts. If the calculation of relative magnitudes of sodium signals expected from the intracellular and interstitial compartments is repeated with the same sodium concentrations used above but with an interstitial water volume fraction of 40%, the relative intracellular and interstitial signal magnitudes for perfused rat hearts become 9% and 91% respectively.

Another study indicated that the interstitial water fraction increases as the duration of perfusion increases, going from 33% after 15 min of perfusion to 34% after 30 min of perfusion to 38% after 60 min of perfusion (raffinose space) (Fisher and Young, 1961). (The interpretation of the raffinose experiment is subject to question given the possibility that sucrose enters cells of perfused rat hearts over time; see Page and Page, 1968.)

A histologic examination of perfused rat heart tissue revealed diffuse interstitial edema following perfusion for one hour at 37°C with modified Krebs-Henseleit bicarbonate buffer containing 1.22 mM calcium and 5.5 mM glucose (Brown et. al., 1968). This interstitial edema was believed to contribute to an increase in the mean water content of perfused rat hearts from 76.9% ± 0.5% for freshly dissected hearts to 80.2% ± 0.3% for hearts which had been perfused for 3 hours. Using the water volume fractions and dry weights from another study of *in vivo* rat hearts (Polimeni, 1974; 0.579 g intracellular water per g wet weight, 0.190 g interstitial water per g wet weight), this change in water content can be calculated to correspond to an increase in interstitial water content from 0.82 grams of water per gram dry weight to 1.55 grams of water per gram dry weight, or an increase of interstitial water volume and hence interstitial sodium by a factor of 1.9. This calculation assumes that the entire increase in water content is attributed to interstitial water, as indicated by the histologic examination noted above. It was suggested that the interstitial edema was caused by the hydrostatic pressure of 68 cm H_2O overcoming the osmotic pressure of the perfusing media.

Two additional points of interest deal with the state of the heart immediately after the heart is removed from the perfusion apparatus. It has been found that a clear fluid exudes from such a heart over time following removal from the perfusion cannula. The amount of expressed fluid is greater than the vascular volume, and probably represents loss of interstitial fluid as the cells go into rigor (Fisher and Young, 1961).

The same study found that a rapid increase in cell permeability appears to occur during 15 minutes following cessation of perfusion, indicated by loss of cellular creatine and cellular uptake of raffinose. This increase in cell permeability did not occur during 15 minutes of anoxia.

4.3. Physical properties of the interstitial matrix

The interstitial matrix has been suggested to be a two phase system consisting of a gel-like phase and a free-fluid phase (Wiederhielm, 1972; Wiederhielm, 1979). The gel phase consists primarily of mucopolysaccharides, while the free-fluid phase contains the majority of the interstitial matrix proteins and may also serve the function of promoting the bulk flow of fluid and solutes from capillaries to cells and back. It has also been suggested that when edema occurs, it is the free-fluid phase that expands greatly (Guyton et. al., 1971).

5. METHODS

Interstitial relaxation times were studied with spectroscopic methods for both control conditions and for the pathologic conditions of global ischemia and interstitial edema. Sodium imaging was utilized to provide further relaxation and imaging intensity data for several pathologic conditions. Described below are the phantoms utilized to test the NMR techniques, the perfused heart preparation, and the NMR pulse sequences which enabled these goals to be achieved. Data analysis procedures, methods of inducing pathologic states, and sodium imaging techniques are also presented in this section.

5.1. Phantoms

Several phantoms were devised in order to validate the NMR pulse sequences used in these experiments. One phantom consisted of a 20 mm o.d. NMR tube filled with 150 mM NaCl. Saline has well-known, monoexponential relaxation characteristics. A second phantom consisted of a latex balloon placed on the end of the perfusion cannula (see below). A small hole was cut in the top of the balloon to allow the fluid which enters from the cannula to leave the balloon. This phantom was used to characterize the T_1 and T_2 behavior of flowing fluid in the perfusion apparatus. A third phantom consisted of an agarose/NaCl gel placed inside a 15 mm o.d. NMR tube, which was placed inside a 20 mm o.d. NMR tube filled with 150 mM NaCl. The gel was prepared by placing 4 g agarose into 100 ml of 150 mM NaCl. The solution was stirred and heated until the agarose dissolved and then poured into a 15 mm o.d. tube and allowed to cool until the gel formed. The gel's volume approximated the volume of a

perfused heart, which was approximately 1 to 2 ml for both frog and rat hearts. The entire 15 mm o.d. tube was then placed in a 20 mm o.d. tube which contained 150 mM NaCl. Both tubes were then sealed. This phantom provides a reasonable "relaxation-time model" of the perfused heart system with agarose representing the heart tissue as a substance having fast, biexponential relaxation times (see Results), and the NaCl solution representing the perfusate as a substance having slow relaxation times. The advantage of the phantom is that the sodium relaxation times of the agarose can be measured separately, thus providing a way of validating the capability of the NMR techniques to quantify the relaxation times of one component (agarose) when the relaxation times of the other component (NaCl solution) are known, but the relative magnitudes of the two components are not known.

5.2. Physiologic Preparations

5.2.1. Frog hearts

Bullfrogs (*Rana Catesbeiana*) were anesthetized with sodium pentobarbital by intraperitoneal injection. The frog heart was excised and placed in a dish of Ringer's solution (Table 5-1) at room temperature. Within 3 minutes, the heart was cannulated at the atrial input and perfused with the Ringer's buffer at room temperature. The Ringer's flowed from the atrial cavity to the venticular cavity from where it diffused into the ventricular tissue, supplying it with energy substrates and oxygen. Perfusate (the terms Ringer's, buffer, and perfusate are used interchangeably) then flowed out of the heart via the aortic outflow tract. This mimics the normal blood flow through frog hearts, which do

not posses coronary arteries. The perfusion flow rate for frog hearts was set to a constant value of 8 ml/min. The cannulated heart was mounted inside a 20 mm o.d. NMR tube and placed in the magnet.

The frog heart perfusion apparatus is shown in Fig. 5-1. The apparatus consisted primarily of two reservoirs, a fluid pump, a plastic cannula with four channels, and flexible tubing to connect the pump to the cannula. One channel of the cannula contained tubing through which the buffer solution flowed to the heart. Two channels contained suction lines to draw fluid out of the NMR tube. The height of one suction line could be varied so that suction could occur either above the heart, in which case the heart was immersed in buffer during the NMR measurements, or below the heart, in which case the heart was suspended in air during the experiment. The other suction line was fixed in position and served as a backup. The fourth channel contained tubing which was used to monitor the intraventricular pressure and heart rate. At the heart, the tubing was connected to one of the two main branches of the aorta. The line was connected to a pressure transducer and filled with fluid to provide uncalibrated monitoring of the pressure produced by the beating heart and hence the heart rate.

Two reservoirs which could be filled with two different buffer solutions were available for use during an experiment. Using a three-way stopcock, the output from each reservoir could be directed either to the cannula and the heart or back to the reservoir. At any given time, the output of one reservoir was directed to the heart while the other was

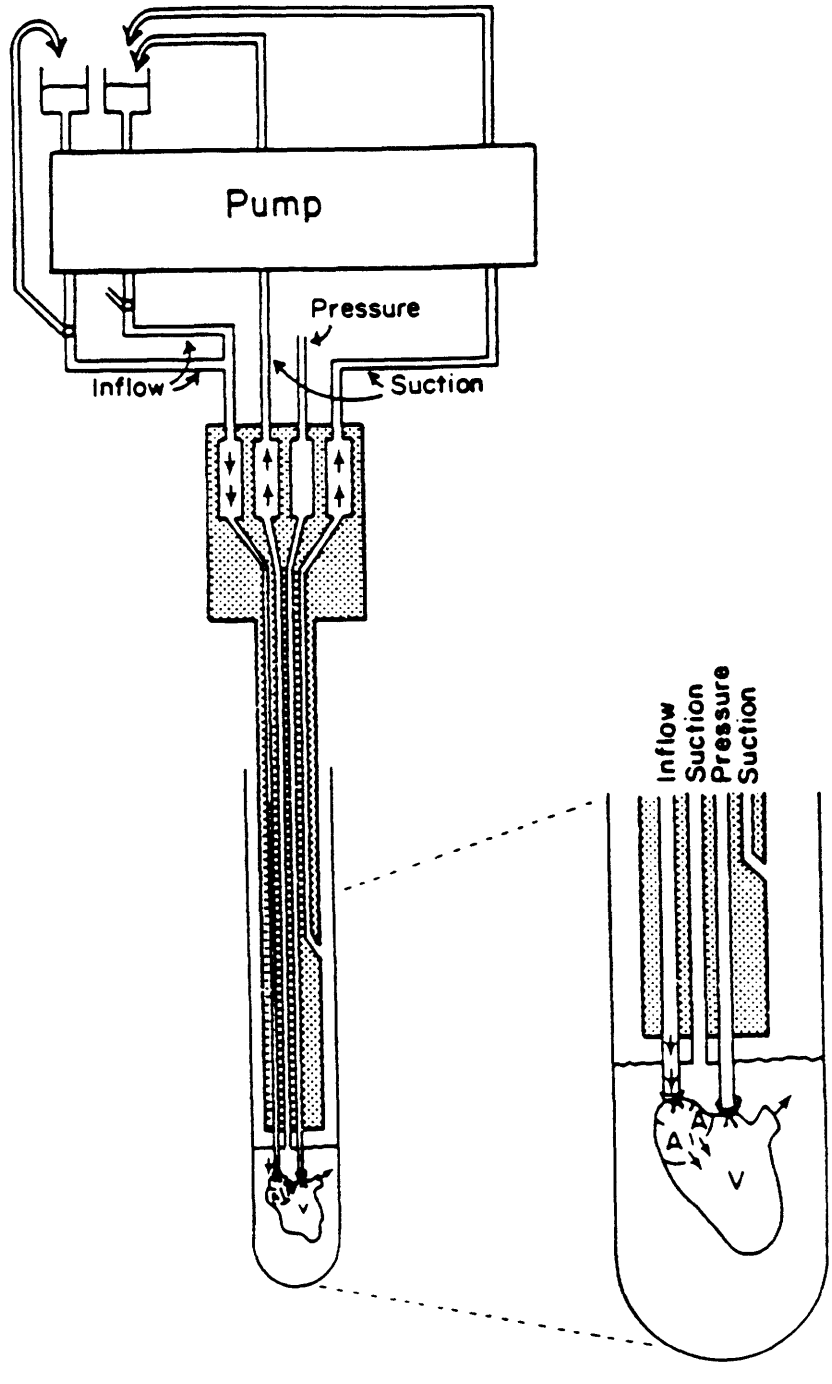

Figure 5-1 Schematic of the frog heart perfusion apparatus. See text for full description.

recirculated. The tubing from each reservoir flowed together at a Y-valve into a single perfusion line just before the plastic cannula, so that by using the three-way stopcocks, the buffer perfusing the heart could be changed without removing the heart from the magnet.

5.2.2. Rat hearts

Rats (Sprague-Dawley) were anesthetized with sodium pentobarbital by intraperitoneal injection. The heart was excised and placed in a dish of iced Krebs Henseleit solution. Within 3 minutes, the heart was cannulated at the aorta and perfused with Krebs Henseleit solution (Table 5-1) at room temperature. A Langendorff, isovolumic preparation was used. In this preparation, the buffer (the terms Krebs-Henseleit, perfusate, and buffer are used interchangeably) flows retrograde down the aorta and enters the coronary arteries at the aortic root, where it flows in the normal forward direction through the coronary vessels. The buffer then flows into the right atrial cavity where it goes to the right ventricle and out through the pulmonary arteries. The perfusion pressure was set to 100 cm of H_2O and determined the flow rate for rats, which varied between 7 and 28 ml/min for different hearts. The cannulated heart was mounted inside a 20 mm o.d. NMR tube and placed in the magnet.

The rat heart perfusion apparatus consisted of two reservoirs, a pump, a plastic cannula, and flexible tubing to connect the pump to the cannula. Again, the cannula contained four channels, one of which was used to contain the tubing through which perfusion fluid flowed, two of which were used as suction lines, and one of which contained the tubing

which was used to monitor the pressure and rate of the heart. One suction line could be positioned either above or below the heart, while the other suction line was fixed and served as a backup. A Latex balloon was connected to the pressure line and inserted into the left ventricle. The balloon was inflated to fill the ventricular cavity, thus creating the isovolumic condition for the perfused rat heart preparation. The fluid filled pressure line was connected to a pressure transducer and the pressure waveform and heart rate were monitored. The pressure waveform could be calibrated, but in all of these experiments, absolute measurements of the developed pressure were not required.

Fluid from each of the two reservoirs, which could be filled with different buffers, was pumped to an intermediate reservoir, the height of which determined the perfusion pressure. The output of each intermediate reservoir could go to the heart or back to the main reservoir. The tubing from each intermediate reservoir to the heart flowed together at a Y-valve to produce a single perfusion line to the heart. At any given time, the option of flowing to the heart was clamped off for one of the two reservoir systems. For the other system, the rate of flow from the intermediate reservoir to the heart was determined by the demands of the heart, while excess fluid provided by the pumps to the intermediate reservoir was recirculated back to the main reservoir. A flow meter was inserted in the main perfusion line to the heart to monitor the rate at which buffer was flowing to the heart. Filters were inserted in each reservoir system between the main reservoirs and the intermediate reservoirs. For each system, two filters in series were used with the

first filter being a glass microfibre type of pore size 2.7 μm (Whatman, GF/D) while the second filter was either a combination of another glass microfibre (Whatman, GF/D) and a membrane filter of pore size 5.0 μm (type MicronSep, Magna Nylon 66), or was simply another glass microfibre type. The membrane filter was not used with some shift reagent buffers because it appeared to cause a buildup of pressure behind the filter with consequent disruption of some tubing connections.

One of the spectroscopic studies (monitoring interstitial edema) involved alternating perfusion of the rat heart with normal buffer and with Krebs/SR buffer. Initial experiments revealed that after perfusion with the shift reagent buffer, reperfusion with normal Krebs Henseleit resulted in a drastic reduction of the flow rate. One possible explanation for this is that mixing of the two buffers can lead to precipitation, due to the free calcium present in the normal Krebs Henseleit and the $Dy(PPP)_2^{-7}$ and calcium present in the shift reagent buffer. By switching directly from perfusion with the shift reagent buffer to normal Krebs Henseleit, such mixing of the two solutions may occur in the perfusion lines and in the heart itself. For this reason a third buffer was prepared which was identical with Krebs with the exception that the calcium chloride concentration was only 0.3 mM. This low calcium buffer was then used for 30 seconds between perfusion with Krebs/SR and normal Krebs Henseleit. As described above, the apparatus was designed in such a way that the Krebs/SR and normal Krebs Henseleit buffers never mixed. The flow rate was then found to be unaffected by repeated alternation of normal Krebs Henseleit and Krebs/SR perfusion.

The low calcium buffer represented a third buffer which needed to flow into the heart in a single experiment. A third intermediate reservoir was therefore created in the perfusion apparatus. The reservoir was filled with buffer by hand (i.e. the pumps did not fill it). This reservoir was at the same height as the other intermediate reservoirs, and the outflow tubing from it joined the outflow tubing from either of the other two intermediate reservoirs, as needed.

After completion of perfusion experiments, the hearts (both frog and rat) were removed from the cannula apparatus, sliced into two halves to expose the ventricle(s), and blotted free of excess fluid for 30 seconds on paper towel. They were then placed into a clean 20 mm o.d. NMR tube and reinserted into the magnet for further measurements. The time elapsed from removal of the heart from the cannula to the beginning of further NMR measurements was never greater than 3 min.

The composition of the Ringer's buffer and the Krebs Henseleit buffer used in the frog and rat heart preparations respectively are listed in Table 5-1. Also listed are the shift reagent (SR) buffers used for frog (Ringer/SR) and rat (Krebs/SR) experiments and a low Ca^{++} buffer. Since EDTA chelates calcium, the concentration of free calcium for all buffers containing EDTA is decreased by the amount of EDTA present. For the low Ca^{++} buffer, the free calcium is estimated to be 0.25 mM or 0.125 mM.

Table 5-1
Composition of buffers

	Ringers	Ringers/SR	Krebs Henseleit	Krebs/SR	Low Ca^{++}
Na	120	120	144	144	144
K	4.8	4.8	5.9	5.9	5.9
Cl	125	95	116	86	84
Ca	1.8	1.8	1.75	3.5	0.75 or 0.625
Glucose	5.56	5.56	11.0	11.0	11.0
H_2PO_4	0.43	0.43	1.2	1.2	1.2
HPO_4	1.58	1.58	0	0	0
Mg	0	0	1.2	1.2	1.2
SO_4	0	0	1.2	1.2	1.2
EDTA	0	0	0.5	0.5	0.5
Pyruvate	0	0	10.0	10.0	10.0
HCO_3	0	0	25.0	25.0	25.0
$Dy(PPP)_2$	0	3.0	0	3.0	0
PPP_2	0	0.9	0	0.9	0

Values are mM. Calcium and $Dy(PPP)_2$ concentrations listed are the amount added to solution. Precipitation and filtering may have altered the final concentrations of these components.

5.3. Shift reagent

The shift reagent used in this work was dysprosium tripolyphosphate ($Dy(PPP)_2^{-7}$) (Gupta and Gupta, 1982). Stock solution of $Dy(PPP)_2^{-7}$ was prepared by adding 26 millimoles of the pentasodium salt of tripolyphosphate ($Na_5P_3O_{10}$, Sigma Chemical Co.) to 100 ml of distilled water. When this dissolved, 10 millimoles of dysprosium chloride ($DyCl_3 \cdot 6H_2O$, Alfa Products) were added. After this dissolved, the pH was adjusted to between 7.0 and 7.5 by addition of a small amount of 1.0 N HCl. The final concentration of $Dy(PPP)_2^{-7}$ in the stock solution was slightly less than 100mM. Note that the ratio of tipolyphosphate to dysprosium is greater than 2 to 1. This has been found to aid in dissolving the reagents in preparation of the stock solution (Burstein and Fossel, 1987c). Note also that the ratio of sodium to $Dy(PPP)_2^{-7}$ in the

stock solution is 13 to 1. This is taken into account when preparing the buffer solutions so as to maintain the desired sodium concentration in the buffer.

For frog heart experiments, the shift reagent buffer contained 3 mM $Dy(PPP)_2^{-7}$, with the concentration of other ions as listed in Table 5-1. For rat heart experiments, the concentration of $Dy(PPP)_2^{-7}$ was also 3 mM, but additional $CaCl_2$ was added to bring the concentration of calcium to 3.5 mM. This was done because $Dy(PPP)_2^{-7}$ is expected to chelate calcium and additional calcium can partially compensate for this. When preparing this shift reagent buffer, calcium chloride was the last component added, but the addition of calcium caused the buffer to become somewhat cloudy even after stirring. The buffer was therefore filtered twice (Nalgene, #2 qualitative) before placing it into the perfusion apparatus.

5.4. Spectroscopy

The goal of the spectroscopy experiments was to characterize interstitial sodium relaxation times during control conditions and during pathologic conditions. In performing these measurements, the challenge was to separate the interstitial sodium signal from the sodium signal of the bath and intracellular compartments. For the control case both interstitial T_1 and T_2 were investigated by the methods described in section 5.4.1.

For experiments involving pathologic interventions, only the fast component of T_2 decay was studied. Characterization of the fast component

of T_2 decay, as opposed to characterization of T_1 and the entire T_2 relaxation behavior of interstitial sodium, was pursued during pathologic studies for two reasons. First, as discussed in the chapter on previous work, the fast component of T_2 decay is the primary feature of sodium relaxation which may contain compartmental or diagnostically useful information, and many of these previous studies have been performed on pathologic tissue. Second, quantification of the fast component of T_2 decay requires less time than the complete relaxation time characterization, enabling more rapid monitoring of changes in the signal during pathology. Therefore, the fast component of T_2 decay was characterized during two pathologic interventions in perfused hearts, global ischemia and extracellular edema. The pulse sequences and methods used for characterizing the fast T_2 decay in pathologic states are described in section 5.4.2.

The sodium spectroscopy relaxation experiments were all performed at room temperature on a Bruker 360 AM wide-bore, vertical-bore spectrometer (Bruker Instruments Inc., Billerica, MA) operating at 95.262 MHz for sodium-23. A broad-banded 20 mm probe was used for the sodium measurements. The typical 90^{o} pulse width for sodium measurements was 30 μs.

5.4.1. Interstitial Relaxation Time Measurements

In order to determine the relaxation characteristics of interstitial sodium, signal from intracellular and bath sodium had to be taken into account. The method described below was utilized to eliminate the bath

signal based on its relaxation times; the remaining (cardiac) signal is due to the intracellular and interstitial sodium. Note that cardiac signal obtained in this fashion refers to cardiac sodium which has relaxation times different than those of the bath sodium (see Discussion). Quantification of the effect of the intracellular sodium signal on the relaxation characteristics of the cardiac signal is described below.

Pulse sequence

To measure cardiac relaxation times, the following pulse sequence was used:

$$180^{*} - ID - 90^{o} - \frac{TE}{2} - 180^{o} - \frac{TE}{2} - AQ \qquad (5\text{-}1)$$

where 180^{*} represents a composite inverting pulse (Freeman et. al., 1980), ID is an inversion delay, TE is the echo time, and AQ is acquisition of the signal. The repetition rate (or TR) used for the pulse sequence was 250 ms. A composite 180^{o} inverting pulse was used instead of a simple 180^{o} pulse in order to reduce the effects of spatial inhomogeneity in the magnitude of the inverting pulse. This sequence is an inversion pulse followed by a delay and then a standard Hahn spin echo pulse sequence. It has been applied to other multicompartment systems for the purpose of separation of the signals arising from each compartment on the basis of relaxation times (Patt and Sykes, 1972; Eisenstadt, 1980). It will be called the Inversion Hahn Echo (IHE) sequence.

By setting ID (or TE) at a given value and varying TE (or ID), the

IHE sequence was run under 3 condititons (described as separate experiments) in order to obtain data which emphasized cardiac T_1 and T_2 decay. The data from these 3 experiments constituted a single data set whose analysis is described later. The experiments, along with the ID and TE values used for each were:

1) T_2 measurement with bath signal eliminated based on its T_1; ID = t' with t' chosen to null the bath signal (and any signal with T_1 similar to bath), vary TE

2) T_1 measurement of total perfused heart system; vary ID, TE = 0.32 ms

3) T_2 measurement of total perfused heart system; no inverting pulse (equivalent to an ID of infinity), vary TE.

Experiments 1, 2, and 3 were performed in a cycled fashion such that a fraction of the signal averages required for experiment 1 was accumulated, then fractions of the data for experiments 2 and 3 were obtained, then the second cycle consisting of another fraction of the averages for experiments 1, 2, and 3 was executed. Typically, 8 cycles were used. The purpose of this was to average small changes in temperature or the heart's condition which may occur during the course of the experiment. This was necessary to enable combination of the experiments into a single data set.

Experiment 1 provides information about the cardiac T_2 decay. If one

assumes that the cardiac sodium has a component with a T_1 less than that of the bath, then, as described in Fig. 5-2, it is possible to choose ID such that bath signal is greatly reduced in magnitude. If a Hahn spin

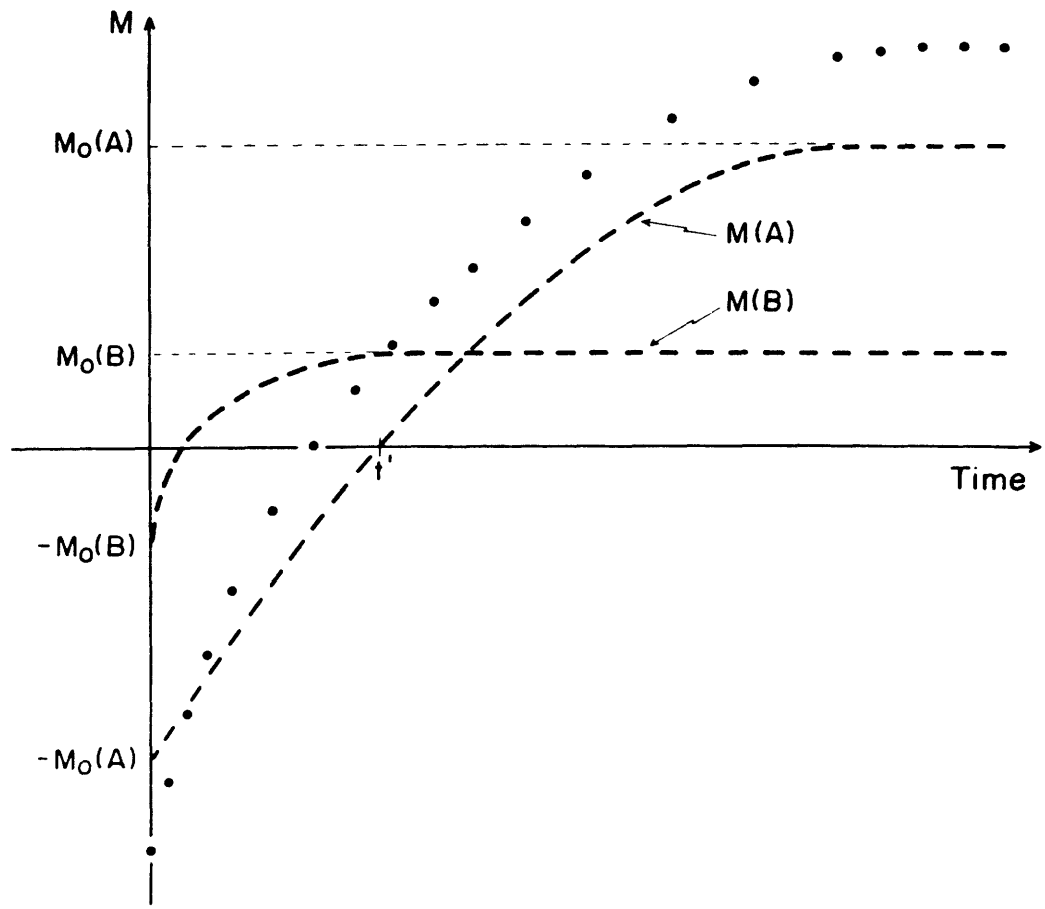

Figure 5-2 Diagram illustrating the application of the Inversion Hahn Echo pulse sequence to the elimination of bath signal. Component labelled M(A) represents the T_1 recovery curve of the bath sodium, with a large amount of signal and a long T_1 time constant. Component M(B) has less signal and a shorter T_1 value and represents the possible behavior of a component of the cardiac signal. Dots are the sum of these two curves. Observation of the signal at the time labelled t' will enable selective detection of the signal from compartment B, because the signal from compartment A is nulled at this point. A Hahn spin-echo sequence which begins at time t' will therefore enable the measurement of T_2 for component B.

echo experiment begins at this ID time, then the T_2 data obtained is predominantly due to any components having a short T_1. By fixing ID to this value and varying TE, information on the T_2 decay of cardiac signal which has a T_1 shorter than that of the bath sodium can be obtained. Since the signal cancellation is not perfect (due to imperfect knowledge of t'), the T_2 time constants reported here were determined from the total fit of all three experiments as described below and not from experiment 1 alone; however, similar results for cardiac T_2 were obtained if the data from only experiment 1 were analyzed.

Determination of the optimal value for t' was done by two methods: 1) the T_1 time constant of the bath sodium was determined in a separate experiment involving perfusate alone; and 2) using the IHE pulse sequence, the signal at ID values near t' and a long TE value (TE = 84 ms) was measured for each perfused heart preparation. As the bath possesses the longest T_2 value, the signal at a long TE value is assumed to be dominated by the bath sodium. The ID value which eliminated this signal provided an estimate of the t' which nulls the bath signal.

Experiment 2 measures the T_1 recovery curve for the entire perfused heart system. It utilizes the IHE pulse sequence with multiple ID values and a fixed echo time of 0.32 ms. The T_1 recovery curve of experiment 2 provides information about the T_1 of the cardiac signal by means of the multiparameter fit described below.

Experiment 3 is a T_2 determination of the entire perfused heart

system and uses a Hahn spin echo pulse sequence. No 180* inverting pulse is applied prior to the Hahn echo sequence, but note that this is equivalent to using the IHE pulse sequence with a very long ID value (an ID of 400 ms was used in the multiparameter fit described below). The purpose of experiment 3 is to provide information about the absolute magnitude of signal with a fast component of T_2 decay, and about the time constant of the slower component of T_2 decay for the multiparameter fit.

Data analysis

The equation which describes the data from an IHE pulse sequence for a compartment described by one T_1 value and one T_2 value, such as the bath, is

$$M_p = M_{op}(1 - Fe^{-\frac{ID}{a}})\, e^{-\frac{TE}{b}}. \qquad (5\text{-}2)$$

F represents [1 - cos(α)] where α is the precise flip angle from the initial 180* pulse, a is the T_1 value, b is the T_2 value, and M_{op} is the total magnitude of the signal with relaxation times a and b. ID and TE are the independent delay times defined above.

From visual inspection of the data from experiment 1, it was found that 2 time constants were needed to specify the T_2 decay of the cardiac signal. Cardiac T_1, in accord with previous findings for intracellular sodium and sodium in agarose gels, is expected to be adequately characterized by a single T_1 value. The equation which describes the data from an IHE pulse sequence for the cardiac component is then

$$M_i = M_{oi}\left(1 - Fe^{-\frac{ID}{c}}\right)\left(De^{-\frac{TE}{d}} + Ee^{-\frac{TE}{e}}\right). \qquad (5\text{-}3)$$

F is the same flip effect as before, c is the T_1 value, and D and E are the fractions of signals present at T_2 values d and e, respectively. The equation used to fit data from the entire perfused heart system, which includes both bath and cardiac contributions, is then the sum of the two equations, $M = M_p + M_i$.

The value of bath T_1 (parameter a) is approximately known and can be fixed before performing the fit. Bath T_1 was estimated from the temperature in the room and a calibration curve between perfusate T_1 and temperature. The uncertainty in this estimate of bath T_1 was judged to be ± 2 ms, and this uncertainty was included in the analysis by performing additional fits of the data with the bath T_1 fixed at the minimum and maximum values within this uncertainty. Bath T_2 was not fixed in the analysis because the flow of bathing solution affected the T_2 decay, making it difficult to quantify the actual T_2 time constant. Therefore, the equation $M = M_p + M_i$ contains 8 free parameters to be specified by 56 total data points obtained from experiments 1, 2, and 3.

Data analysis was performed by fitting integrals of the resonances to the sum of equations (5-2) and (5-3) for control hearts, and to equation (5-4) for pathologic hearts. A gradient expansion algorithm (Marquardt, 1963; Bevington, 1969) implemented in Basic on a personal computer was used for curve fitting. This allowed flexibility in specifying the form

of the non-linear equations which were used.

Effect of the intracellular signal

As stated earlier, the signal referred to as cardiac contains a contribution from both interstitial and intracellular ions. In order to determine the relaxation characteristics of interstitial ions, the intracellular sodium relaxation times and signal magnitude must be known. Intracellular relaxation times have been previously measured in perfused frog hearts using the addition of a shift reagent to the buffer (Burstein and Fossel, 1987a). The effect of doubling the concentration of shift reagent on the intracellular relaxation times was found to be negligible, indicating that the intracellular relaxation times are probably not altered due to susceptibility effects in perfused heart preparations (Burstein and Fossel, 1987a).

Since the intracellular relaxation times of rat hearts had not been determined, they were measured in 4 hearts in separate experiments. Krebs/SR buffer was utilized, and the intracellular signal magnitude (the integral of the unshifted resonance) was determined with a Hahn spin echo pulse sequence and 12 echo times ranging from 0.62 to 60 ms to determine intracellular T_2. Intracellular T_1 was measured with an inversion recovery pulse sequence and 10 ID values ranging from 1 to 400 ms (9 ID values less than 40 ms).

Following NMR experiments utilizing the IHE pulse sequence, which were performed during perfusion with a normal buffer, the magnitude of the

intracellular sodium signal was determined by perfusing several hearts with a buffer containing shift reagent. After 20 to 30 min of perfusion with the shift reagent buffer (either Ringers/SR or Krebs/SR depending on the heart type), the signal stabilized and NMR measurements of the intracellular magnitude were obtained. The hearts which were perfused with shift reagent were returned to normal perfusion before being removed from the perfusion apparatus.

Knowing the intracellular magnitude and relaxation times, the intracellular contribution to the cardiac measurements was subtracted to yield interstitial relaxation times. Comparison of these purely interstitial relaxation times with relaxation measurements of the cardiac signal revealed differences of less than 15% in the relaxation times of 3 frog and 2 rat hearts (see Results). This is due to the fact that the intracellular signal was found to have a magnitude which was a small fraction of the magnitude of the cardiac signal and had similar relaxation times. Therefore, the majority of the hearts did not receive shift reagent in the buffer due to the small error incurred by not correcting for intracellular signal, the time required for the shift reagent to completely wash in and out of the heart, and possible physiological effects of the shift reagent on measurements performed subsequent to addition of the shift reagent, such as the blotted heart measurements. Differences in these relaxation times from those of pure interstitium of 15% or less were deemed of minor importance due to the fact that the goal of these interstitial relaxation time measurements was not to obtain a high precision, but to report for the first time the general

characteristics of interstitial sodium relaxation.

Finally, NMR measurements of blotted heart tissue were performed. Magnitude, T_1, and T_2 measurements were done on this non-perfused heart tissue, with magnitude measurements being relative to the previous experiments where cardiac signal was obtained utilizing the IHE pulse sequence. T_1 measurements used an inversion recovery pulse sequence, while T_2 measurements used a Hahn spin echo pulse sequence. T_1 data from non-perfused heart tissue were fit to a single exponential recovery curve, while T_2 data were fit to a biexponential decay curve.

5.4.2. Fast component of T_2 decay during global ischemia and interstitial edema

The goal of the global ischemia experiment was to determine if the fast component of T_2 decay is affected by a severe pathology, and to characterize changes in the fast T_2 signal for this intervention in perfused hearts. The fast T_2 signal from the interstitial compartment was not distinguished from the intracellular signal for the global ischemia experiment because measuring intracellular signal requires the use of SR, and it is impossible to switch between normal buffer and a SR buffer when there is no flow to the heart. Thus subtraction of intracellular signal (obtained with SR perfusion) from cardiac signal (obtained with normal buffer perfusion) to yield interstitial signal was not possible during global ischemia. Cardiac signal in the presence of SR buffer is not representative of normal cardiac signal due to alteration of interstitial relaxation times by the SR. Also, determination of typical intracellular

changes during global ischemia with the use of $Dy(PPP)_2^{-7}$ on a separate series of hearts would not be reliable due to degradation of $Dy(PPP)_2^{-7}$ by membrane phosphatases (Boulanger and Vinay, 1989) which are probably more likely if the SR remains stationary in tissue for too long a period of time. The frequency separation of intra- and extracellular signals was indeed found to decay over time for one rat heart which contained Krebs/SR buffer just prior to stopping perfusion. After 3 hours, no compartmental signal separation was detectable.

The goal of the interstitial edema experiment was to determine if the amount of interstitial sodium signal with a fast component of T_2 decay was altered during interstitial edema. Since the amount of intracellular sodium signal with a fast component of T_2 decay has been shown to vary with pathology (Burstein and Fossel, 1987a), the possibility that the amount of fast T_2 signal in the interstitial space can vary would limit the capability of pulse sequences which emphasize the fast T_2 signal to attribute changes in NMR signal to a specific compartment in studies of pathology. By inducing interstitial edema, the amount of sodium in the interstitial space was increased without significantly altering the amount of sodium in the intracellular space, thus allowing the changes in relaxation behavior to be attributed to interstitial sodium. The constancy of intracellular sodium magnitudes and relaxation times during interstitial edema was verified with the use of SR as described below.

Three series of experiments for interstitial edema studies are described below. The first series alternated measurements of the total

myocardial fast component of T_2 decay (during perfusion with normal Krebs Henseleit buffer) with fast T_2 measurements of intracellular sodium (during perfusion with Krebs/SR buffer). The second series tested possible effects of the SR buffer on interstitial measurements by monitoring the total myocardial fast T_2 decay without use of SR. The third series examined a specific aspect of the SR buffer, namely the low levels of free calcium in the SR buffer, by performing the same experiment as in series one, but with a low calcium buffer substituted for the Krebs/SR buffer.

Pulse sequence and data analysis

For measurements of T_2 relaxation in pathologic states, a Hahn spin echo pulse sequence with 18 or 27 data points consisting of echo times between 0.32 and 90 ms was used. The experimental dead time was 0.12 ms, which is included as part of the echo time. The recycle delay was 250 ms, 128 or 256 averages were collected for each data point, and the entire T^2 measurement required 15 to 35 minutes.

The T_2 decay of sodium signal arising from the perfused heart preparation can be characterized using the equation

$$M = M_f e^{-\frac{TE}{T_{2f}}} + M_s e^{-\frac{TE}{T_{2s}}}. \qquad (5\text{-}4)$$

M represents the magnitude of the signal acquired, T_{2f} refers to the fast time constant with magnitude M_f, T_{2s} refers to the slow time constant with magnitude M_s, and TE is the echo time. The M_f and T_{2f} parameters are of

primary interest as discussed above, while the M_s and T_{2s} parameters are expected to contain a contribution from the perfusate buffer and are therefore less useful.

When using Eq. (5-4) to determine M_f and the other parameters, one must know the accuracy to which each parameter can be determined in order to know if any change in a given value is significant. In addition to the error estimate returned by the fitting algorithm (Marquardt, 1963; Bevington, 1969), an additional evaluation of the error of each parameter was undertaken by creating simulated data with characteristics similar to those obtained from actual T_2 measurements on the perfused heart system. Random noise with a Gaussian magnitude distribution was added to the simulated data. The standard deviation of the noise added was similar to the estimate of uncertainty of signal magnitudes present in actual T_2 measurements. Six different parameter sets were used to create the simulated data, and each parameter set had different ratios of T_{2f} to T_{2s} and M_f to M_s. The ratios were chosen to correspond to the range of data observed in numerous experiments on perfused heart under control and pathologic conditions. The goal was to determine the error in measurements of M_f and T_{2f} for relaxation curves of varying characteristics. M_f was fixed to 10 (arbitrary units) and T_{2s} was fixed to 30 ms for each parameter set. M_s was set to either 110, 180, or 250 (same units as for M_f), and T_{2f} was set to either 2 ms or 5 ms. Ten sets of simulated data with random noise were created for each parameter set, and the simulated data was analyzed according to equation (5-4). Each data set created used the same 27 TE values as were utilized in T_2

determinations on perfused hearts.

One possible error not accounted for by the analysis of simulated data presented above was the possibility that T_2 data from the heart contained 3 or more time constants, but was being fit to 2 time constants due to S/N limitations and similarity of some of the time constants. M_f and T_{2f} are less well defined in this case, and may be affected by changes in magnitudes or time constants of the slower relaxation time components, even if the magnitude and time constant of the fastest relaxation time component is unchanged. To test this possibility, simulated data using 9 parameter sets were created, each with 3 time constants. The sets are listed in Table 5-2, and are presented in 3 groups of 3 (set numbers 1 to 3, 4 to 6, and 7 to 9; see below). Within each group of parameter sets, M_{sb} was varied because it is partially derived from the bath signal, which can vary a great deal in magnitude, and may also be partially derived from T_2 components of interstitial sodium which have long time constants. The variation in M_{sb} was chosen to be similar to variations in the magnitude of signal with a slow component of T_2 decay which occured during control and pathologic conditions in perfused hearts. Biexponential fits according to (5-4) were performed on data produced using these 9 parameter sets to determine the dependence of fitted parameters M_f and T_{2f} on changes in the simulated parameters for the slower time constants of a 3 time constant parameter set. Noise was not added to the data created. Each data set created used the same 27 TE values as were utilized in T_2 determinations on perfused hearts.

Table 5-2
Three component parameter sets

Set #	1	2	3
M_f	10	10	10
T_{2f} (ms)	2	2	2
M_{sa}	15	15	15
T_{2sa} (ms)	25	25	25
M_{sb}	95	165	235
T_{2sb} (ms)	33	33	33

Set #	4	5	6
M_f	10	10	10
T_{2f} (ms)	2	2	2
M_{sa}	90	90	90
T_{2sa} (ms)	25	25	25
M_{sb}	20	90	160
T_{2sb} (ms)	35	35	35

Set #	7	8	9
M_f	10	10	10
T_{2f} (ms)	2	2	2
M_{sa}	90	90	90
T_{2sa} (ms)	20	20	20
M_{sb}	20	90	160
T_{2sb} (ms)	40	40	40

The group of parameter sets 1 to 3 was chosen to simulate the 3 T_2 relaxation time components actually obtained from the IHE pulse sequence applied to rat hearts. The correspondence between parameters of Table 5-2 for this group and parameters of the fit to the IHE sequence (section 5.4.1.), respectively, is as follows: $M_f = M_{oi}*D$, $T_{2f} = d$, $M_{sa} = M_{oi}*E$, $T_{2sa} = e$, $M_{sb} = M_{op}$, and $T_{2sb} = b$. Parameter sets 4 to 6 were chosen to have a larger contribution from the middle relaxation time component, M_{sa}. This group was chosen in case the IHE pulse sequence causes an under-representation of the magnitude of myocardial signal with the slower T_2 time constant (parameter M_{sa}). The time constants for sets 4 to 6 were chosen because they produced biexponential fits to the parameter set which were similar to T_2 data actually obtained from perfused rat hearts.

Parameter sets 7 to 9 were chosen to be similar to sets 4 to 6, except the difference in the 2 slower time constants was greater.

Global ischemia experiment

Global ischemia was induced by stopping the flow of all perfusate to the heart by placing a clamp on the perfusion line to the heart. A T_2 measurement was obtained for each heart before global ischemia was induced during a period of 40 min to 80 min of perfusion with normal Krebs Henseleit. Additional T_2 measurements were then performed at 25 min to 200 min following initiation of global ischemia. All of the T_2 data was biexponential in nature as determined by non-linearity on semilogarithmic plots and was therefore characterized using Eq. (5-4).

Interstitial edema experiment

Based on previous work on compartmental volumes in perfused rat hearts, the method of induction of interstitial edema will be to maintain the perfusion for several hours or more. The perfusion pressure of 100 cm H_2O should be sufficient to induce edema since the perfusing media, Krebs Henseleit buffer, is lacking in vascular osmotic factors such as large proteins. Comparison of relaxation measurements taken soon after initiating perfusion with measurements taken following several hours of perfusion should enable comparison of the sodium relaxation times of the heart under varying degrees of interstitial edema.

Since the purpose of studies performed on hearts experiencing interstitial edema is to quantify changes in the fast component of T_2

decay of the interstitial space, it is necessary to quantify and subtract the contribution of intracellular sodium to the total fast T_2 sodium signal in order to obtain interstitial fast T_2 data. This is done by the use of the shift reagent $Dy(PPP)_2^{-7}$.

The first series of experiments in the interstitial edema studies (n = 3 hearts) underwent the following series of measurements. Initial T_2 measurements were obtained during a period of 40 min to 80 min perfusion with normal Krebs. Then, following initiation of perfusion with shift reagent buffer, a period of time between 10 and 20 minutes was spent waiting for the resonances to establish a stable position. Then, a T_2 measurement of the unshifted intracellular resonance was performed. For these intracellular T_2 measurements, 12 data points with echo times between 0.32 and 80 ms were used. The recycle delay was again 250 ms and 256 averages were obtained, requiring about 15 minutes for the T_2 measurement. The sequence of NMR measurements then consists of alternating T_2 measurements performed during perfusion with normal Krebs with intracellular measurements performed during perfusion with shift reagent buffer. This process continued for up to 3 Krebs/Shift reagent cycles requiring 3 to 6 hours.

For the second series of hearts in the interstitial edema experiment (n=4), relaxation measurements were obtained early in the course of perfusion and after several hours of perfusion without using shift reagent at all during this time. The final measurement performed on 2 of these hearts was obtained during perfusion with shift reagent to gain

information on the intracellular sodium contribution in the previous measurements.

The third series tested the possibility that the low levels of free calcium in the SR buffer affected the fast component of interstitial T_2 decay. The value of Mf was monitored in two hearts perfused with alternating normal and low calcium buffers, with timing similar to the procedure used for alternating normal and shift reagent buffers of the first series of interstitial edema experiments. The low calcium buffer had no shift reagent and estimated free calcium concentrations of 0.25 mM for one heart and 0.125 mM for the other heart.

All of the T_2 data from the interstitial edema experiment was biexponential in nature as determined by non-linearity on semilogarithmic plots and was therefore characterized using equation (5-4).

5.5 Sodium imaging

The procedure for sodium imaging experiments was to obtain a sodium image at a short (1.6 to 2.4 ms) and a long (20 to 25 ms) echo time. Images during control conditions, and after inducing a pathologic state were obtained. The pathologic states studied include interstitial edema, global ischemia and global ischemia followed by reperfusion, coronary occlusion, low-flow and low-flow followed by reflow, and ouabain toxicity. For all hearts, proton images were also obtained to determine the specific anatomy and orientation of each perfused heart. For some hearts, a perfusion image (described below) or a ^{31}P spectrum was also obtained.

By obtaining sodium images at both short and long echo times, information about the sodium signal magnitude and relaxation characteristics was obtained which was unavailable from spectroscopic studies. The intensity of the signal on the short echo time image provided data on the myocardial sodium density. Sodium density refers to a volume average of sodium signal, as opposed to the total sodium signal obtained in a spectroscopic experiment. Due to the presence of multiple sodium compartments with differing sodium concentrations in tissue, the sodium density and total sodium signal change by differing percentages when the sodium content of just one compartment or the other is altered (see Theory). Differences between the sodium imaging intensity at the short echo time and the total myocardial sodium density, which is of more interest, are presented below.

Comparison of the sodium intensities at the two different echo times should aid in determining the relaxation characteristics of the myocardium. In particular, imaging should enable study of the slower components of T_2 decay, namely those relaxation components which are not grouped with the fast component of T_2 decay (time constant of around 2 ms) on data analyses. Study of the slow T_2 was not possible in a spectroscopy experiment since signal arising from myocardium could not be distinguished from signal arising from bathing solution, both of which have a slow T_2 decay. Also, comparison of the sodium intensities at the two echo times should enable determination of the density of the fast component of T_2 decay by subtracting the image intensity at the long echo time from the image intensity of the short echo time. This information differs from

spectroscopic fast T_2 data in that it provides fast T_2 densities instead of total fast T_2 magnitude.

The imaging experiments were performed on either the 360 AM spectrometer (operating at 95.262 MHz for sodium) or on a 4.7 Tesla 30 cm bore Bruker BIOSPEC (operating at 52.93 MHz for sodium). Both were equipped with a microimaging accessory consisting of 5 cm gradient coils. Both magnets were also used for proton imaging, operating at 360.14 MHz for the 360 AM and at 200.25 MHz for the BIOSPEC. The radiofrequency coils used in the microimaging accessory of each magnet were dual coils tuned to sodium and protons. Spectra of phosphorous-31 were obtained using the 360 AM (^{31}P resonant frequency of 145.789 MHz) with the microimaging accessory and dual radiofrequency coils tuned to phosphorous and protons.

5.5.1. Imaging pulse sequences

A Hahn spin echo sequence was used for all sodium images, and images were obtained at a short (1.6 or 2.4 ms) and a long (20 or 25 ms) echo time for each experiment. A selective 90^{o} excitation pulse and a non-selective 180^{o} refocussing pulse were utilized. For sodium images, a repetition time of 100 ms, a 128x64 matrix, and 100, 200, or 400 averages were utilized requiring 13 to 50 minutes for data acquisition. The receiver bandwidth for sodium images was 20 kHz for the majority of the experiments. Early sodium images were obtained with a receiver bandwidth of 50 kHz or 25 kHz. The field of view was 4, 5, or 6 cm, and slice thickness was 7 or 8 mm.

Proton images were obtained with a gradient echo pulse sequence using a repetition time of 5.2 ms and an echo time of 1.6 ms. The matrix was 128x64, 1 average was used, and the image was obtained in approximately 350 ms. For the experiment when a coronary artery was occluded, a perfusion image was obtained. For this, the region of myocardium supplied by the occluded artery was observed by imaging the distribution of a magnetic resonance contrast agent in the perfused regions of the heart (Atkinson et. al., 1990). For some hearts which experienced global ischemia, ^{31}P spectra were obtained using a repetition time of 3 sec, an excitation pulse with a flip angle of about 60^{o}, and 256 averages. The ^{31}P spectrum enabled monitoring the ratio of high energy phosphates (ATP) to low energy phosphates (inorganic phosphates).

5.5.2. Limitations of sodium imaging methods

The image acquired with an echo time of 1.6 to 2.4 ms does not acquire all of the sodium signal with a fast T_2 time constant. A 2 ms echo time will acquire only 37% of the full magnitude of signal which has a 2 ms T_2. Thus the image at a short echo time does not provide a measure of the total myocardial sodium density, but rather reveals the image intensity at the shortest echo time obtainable with the methods and hardware utilized in this work (see below). The difference between this image and the true sodium density depends on the amount of signal with a fast T_2 time constant. Further discussion of this difference for the perfused heart preparation is presented later (see Discussion).

The primary limiting factors for producing the shortest possible

echo time are the time required to produce the initial selective pulse and the time required for the gradients to attain the specified amplitude. The echo time for the Hahn spin echo sequence employed in this study is determined by

$$TE/2 = d90^{o}/2 + dG + d180^{o}/2$$

where TE/2 is half the echo time, $d90^{o}$ is the duration of the selective 90^{o} pulse, dG is the time required for the gradients to rise to desired amplitude for the desired encoding period and then to return to zero, and $d180^{o}$ is the duration of the non-selective 180^{o} refocussing pulse. Substituting in the respective values used to obtain the 1.6 ms echo time, one obtaines

$$TE/2 = 0.35 \text{ ms} + 0.4 \text{ ms} + 0.05 \text{ ms} = 0.8 \text{ ms}.$$

Maximal power was used for the selective pulse, and the duration was 0.7 ms. The 180^{o} pulse duration above is for a simple 180^{o} pulse. Later experiments utilized a composite 180^{o} pulse (Freeman et. al., 1980) of twice the duration to eliminate "edge effects" caused by inhomogeneous RF fields produced near the RF coil. Shorter echo times could probably be obtained by shortening the initial selective pulse (use less than a 90^{o} pulse or increase the power of the radiofrequency amplifiers) or by allowing less time for the gradients to stay at the desired amplitude. The latter alternative would require higher gradient power in order to provide the same encoding effect. This is feasible since the full power

of the gradient amplifiers was not used in the imaging sequences employed here.

The primary limitation of shorter duration gradient pulses is that the gradient used during data acquisition must be at a stable value in order for the frequency-to-spatial-location correspondence to be maintained in the first dimension of an image. Also, the gradient amplitudes produced for one of the gradients (the phase encoding gradient, which specifies spatial information in the second dimension of an image) are varied in several discrete steps to obtain an image. With very short duration gradient pulses, the gradient amplitudes actually produced may not be linearly related to the amplitudes specified, which could produce distortions or artifacts in the image since the processing algorithm expects linear steps for the phase encoding gradient.

An alternative to shorter duration gradient pulses is to utilize a pulse sequence which selects a slice with a combination of selective pulses before the 90^{o} excitation pulse (to affect all volumes which are not to be imaged) and a non-selective 90^{o} excitation pulse (Perman et. al., 1989). The non-selective pulse is shorter in duration, which enables a shorter echo time.

Choice of the longer echo time of 20 to 25 ms was based on S/N considerations. In general, as the echo time is lengthened, the image is more strongly weighted for signal with slow relaxation times. However, at longer echo times the signal intensity, and thus the S/N, is lower. The

echo time of 20 to 25 ms was chosen to be as long as possible while still providing sufficient S/N to visualize the perfused heart.

Initially, the images were obtained in a serial fashion--i.e. an image at the shorter echo time was acquired, then an image at the longer echo time was acquired, etc. Since a typical image requires 25 minutes, this procedure may produce some difficulty in comparing the images from different echo times due to the potential for changes in the heart's condition to occur between the center time of subsequent image acquisitions. Later experiments (heart numbers 3, 5, and 9 of Table 6-9 in Results) were performed so that the short and long echo images were acquired "simultaneously" (fractions of the total number of averages for one image were interleaved with fractions of the total averages for the other image) so as to avoid this potential difficulty.

5.5.3. Noise evaluation and reduction

Since sodium imaging suffers from a low S/N, any reduction in the noise level would improve the quality of information obtained from a sodium image. Therefore, efforts were made to analyze the sources of noise in the system. Methods to reduce the noise level were then suggested and, when possible, implemented. All of this work was performed on the 360 AM, since that system was used for most of the imaging work and had the most problems with S/N.

The spectral characteristics of the noise were evaluated by acquiring data with no excitation pulse, and using a wide receiver

bandwidth of 100 kHz. The spectrometer was configured as if a sodium image were going to be acquired, which means that the microimaging probe was inserted and preamplifiers and gradient amplifiers were connected to the probe. A Fourier transform of this data revealed the spectral content of the noise, shown in Fig. 5-3. The center of this spectrum is 95.262 MHz, the resonant frequency for sodium for the 360 AM. Two large noise sources are observed, one at 95.3 MHz, and a broad one at 95.225 MHz. (The noise source at 95.225 MHz is believed to be related to the 95.3 MHz noise source. The difference between 95.225 MHz and the center frequency of 95.262 MHz is the same as the difference between 95.3 MHz and the center frequency. This mirroring about the center frequency is maintained when the center frequency is changed slightly. Also, when a narrow receiver bandwidth (e.g. 5 kHz) is used to obtain a noise spectrum, much more noise is present at 95.3 MHz than at 95.225 MHz.) When a receiver bandwidth of 20 kHz centered around 95.262 MHz is used for the imaging studies, the contribution of noise from the background level as well as the major noise sources is significant. Not observeable on this noise

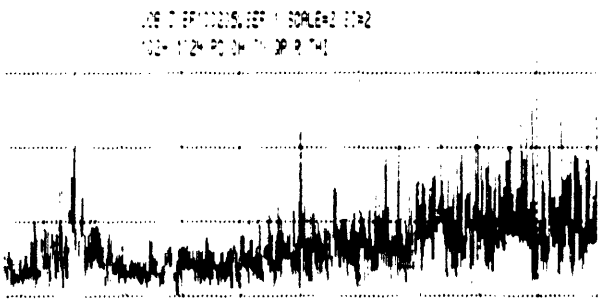

Figure 5-3 Spectrum of noise near the sodium resonance frequency for 360 AM spectrometer (magnetic field of 8.46 T). The center of the spectrum is 95.262 MHz, and the width of the spectrum is 100 kHz. The characteristics of this spectrum are discussed in the text.

spectrum is the fact that other frequencies near the sodium reference (e.g. 95.1 MHz) contain significantly less noise. Changing the field of the magnet slightly would change the sodium resonant frequency and would enable one to operate in a frequency regime which is more favorable to sodium imaging. However, the field strength of a superconducting magnet cannot be easily varied. Therefore, the field would need to be left at the new value for all studies. This would present two difficulties. One is that the resonant frequency of all other nuclei would be changed, which would affect other users of the system. The other is that certain electronic circuits, especially circuits which enable frequency locking on a deuterium signal, are fixed frequency circuits from the manufacturer.

Further analysis of the noise was undertaken by determining the amount of noise generated by each component of the spectrometer system. This is done by connecting each component of the system in stages, and determining the additional noise generated by each stage. This series of spectra, along with spectra obtained utilizing the noise reduction techniques discussed below, are presented in Fig. 5-4. It is clear that most stages of the system contribute an additional noise component, with a significant contribution arising from the gradient cables.

Three primary means were utilized to reduce the noise. The first method discovered was simply to provide a good connection at both ends of the preamplifier-probe cable. Triple shielded cables are customarily used with this magnet, but the ground connection at each end appears to be less than ideal. By taping the cable to a fixed object (such as the base of

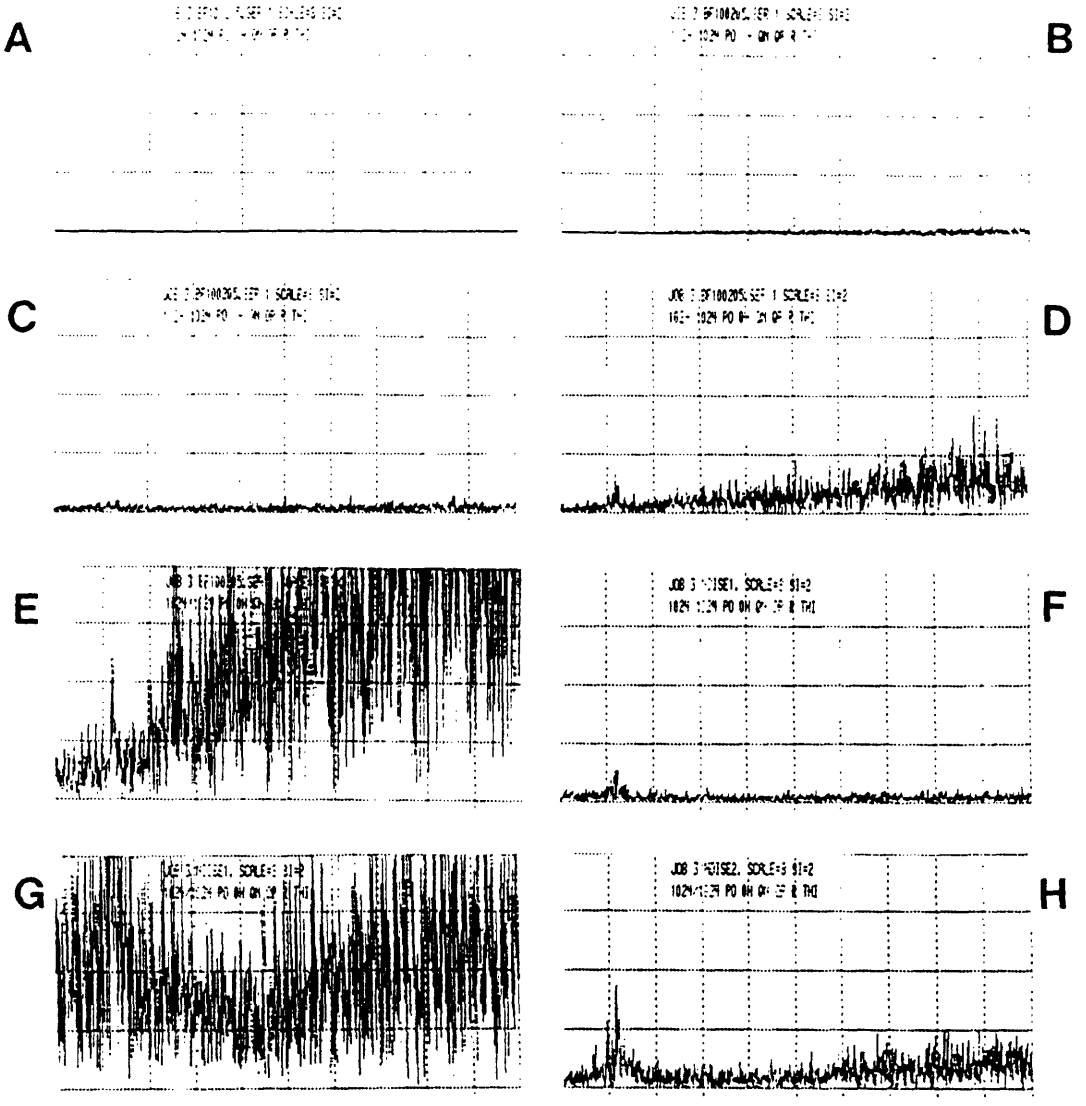

Figure 5-4 Noise spectra obtained with various hardware connections. Each successive spectrum has an additional connection compared to previous spectrum: (A) spectrometer console alone; (B) cable from console to preamplifier (console-preamp cable) connected to console but not to preamplifier; (C) console-preamp cable connected to preamplifier, but preamp-probe cable not connected to preamplifier (50 Ω resistor attached to preamplifier in place of preamp-probe cable); (D) preamp-probe cable connected to preamplifier, but not to probe (preamp-probe cable terminated with 50 Ω resistor); (E) preamp-probe cable connected to microimaging probe; (F) preamp-probe cable "taped" so as to improve connection at both ends (see text); (G) gradient cables connected to probe; (H) RF filter inserted in gradient line (see text).

the magnet) in such a manner that a lateral force is applied at each end of the cable, the noise level can be significantly reduced in some circumstances.

A second factor which affects the noise is the placement of cables, metal objects and people in the room. As one moves about the room while observing the noise signal, fluctuations in the noise occur. Based on this, certain arrangements of cables and metal objects were found to result in lower noise levels. No specific arrangements were found to work every day. The most important factor was usually placement of the gradient cable. An aluminum ladder situated near the magnet helped on some days. Also noted was the importance of removing "extra" cables from the region near the bottom of the magnet.

The final approach to reducing noise was to place an RF filter in the gradient cable line. This filter is diagrammed in Fig. 5-5 and results in a substantial reduction of the noise arising from the gradient cable.

5.5.4. Sodium imaging experiments of pathologic states

Sodium imaging was conducted in the presence of several pathologic interventions. Global ischemia was induced by clamping the flow of perfusate to the heart. In some cases, the hearts were then reperfused by releasing the clamp after a 30 to 200 min duration of ischemia. Coronary occlusion was performed by passing a suture around tissue which included the left coronary artery. Low flow was induced by partial clamping of the

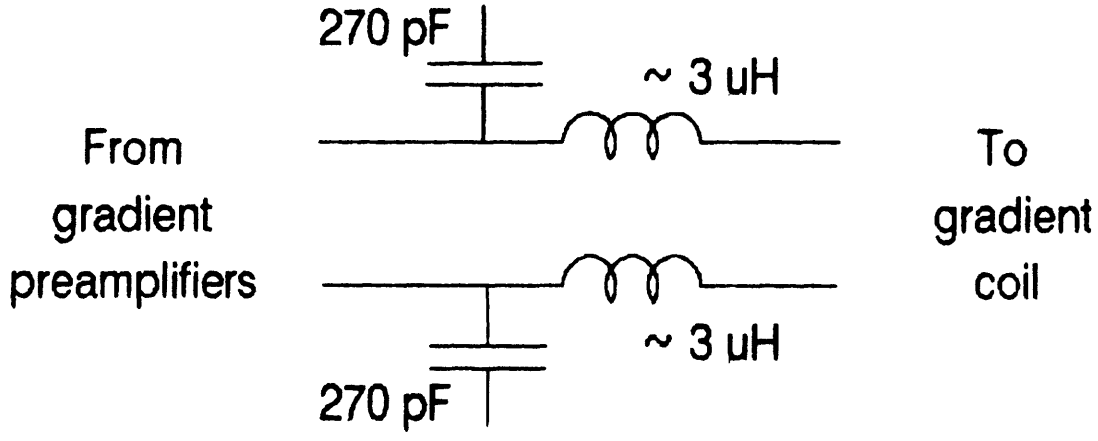

Figure 5-5 Electronic circuit to reduce contribution of radiofrequency noise of gradient cables to the signal detected in a sodium NMR experiment. This circuit is placed in-line with 1 gradient coil. Thus three such circuits are necessary--one each for x, y, and z gradients.

perfusion line, producing flow rates of about 5% of normal. Ouabain toxicity was achieved in rat hearts by adding ouabain to the perfusate buffer to achieve a concentration of 200 uM.

Initial sodium images at both short and long echo times were obtained from each heart during normal perfusion. Then following 60 to 120 min of normal perfusion, the pathologic intervention described above was implemented. Subsequent sodium images at both short and long echo times were obtained.

5.5.5. Quantification of image intensity

A sodium image intensity was obtained from each image in the following manner. The mean integral intensity was obtained at 6 to 8 spots over the heart tissue, taking care to avoid the right ventricular

cavity which had been located by previous proton images. Care was also taken to avoid sodium signal from the left ventricular cavity and from the exterior surface of the heart. However, since the sodium images of the perfused heart were not gated, some contamination from these sources was possible. The region of interest used for mean integral measurements was a circle or square of dimensions slightly less than the thickness of the wall of the heart. These 6 to 8 measurements were averaged to obtain the mean intensity over the region of the heart (MIOH) and the standard deviation of the 6 to 8 measurements was computed. The mean integral of the background intensity (MIB) was obtained by measurements over a large region of interest which did not include the heart. Since the images were magnitude only, the MIB was positive. This background signal will produce a positive contribution to the MIOH in images where the signal from the heart tissue is small (Henkelman, 1985). To correct this, the background intensity was accounted for via a numerical integration approach which assumed that the background signal had a gaussian distribution (Henkelman, 1985). The inputs to the numerical integration were the MIB and the MIOH, and the output was the image intensity actually due to the heart tissue itself (MIH). To determine if changes in MIH were significant, a t-test for independent data was applied using a significance level of 0.05.

6. RESULTS

6.1. Phantoms

The T_1 and T_2 values for sodium in both Ringers and Krebs Henseleit buffer were found to be equal with a value of 56 ms at room temperature. With small variations in room temperature of 24 ± 2°C, this relaxation time was found to vary by about ± 1.5 ms. The T_1 relaxation time of the phantom with Ringers flowing at a rate comparable to that in the perfused heart preparation (8 ml/min) was found to be the same as the T_1 with no flow. However, the T_2 of this phantom was found to be 15 ms shorter, presumably due to sodium movement within B_o inhomogeneities. The actual T_2 in the perfused heart preparations can be shorter than this due to the additional movement of the heart. Up to echo times of 100 ms, this T_2 decay was accurately characterized by a single exponential process. At greater echo times, the signal dropped off more rapidly than an exponential process would dictate, but this was not a problem as the maximum echo time used for T_2 measurements was 90 ms.

The IHE pulse sequence was applied to a phantom of 150 mM NaCl to determine if the pulse sequence produced artifactual signals or relaxation times. With ID fixed near the value which would completely cancel the sodium signal, the T_2 decay was measured and found to agree with the T_2 value obtained using a Hahn spin echo sequence. With TE fixed to a short value (0.32 ms), ID was varied to obtain a T_1 recovery curve, and the T_1 value obtained agreed with that found from an inversion recovery pulse sequence. Therefore, the IHE pulse sequence does not appear to produce artifacts in relaxation times under these conditions.

The agarose, when studied separately, was found to have sodium relaxation times of T_1 = 38.5 ± 0.3 ms (mean ± SD), and T_2 = 5.4 ± 0.3 ms (59.5 ± 2.5%) and 36.2 ± 2.3 ms (40.5 ± 2.5%). These values were determined by an inversion recovery pulse sequence for T_1 and by a Hahn spin echo sequence for T_2. When the IHE pulse sequence and 8 parameter fit was applied to the agarose + NaCl phantom, the relaxation times of agarose and the relative magnitudes of signal from NaCl solution and agarose agreed well with the value found in the separate experiments (n=2). The maximum difference in relaxation times between these values and the separately determined agarose values was 18%, while the maximum error in the estimate of the magnitude of agarose signal was at most 22%. The ID value which resulted in nulling of the signal from the NaCl solution was set in the same fashion for this phantom as it was for the perfused hearts, namely by monitoring the signal at long echo times while trying different ID values.

6.2. Spectroscopy

6.2.1. Interstitial relaxation time measurements

Physiologic response

Frog hearts perfused with Ringers solution beat steadily for up to 24 hours. Rat hearts perfused with Krebs Henseleit buffer beat steadily for 5 to 8 hours. The total duration of the interstitial relaxation experiment was approximately 4 hours.

When shift reagent buffer was used for intracellular measurements (after measurements of cardiac relaxation times were obtained while the

heart was perfused with normal buffer, see below), both the rate and force of contraction decreased during perfusion with the shift reagent, presumably due to the chelating of free calcium by the shift reagent. For frog hearts, the duration over which the beat was regular and detectable was not appreciably decreased by perfusion with shift reagent. For rat hearts the force of contraction decreased to approximately 10% of normal, and the duration over which its beat was detectable was reduced to about 2 hours. Experiments with shift reagent required 1 hour.

Relaxation time data for perfused hearts

Cardiac relaxation times were measured for 6 frog hearts during perfusion with Ringers. For rat hearts, 5 cardiac relaxation time measurements were performed on 3 rat hearts (two hearts were measured twice) during perfusion with Krebs Henseleit. A typical interstitial T_2 decay curve obtained from a frog heart using the IHE pulse sequence with the perfusate signal nulled (described as experiment #1 in the methods chapter) is shown in Fig. 6-1. The intracellular contribution, as determined by shift reagent experiments, has been subtracted from this curve in order to illustrate the fact that purely interstitial signal has a distinct biexponential behavior. The biexponential character of the interstitial decay, as seen by its non-linear character on the semilogarithmic plot, was apparent for every heart used in the experiments.

The cardiac relaxation time measurements are summarized in Table 6-1, and are expressed as mean ± SD. T_1 data was fit with a single

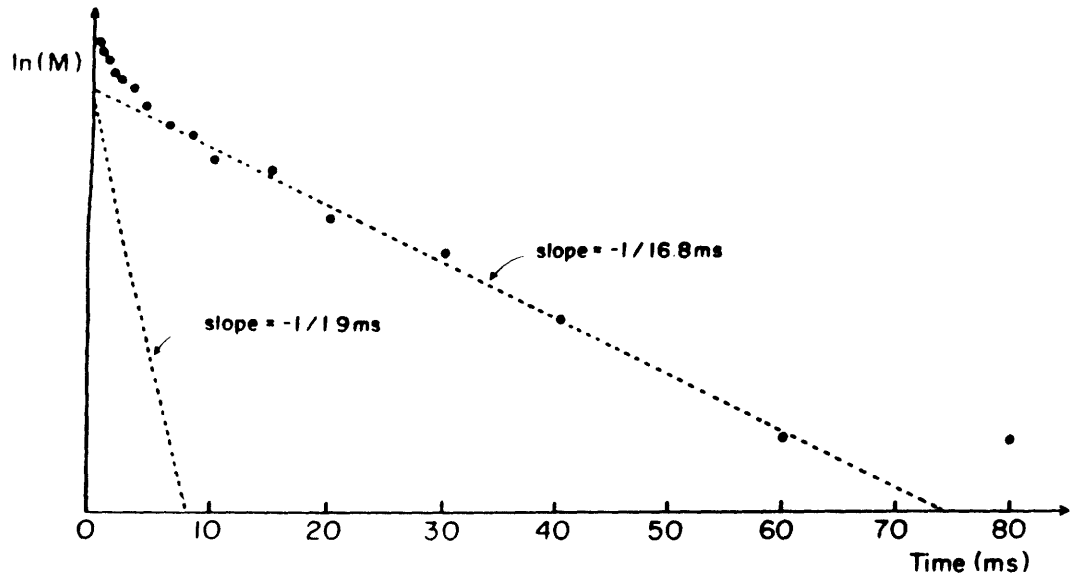

Figure 6-1 T_2 relaxation curve for interstitial sodium of a frog heart using the IHE pulse sequence. The intracellular signal as measured with shift reagent has been subtracted from the cardiac signal to produce this interstitial data. The magnitude of the subtracted intracellular signal was equal to 10% of the cardiac magnitude. The T_2 time constants of the subtracted signal were 2 ms (50%) and 16 ms (50%).

Table 6-1
Cardiac Sodium Relaxation Times in Perfused Hearts

	Frog	Rat
n	6	5
T_1(ms)	31.6 ± 3.0	27.3 ± 1.6
$\%T_{2f}$	37.2 ± 7.4	42.2 ± 4.7
T_{2f}(ms)	1.9 ± 1.0	2.1 ± 0.3
$\%T_{2s}$	62.8 ± 7.4	57.8 ± 4.7
T_{2s}(ms)	25.2 ± 1.3	26.3 ± 3.2

exponential time constant, while T_2 was fit with two time constants, designated fast (f) and slow (s) with relative amplitudes of $\%T_{2f}$ and $\%T_{2s}$. The data was also analyzed assuming possible variations in bath T_1 as discussed earlier. The possible range of the mean cardiac T_1 was found

to be 29.1 ms to 33.6 ms for frog hearts and 24.3 ms to 29.9 ms for rat hearts. The possible range of the mean cardiac fast T_2 values was found to be 1.8 ms to 2.1 ms for frog hearts and 2.0 ms to 2.2 ms for rat hearts, while for the cardiac slow T_2 values the range was 21.0 to 26.6 for frog hearts and 20.1 to 28.2 ms for rat hearts.

Table 6-2 and Table 6-3 list the small effect intracellular sodium signal has on combined interstitial and intracellular relaxation times of frog and rat hearts. The cardiac relaxation times were obtained from the 8 parameter fit of the raw data. The intracellular magnitude was obtained during perfusion with shift reagent, while the intracellular relaxation times were characterized previously in frog hearts (Burstein and Fossel, 1987a), and were measured in separate experiments on 4 hearts for rats. The purely interstitial relaxation times were obtained by the 8 parameter fit of the data after the intracellular contribution had been subtracted from the raw data. These values illustrate the validity of using the

Table 6-2
Comparison of magnitudes and relaxation times of total cardiac, intracellular, and interstitial compartments
Frog Hearts (n=3)

	Cardiac	Intracellular	Interstitial
Relative Magnitude(%)	100	8.4 ± 4.9[+]	93.4 ± 6.1[+]
T_1(ms)	29.4 ± 3.9	22.4 ± 3.0	30.7 ± 4.4
$\%T_{2f}$	41.6 ± 7.3	48.0 ± 8.0	40.3 ± 8.6
T_{2f}(ms)	1.8 ± 1.0	2.0 ± 1.3	1.8 ± 1.1
$\%T_{2s}$	58.4 ± 7.3	52.0 ± 8.0	59.7 ± 8.6
T_{2s}(ms)	23.8 ± 0.9	16.4 ± 4.2	24.5 ± 0.8

[+]Intracellular and interstitial magnitudes are relative to cardiac magnitude.

Table 6-3
Comparison of magnitudes and relaxation times of total cardiac, intracellular, and interstitial compartments
Rat hearts (n=2)

	Cardiac	Intracelular	Interstitial
Relative magnitude(%)	100	21.7 ± 9.3[+]	81.9 ± 1.4[+]
T_1(ms)	31.0 ± 1.5	23.0 ± 2.5	34.2 ± 4.9
$\%T_{2f}$	28.4 ± 18.4	23.8 ± 6.0	31.1 ± 20.3
T_{2f}(ms)	1.7 ± 1.3	2.6 ± 1.5	1.5 ± 1.5
$\%T_{2s}$	71.6 ± 18.4	76.2 ± 6.0	68.9 ± 20.3
T_{2s}(ms)	22.5 ± 6.0	19.0 ± 1.1	25.0 ± 7.4

[+]Intracellular and interstitial magnitudes are relative to cardiac magnitude.

combined interstitial and intracellular sodium signal as a good estimate of interstitial relaxation times.

Relaxation time data for non-perfused hearts

The relaxation times of non-perfused heart tissue are presented in Table 6-4. These values changed by less than 10% over 21 hours of observation for frog hearts and by less than 20% over 21 hours of observation for rat hearts. The direction of the changes was consistently toward shorter relaxation times. The magnitude of signal obtained from this preparation is also of interest. For frog hearts, the magnitude of

Table 6-4
Sodium Relaxation Times of Non-perfused Heart Tissue

	Frog	Rat
n	3	3
T_1(ms)	42.4 ± 1.6	43.4 ± 4.9
$\%T_{2f}$	38.3 ± 4.9	26.7 ± 4.0
T_{2f}(ms)	3.3 ± 0.7	3.4 ± 0.6
$\%T_{2s}$	61.7 ± 4.9	73.3 ± 4.0
T_{2s}	36.3 ± 4.1	39.6 ± 5.0

the signal from non-perfused hearts was 1.9 ± 0.4 (n = 3) times as large as the cardiac signal estimated from perfused hearts, while for rats the non-perfused magnitude was 2.8 ± 0.5 (n = 3) times as large as the cardiac signal estimated from perfused hearts. Possible interpretations of this will be presented later (see Discussion). The magnitude of this non-perfused tissue signal was constant from 3 minutes to 21 hours following cessation of perfusion.

6.2.2. Measurements of the fast component of T_2 decay during global ischemia and interstitial edema

Physiologic response

Induction of global ischemia resulted in cessation of beating within 1 min. If the rat heart was reperfused within 60 minutes, then the developed pressure recovered to 50-80% of original values.

In response to a long duration of perfusion, as needed for induction of interstitial edema, rat hearts perfused with Krebs Henseleit alone beat steadily for 5 to 10 hours with a slow decline in developed pressure to 50% to 80% of original values over that time. The flow rate ranged between 16 and 23 ml/min for various hearts and tended to decrease to 8 to 12 ml/min by the end of the experiment.

For rat hearts which were perfused with alternating normal buffer and shift reagent buffer, the response was as follows. Early in the time course of the experiment, perfusion with shift reagent buffer resulted in an immediate drop in developed pressure to 20% to 30% of original values.

Reperfusion with normal Krebs resulted in a recovery of developed pressure to 70% to 100% of original values. After 5 to 6 hours of alternating shift reagent and normal perfusion, the developed pressure during normal Krebs perfusion was 40% to 60% of original values, while during shift reagent perfusion the pressure dropped to 8% to 16% of these values (or 4% to 8% of the original values at the beginning of the experiment). In one instance the heart ceased beating during perfusion with shift reagent, and recovered an irregular beat during perfusion with normal Krebs. The flow rate during perfusion with shift reagent buffer was either unchanged from the flow rate during perfusion with normal Krebs, or exhibited a slight decrease of 3 to 7 ml/min versus normal Krebs perfusion. Over time the flow rate for these alternating shift reagent and normal Krebs perfused hearts exhibited characteristics very similar to those for hearts perfused with only normal Krebs, with a slow decline from 17 to 28 ml/min to 8 to 10 ml/min.

Analysis of simulated data

One simulated data experiment involved creating 10 simulated data sets for each of six biexponential parameter sets. The mean of the noise added to each of the simulated data sets was zero. The standard deviation of the random Gaussian noise added to each of the simulated data sets was 0.9 (arbitrary units) which compares to the total signal magnitude of the parameter sets of 120, 190, or 260. This noise level is comparable to the typical difference between the curve obtained by fitting heart T_2 data to equation 5-4 and the actual data point. It is also comparable to the estimate of how precisely the integral magnitude can be determined in a

typical sodium spectrum.

The average fitted parameters determined by analyzing this simulated data according to Eq. 5-4 are presented in Table 6-5. One conclusion which can be drawn from this analysis is that the mean of each of the fitted parameters for the ten trials tends to be very close to the ideal (before noise was added) parameters. No systematic errors in any parameters with varying T_{2f} and M_s are noted. One can also determine that when T_{2f} is 2 ms, the standard deviation of the fitted M_f is about 11% of M_f, while when T_{2f} is 5 ms, the standard deviation of the fitted M_f is about 19% of M_f.

Table 6-5
Biexponential Fits to Biexponential Simulated Data

	Ideal	Fitted	Ideal	Fitted
Mf	10.0	10.3 ± 1.1	10.0	10.2 ± 1.3
T2f(ms)	2.0	2.0 ± 0.6	5.0	4.7 ± 1.3
Ms	110.0	109.8 ± 1.3	110.0	110.1 ± 1.7
T2s(ms)	30.0	30.1 ± 0.5	30.0	30.0 ± 0.4
Mf	10.0	9.9 ± 1.1	10.0	10.4 ± 2.1
T2f(ms)	2.0	2.3 ± 0.6	5.0	5.3 ± 1.2
Ms	180.0	179.7 ± 1.5	180.0	179.6 ± 2.1
T2s(ms)	30.0	30.0 ± 0.3	30.0	30.1 ± 0.3
Mf	10.0	10.1 ± 1.2	10.0	10.1 ± 2.4
T2f(ms)	2.0	2.2 ± 0.4	5.0	5.3 ± 1.6
Ms	250.0	249.7 ± 0.8	250.0	249.8 ± 2.3
T2s(ms)	30.0	30.0 ± 0.1	30.0	30.0 ± 0.3

Ideal refers to intitial parameter values used to create the simulated data. Random noise was then added to the simulated data (described in text) and this data was fit to a biexponential function. Fitted values are presented as mean ± SD. N=10 for each parameter set.

A second simulated data experiment explored biexponential fits to data which was actually derived from 3 T_2 time constants. The results of this analysis are presented in Table 6-6. They reveal that for sets 1 to 3 and sets 4 to 6, the fitted values of M_f and T_{2f} are relatively independent of changes in the distribution of slower relaxation time components. Sets 1 to 3 are believed to be the most likely representation of the actual distribution of T_2 data in the perfused heart, as they are

Table 6-6
Biexponential fits to 3 component simulated data

	Ideal	Fitted	Ideal	Fitted	Ideal	Fitted
Set #	**#1**		**#2**		**#3**	
Mf	10.0	10.3	10.0	10.3	10.0	10.3
T2f	2.0	2.1	2.0	2.1	2.0	2.1
Msa	15.0		15.0		15.0	
T2sa	25.0		25.0		25.0	
Ms(b)	95.0	109.7	165.0	179.7	235.0	249.7
T2s(b)	33.0	31.9	33.0	32.3	33.0	32.5
Set #	**#4**		**#5**		**#6**	
Mf	10.0	10.6	10.0	11.6	10.0	12.0
T2f	2.0	2.2	2.0	2.5	2.0	2.7
Msa	90.0		90.0		90.0	
T2sa	25.0		25.0		25.0	
Ms(b)	20.0	109.3	90.0	178.1	160.0	247.5
T2s(b)	35.0	26.8	35.0	30.0	35.0	31.5
Set #	**#7**		**#8**		**#9**	
Mf	10.0	13.8	10.0	24.0	10.0	27.5
T2f	2.0	3.1	2.0	5.7	2.0	6.4
Msa	90.0		90.0		90.0	
T2sa	20.0		20.0		20.0	
Ms(b)	20.0	105.6	90.0	164.5	160.0	230.8
T2s(b)	40.0	23.8	40.0	31.4	40.0	34.3

Ideal refers to the parameters used to create the simulated data. No noise was added to this data. The fitted values are biexponential fits to the simulated data. Ms(b) and T2s(b) refer to the third component for ideal parameters and to the second component of fitted values.

derived from the 3 T_2 components determined by experiments utilizing the IHE pulse sequence and analysis. Since the IHE analysis may underrepresent the slower cardiac relaxation components (see Discussion), sets 4 to 6 were created and analyzed. There is a tendency for the biexponential fits to overestimate the M_f value by 10 to 20% for sets 4 to 6, but this is a small error relative to the changes in M_f noted in the pathology experiments below.

Sets 7 to 9 illustrate a large dependence of fitted values for M_f and T_{2f} on the distribution of the slower relaxation time components. These data sets illustrate the limitations of fitting a complex system such as a perfused heart to only 2 T_2 time constants. The parameters determined in the biexponential fit must be considered to be a characterization of the perfused heart system, and not an absolute determination of the distribution of time constants which may be present. Data sets 7 to 9 are not believed to represent the T_2 curves obtained in this study for two reasons. First, for these data sets, the difference in the two slow time constants (20 ms and 40 ms) is large enough that the T_2 decay curve may be noticeably triple exponential in character. Also, the M_f and T_{2f} values are both observed to increase as M_{sb} increases in sets 7 to 9 of Table 6-6. As described below, in this study, systematic changes in M_f were noted to occur during pathologic interventions without corresponding changes in T_{2f}.

Measurements of fast T_2 decay

A typical T_2 decay curve obtained from a perfused rat heart is shown

in Fig. 6-2. The biexponential character of the data, as seen by its non-linear character on the semilogarithmic plot, was apparent for every heart used in the experiments.

Five T_2 measurements were obtained on 4 hearts during global ischemia. The value of M_f, the magnitude of signal with a fast T_2 time constant, is plotted as a function of duration of ischemia in Fig. 6-3. It should be stressed that M_f is an absolute magnitude determined by equation 5-4 and not a percent. Three of the four hearts exhibited large increases in M_f, with M_f measurements during ischemia averaging 3.3 times the M_f measurements obtained prior to ischemia. The one heart which

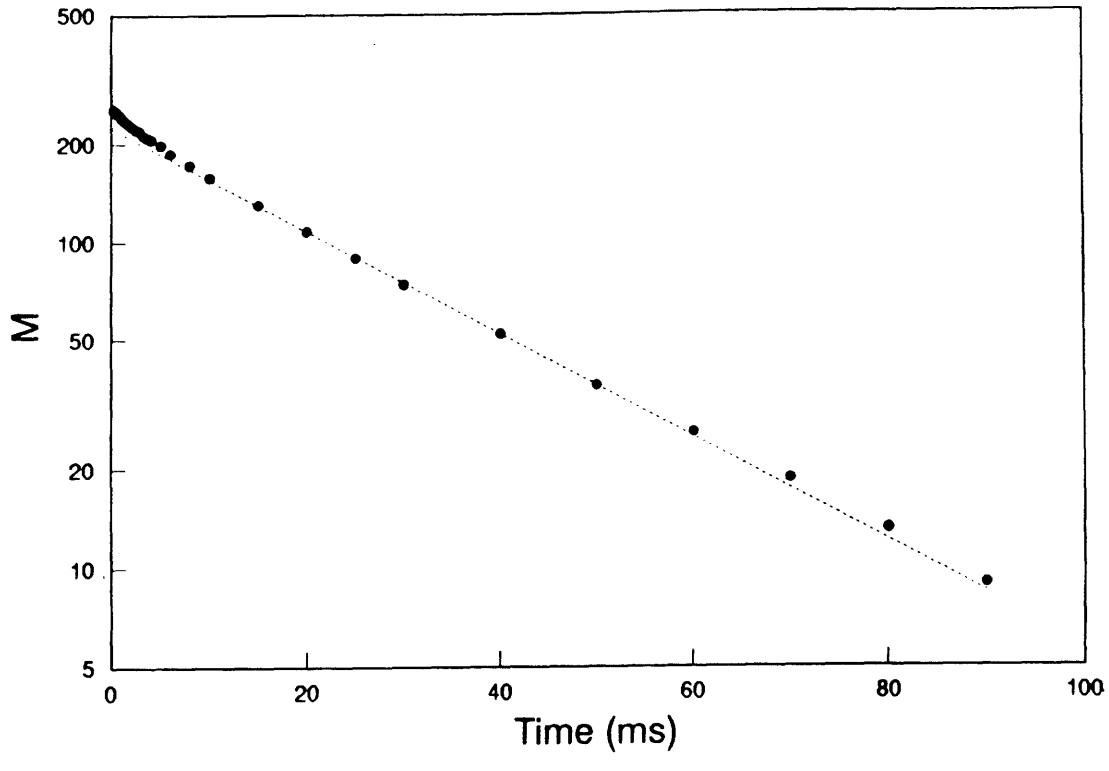

Figure 6-2 T_2 decay curve from perfused rat heart. Dashed line is the slow component of a biexponential fit to the data.

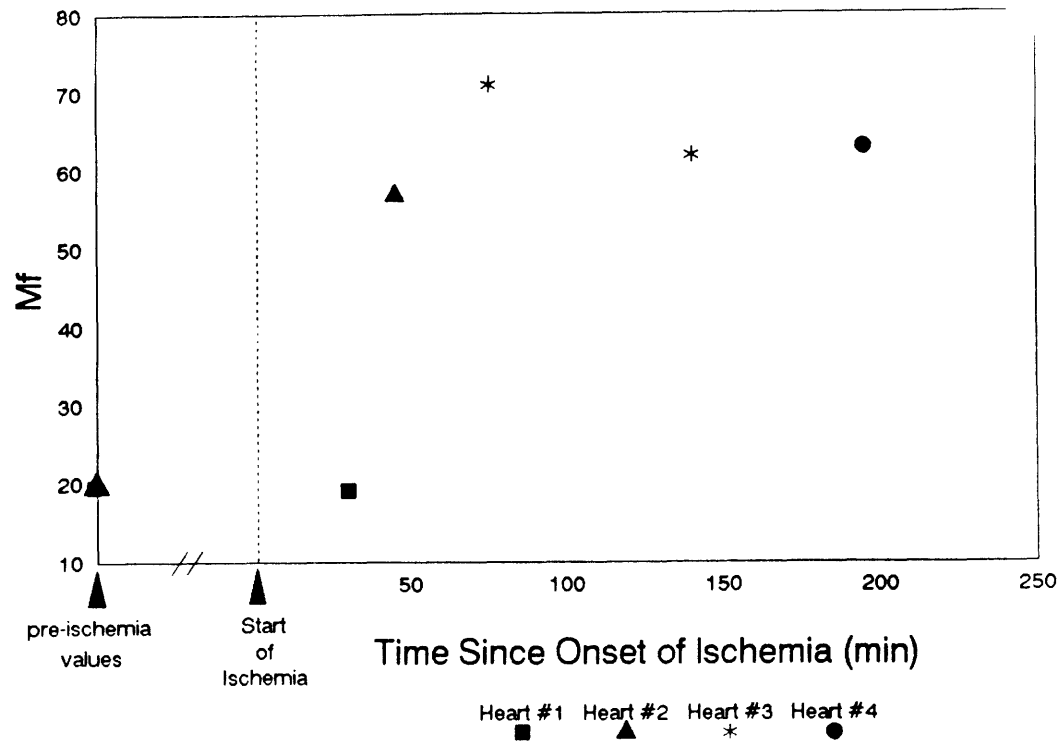

Figure 6-3 Magnitude of signal with a fast T_2 time constant versus duration of ischemia for four rat hearts. The pre-ischemia measurements were normalized to a value of 20 (arbitrary units).

exhibited no change in its M_f value was measured after only 28 minutes of ischemia.

No significant trends in T_2f were observed as a result of global ischemia, with values ranging from 1.7 to 5.5 ms. M_s and T_2s are not considered useful due to the possibly variable amount of perfusate signal arising from the ventricle and bath which may contribute to these parameters.

For the extracellular edema experiment, T_2 relaxation data was obtained for 3 hearts which underwent alternating normal and shift reagent

perfusion, for 4 hearts which were perfused with normal Krebs Henseleit, and for 2 hearts which underwent alternating normal and low calcium perfusion. Two of the 4 hearts which had normal Krebs Henseleit perfusion for the duration of the experiment received shift reagent perfusion at the conclusion of the experiment to verify that the intracellular sodium magnitude had remained small relative to the extracellular signal. These T_2 results are presented in Table 6-7 for the alternately normal and shift reagent perfused hearts, and in Table 6-8 for the hearts which had normal Krebs Henseleit perfusion for the duration of the experiment. All values are expressed as mean ± SD.

The values for M_f from Table 6-7 indicate that the magnitude of the fast component of T_2 relaxation of the entire perfused heart system is increasing by a factor of nearly 5, while the magnitude of the fast component of intracellular T_2 relaxation is stable. As described above, two hearts whose data is incorporated into Table 6-8 received shift reagent perfusion at the conclusion of the experiment. The intracellular Mf for these two hearts was 11.4% and 13.2% of the total Mf measured at the later time (the second line of Table 6-8) for each heart. This indicates that the intracellular signal is too small to account for the increases in M_f observed in the absence of shift reagent. The data from one of the hearts of the alternate normal and shift reagent perfusion series, and from one of the hearts which had only normal buffer perfusion until a final shift reagent measurement, are presented in Fig. 6-4.

Concerning the hearts which underwent alternate normal and low

Table 6-7

T_2 relaxation measurements during interstitial edema with alternating normal and shift reagent perfusion (n=3)

	time (min)	M_f	T_{2f}	M_s	T_{2s}
Heart	40-55	7.4 ± 1.8	3.0 ± 1.2	92.6 ± 15.7	29.4 ± 2.5
Intrac.	90-110	2.0 ± 0.7	1.6 ± 0.4	2.0 ± 0.6	22.1 ± 4.5
Heart	137-200	21.7 ± 6.6	3.7 ± 0.2	121.2 ± 8.4	28.2 ± 3.5
Intrac.	177-260	1.9 ± 0.7	0.9 ± 0.1	2.4 ± 1.2	20.0 ± 2.2
Heart	226-320	35.6 ± 9.4	3.7 ± 0.6	119.7 ± 6.7	25.7 ± 2.2
Intrac.	280-324	1.9 ± 0.9	1.1 ± 0.5	2.0 ± 1.1	18.3 ± 6.6

Rows labelled heart refer to T_2 measurements of the sodium signal from the entire perfused heart system while on Krebs Henseleit perfusion, while rows labelled intrac. refer to T_2 measurements of the unshifted intracellular resonance while on shift reagent perfusion. Magnitudes are in arbitrary units, with $M_f + M_s$ set equal to 100 for the first row. Time is measured from the initiation of perfusion to the midpoint of the T_2 measurement. A range of time values is indicated for each row because a given measurement for each heart occurred at a slightly different time following the start of perfusion due to a variable time required between washing in and washing out of the shift reagent for each heart. Note large increase in M_f of entire heart while M_f of intracellular sodium remains fairly constant.

Table 6-8

T_2 relaxation measurements during interstitial edema without using shift reagent (n=4)

	time (min)	M_f	T_{2f}	M_s	T_{2s}
Heart	140-270	7.0 ± 2.0	2.9 ± 0.6	93.0 ± 2.0	35.7 ± 3.3
Heart	350-500	12.0 ± 4.3	4.1 ± 2.0	125.9 ± 20.0	38.4 ± 1.0

T_2 measurements were made on the sodium signal from the entire perfused heart system. $M_f + M_s$ is normalized to 100 for the first row. Time is measured from the initiation of perfusion to the midpoint of the T_2 measurement. A range of time values is indicated for each row because a given measurement for each heart occurred at a different time following the start of perfusion.

calcium perfusion, the final Mf measured during perfusion with normal buffer (after 3 cycles of alternating buffers) was 21% and 32% higher than

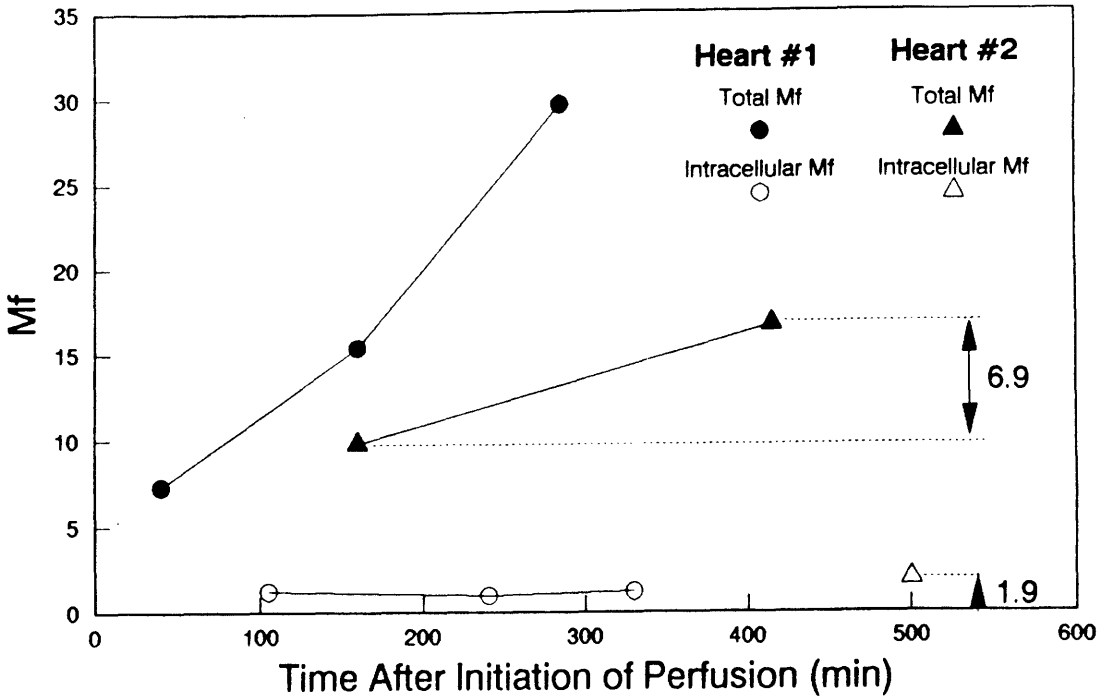

Figure 6-4 The magnitude of signal with a fast component of T_2 decay (Mf) versus time of perfusion for two rat hearts. Mf is measured in arbitrary units. Heart #1 experienced perfusion with alternating normal and shift reagent buffers. Note the large increase in total Mf and the stability of intracellular Mf. Two other hearts exhibited similar trends. Heart #2 was perfused only with normal buffer until a final intracellular measurement with shift reagent. Note that the increase in total Mf is greater than final intracellular Mf. Three other hearts exhibited similar trends.

the initial Mf measured during perfusion with normal buffer. This magnitude of change is similar to the change noted for those hearts when no shift reagent buffer was used (Table 6-8), indicating that it is not the low free calcium aspect of the shift reagent buffer which led to unusually large increases in Mf when alternating normal and shift reagent buffers are used.

6.3. Sodium imaging

Sodium images were obtained at short and long echo times for 9 rat

hearts which underwent various interventions. Sodium images from a heart before and after coronary occlusion are presented in Fig. 6-5, along with the corresponding proton images. One can notice that a loss of sodium intensity is present at both short and long echo times, but that it is somewhat more distinct at the longer echo time. Similar findings on sodium images during coronary occlusion were observed in several other hearts, but were not quantified. The preservation of the proton signal intensity in the occluded region confirms that the heart has not "collapsed", and that the loss of sodium intensity is due to changes withing the tissue. The perfusion image demonstrates clearly the correspondence between the region with little or no flow and the region with decreased sodium intensity.

Sodium images and corresponding proton images from a heart before ischemia and after reperfusion are presented in Fig. 6-6. A large increase in the sodium imaging intensity at both short and long echo times can be seen. A series of phosphorous spectra depicting the energetic state of this heart at various times is shown in Fig. 6-7.

Figure 6-5 (next two pages) Before occlusion: (A) proton image; (B) sodium image, TE = 2.4 ms; (C) sodium image, TE = 20 ms. After occlusion of a coronary artery: (D) proton image 40 minutes after occlusion; (E) perfusion image 25 minutes after occlusion; (F) sodium image 60 minutes after occlusion, TE = 2.4 ms; (G) sodium image 80 minutes after occlusion, TE = 20 ms. The field of view for the proton images was slightly smaller than for the sodium images, and thus the heart appears somewhat larger in the proton images. The heart in these images is referred to as heart #7 in Table 6-9.

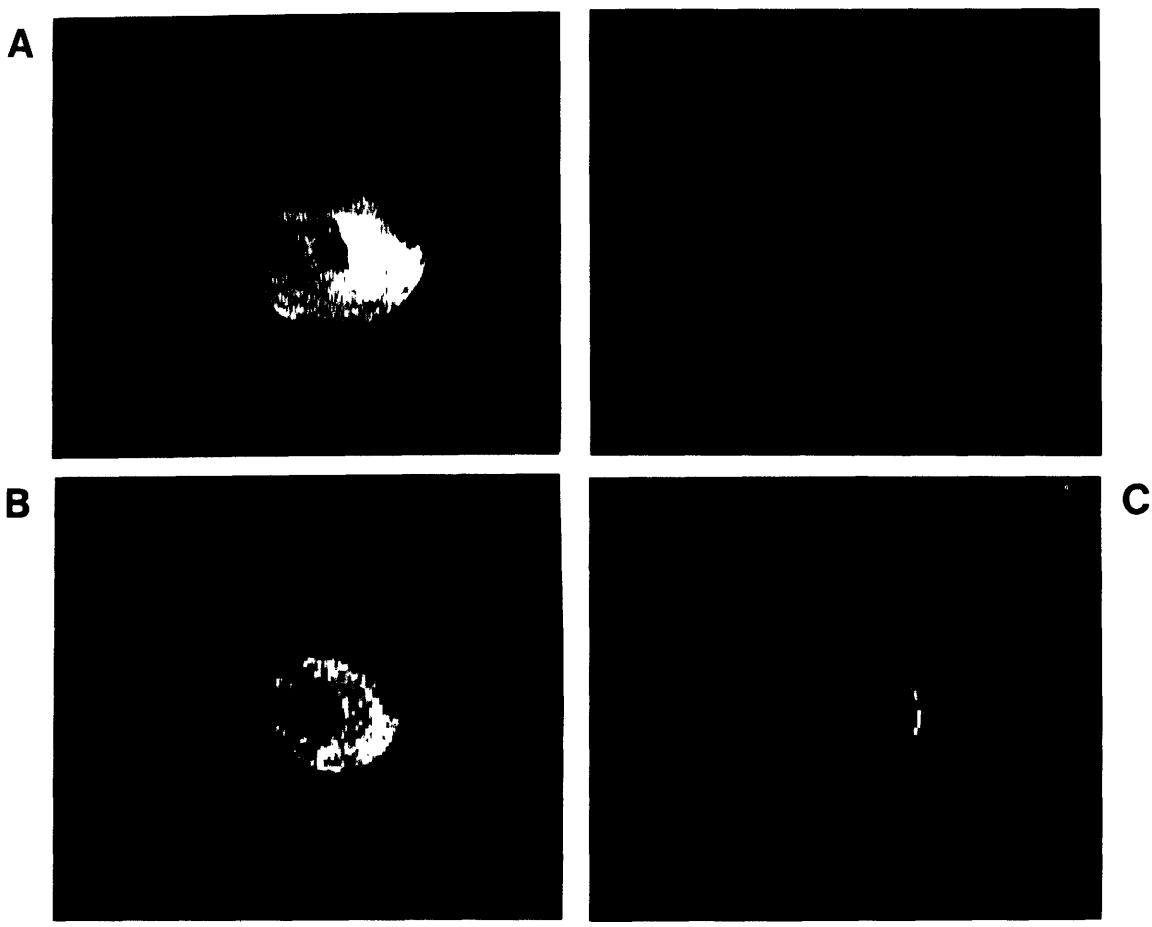
A
B
C

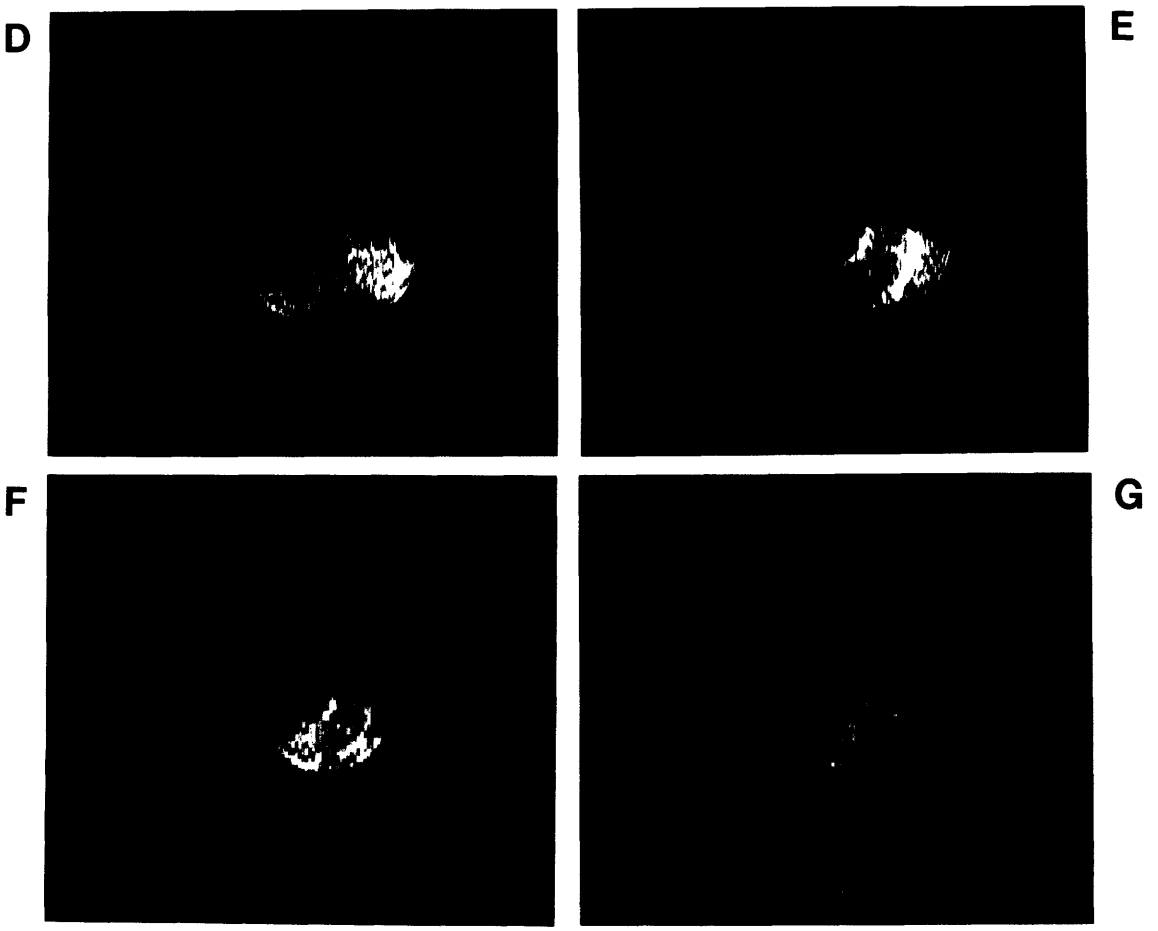
D
E
F
G

Figure 6-6 (next page) Sodium images of a perfused rat heart which underwent global ischemia and reperfusion. Before global ischemia: (A) sodium image, TE = 1.6 ms; (B) sodium image, TE = 20 ms. After 3 hours of global ischemia and 1 hour of reperfusion: (C) sodium image, TE = 1.6 ms; (D) sodium image, TE = 20 ms. The region of high intensity signal toward the top of the heart image (especially noticeable in (A)) is due to buffer in the right ventricle. The heart in these images is referred to as heart #4 of Table 6-9.

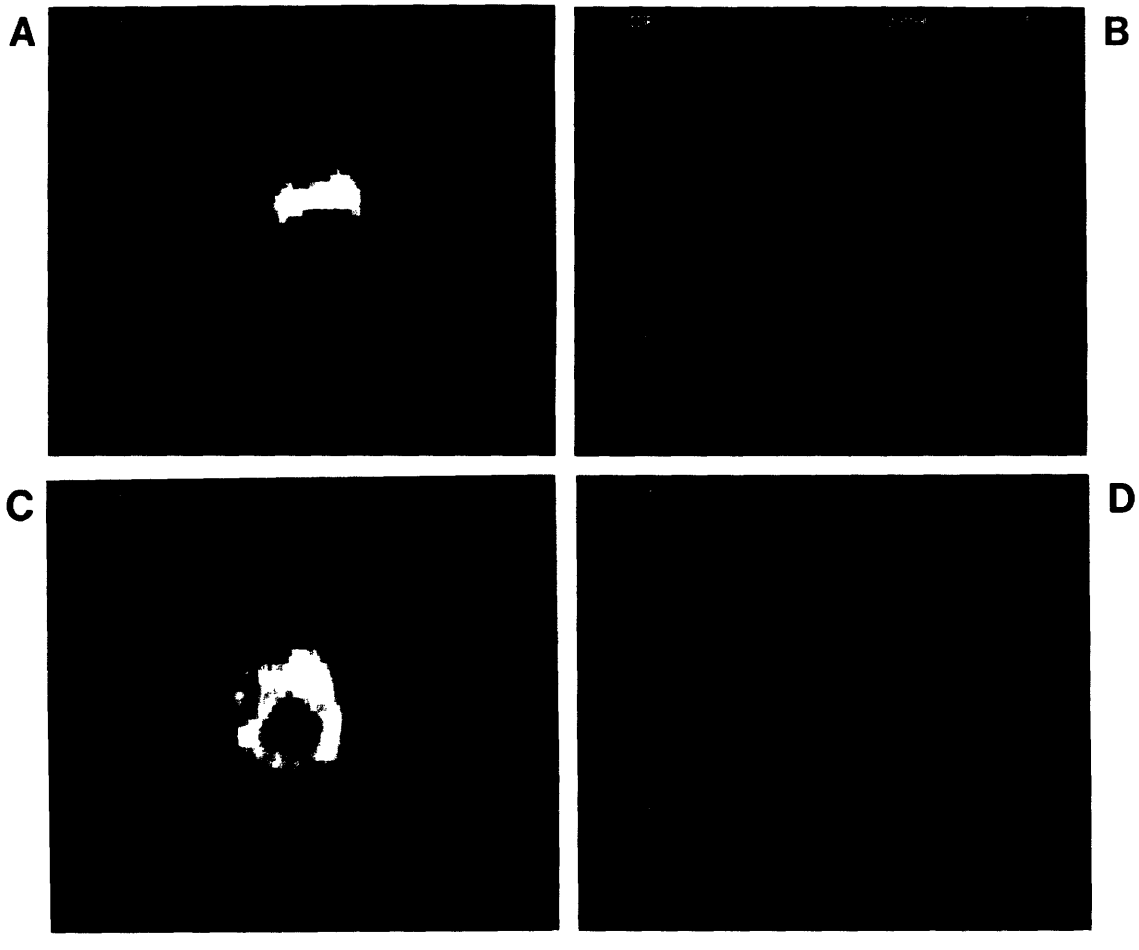
A
B
C
D

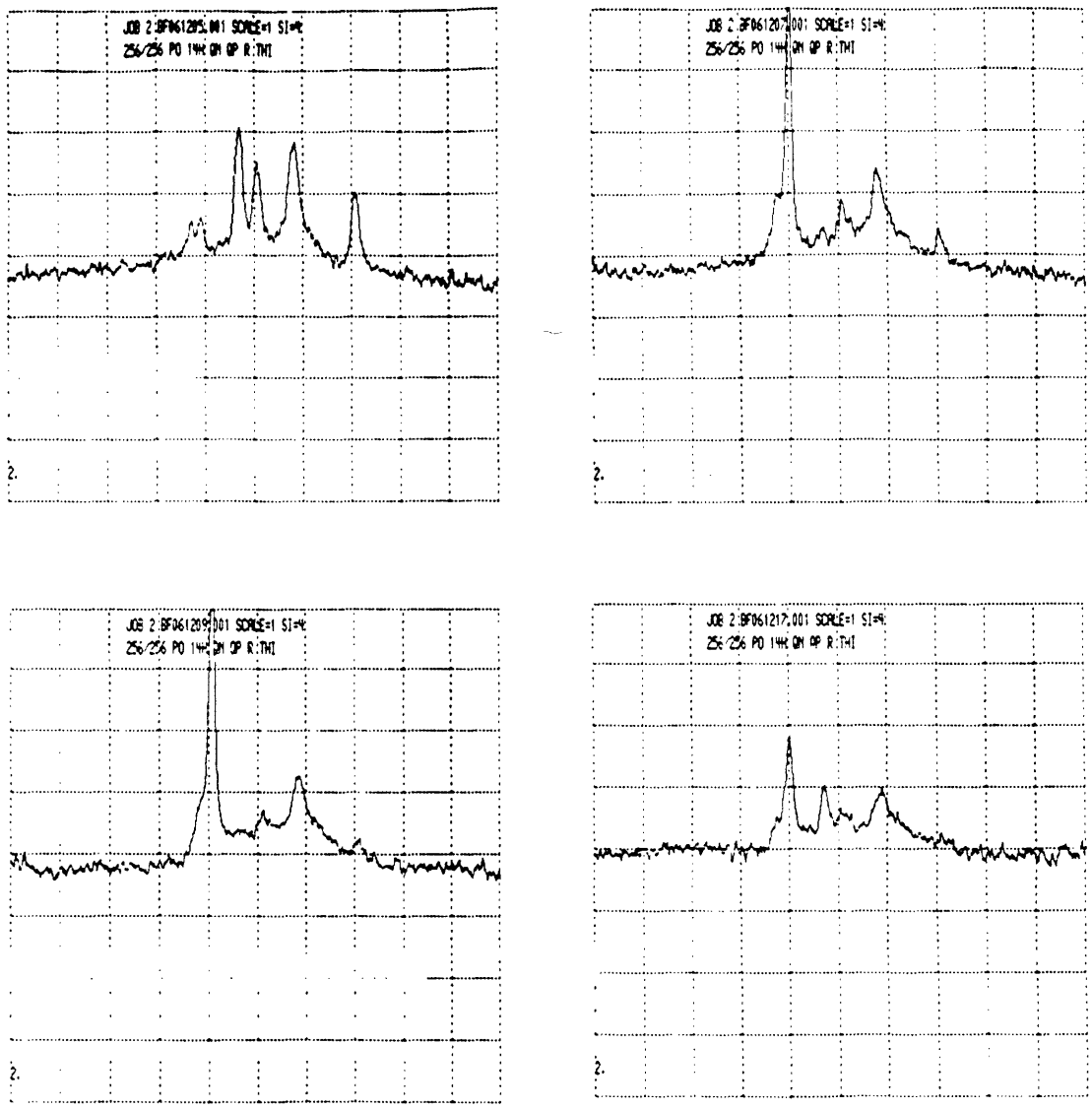

Figure 6-7 ^{31}P spectra of heart shown in Fig. 6-6: (A) just before inducing global ischemia. The three resonances on the right refer to the three phosphates of adenosine triphophatase (ATP). The resonance to the left of those three is phosphocreatine. The less well discriminated resonances on the left of the spectrum refer to the sugar phosphates and to inorganic phosphates. (B) Spectrum 25 minutes after inducing global ischemia. (C) 55 minutes after inducing global ischemia. (D) Spectrum obtained following 3 hours of global ischemia and 2 hours of reperfusion. Note the decrease in ATP and phosphocreatine and the increase in inorganic phosphate during global ischemia. With reperfusion, the inorganic phosphate resonance decreases in magnitude, and the phosphocreatine resonance partially recovers.

Sodium and proton images of a heart after 2.5 hours and after 9.5 hours of perfusion are presented in Fig. 6-8. An increase in image intensity is noticeable at the short echo time, but not at the long echo time for this particular heart. This duration of perfusion is expected to lead to interstitial edema.

The intensity measurements from these images are presented in Table 6-9, along with a description as to the timing of each measurement in relation to the intervention. One feature which can be noted from the imaging data is that the S/N present in the images and in the intensity measurements is somewhat low, such that detection of significant differences or changes is difficult. As discussed below (see Discussion), the low S/N limited the ability to draw conclusions about changes in fast or slow T_2 decay due to pathology.

Figure 6-8 (next page) Sodium images, proton images, and a ^{31}P spectrum of a perfused rat heart which experienced a long duration of perfusion. (A) Proton image after 4 hours of perfusion; (B) ^{31}P spectrum after 5 hours of perfusion; (C) and (D), sodium images after 2.5 hours of perfusion, TE = 1.6 and 20 ms respectively; (E) and (F), sodium images after 9.5 hours of perfusion, TE = 1.6 and 20 ms respectively. The field of view in the proton image (A) was smaller than for the sodium images, and thus the heart appears larger in the proton image. The heart in these images is referred to as heart #3 in Table 6-9.

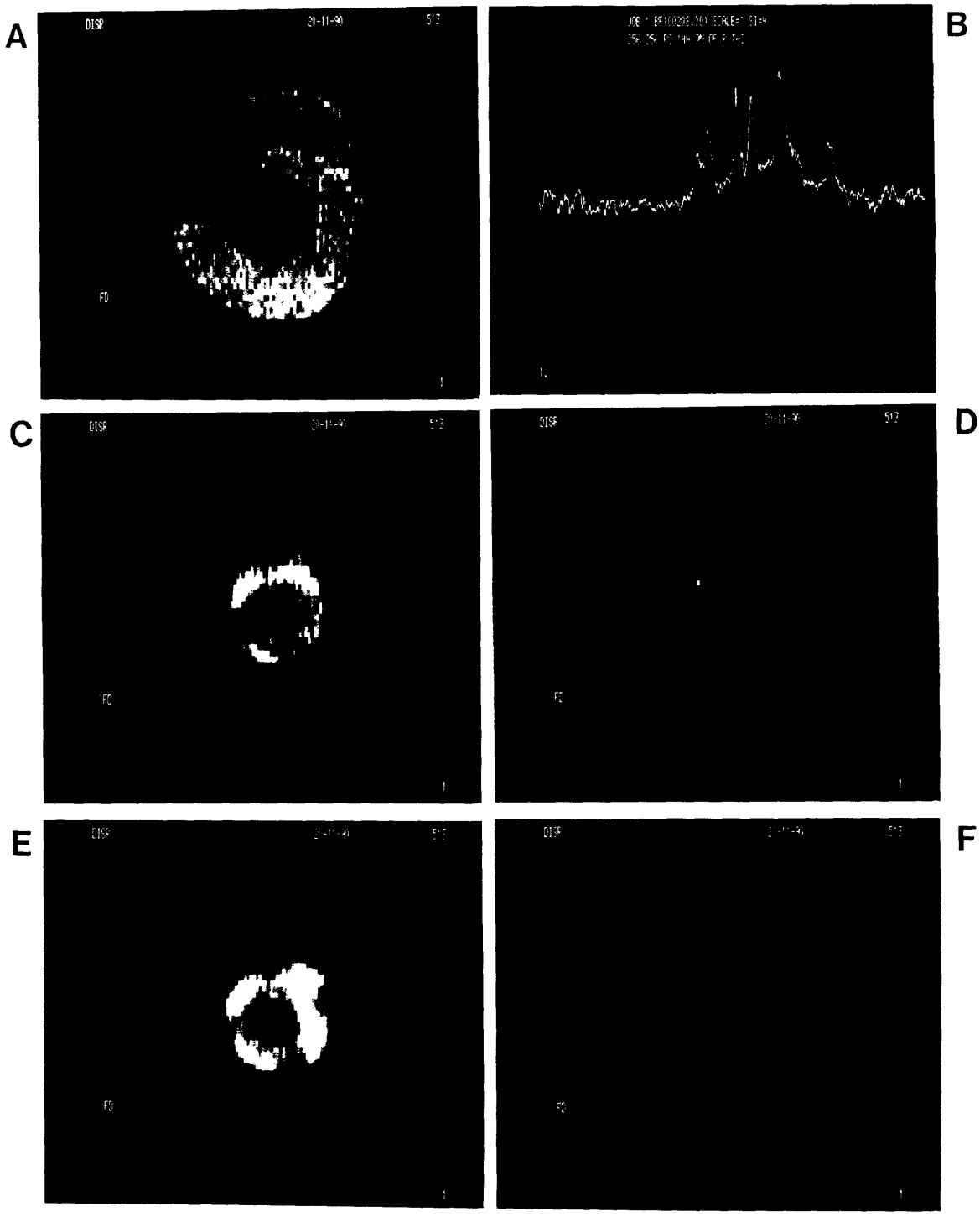
A
B
C
D
E
F

Table 6-9

Sodium imaging intensity at short and long echo times for various interventions

Heart #	Intervention	Timing	Intensity: Short TE	Intensity: Long TE
1	Perfusion	120 min perf.	10.0 ± 0.7	4.0 ± 0.3
		300 min perf.	10.8 ± 1.1	4.8 ± 0.5*
2	Perfusion	90 min perf.	10.0 ± 1.3	3.7 ± 0.6
		350 min perf.	11.8 ± 1.2*	5.1 ± 0.6
3	Perfusion	155 min perf.	10.0 ± 1.0	4.2 ± 0.7
		575 min perf.	13.3 ± 1.6*	4.3 ± 0.5
4	Global ischemia/ reperfusion	before isc.	10.0 ± 1.9	5.0 ± 1.1
		during isc.	13.6 ± 1.6*	3.6 ± 0.6*
		reperfusion	19.2 ± 3.4*	9.5 ± 1.2*
5	Global ischemia/ reperfusion	before isc.	10.0 ± 0.9	4.4 ± 0.8
		during isc.	8.2 ± 1.4*	3.3 ± 0.9*
		reperfusion	12.3 ± 0.8*	5.3 ± 1.1*
6	Global ischemia/ reperfusion	before isc.	10.0 ± 2.0	3.6 ± 0.8
		reperfusion	12.3 ± 2.7	6.5 ± 1.0*
7	coronary occ. (non-occ. side)	before occ.	10.0 ± 1.0	3.7 ± 0.1
		after occ.	12.3 ± 2.7	6.5 ± 1.0*
7	coronary occ. (occ. side)	before occ.	10.0 ± 2.5	4.5 ± 0.4
		after occ.	6.2 ± 0.5*	2.2 ± 0.1*
8	low flow/reflow	before lwfl.	10.0 ± 0.7	2.8 ± 0.3
		during lwfl.	8.8 ± 0.8*	3.0 ± 0.3
		reflow	13.3 ± 0.8*	3.2 ± 0.3
9	ouabain toxicity	before ouab.	10.0 ± 1.0	3.8 ± 1.1
		after ouab.	12.5 ± 1.0*	4.7 ± 0.7

*Indicates that the intensity measurement is significantly different than the intensity measurement immediately above ($p < .05$, t test, uncorrelated data).

7. DISCUSSION

The objective of this work was to characterize the NMR relaxation times of interstitial sodium in the heart, thereby determining the extent to which relaxation characteristics can be exploited to yield compartmental (i.e., intracellular versus interstitial) sodium NMR data. The perfused frog and rat heart model enabled this study to be performed on functioning tissue under both control and pathologic conditions. In order to study the interstitial sodium, the sodium signal of the myocardium had to be separated from the sodium signal of the bath outside the heart and inside the ventricular cavity. In addition, the effect of the intracellular sodium signal needed to be taken into account. By utilizing the known relaxation properties of bath sodium and the addition of shift reagents to quantify intracellular sodium, the spectroscopic study of relaxation properties of interstitial sodium was possible, with the limitations described below. Sodium imaging provided another method of obtaining signal from heart tissue by spatially separating the sodium signal of heart tissue from bath signal.

With these techniques, a component of the interstitial sodium was found to have relaxation characteristics very similar to the intracellular sodium for perfused hearts under control conditions. In addition, the fast component of T_2 decay attributable to the interstitial space was found to increase during pathologic conditions in the perfused heart. The implications and limitations of these studies are described below.

7.1. Interstitial relaxation measurements

The first technique used to observe the cardiac sodium relaxation relied on nulling the signal from the sodium in the bathing solution on the basis of its known relaxation properties. Therefore, if the cardiac signal, or a component of the cardiac signal, has relaxation times similar to those of the bath, then these methods will not be able to observe and quantify this signal. Thus, in characterizing the cardiac signal in this way, it is important to realize that only cardiac components which have shorter relaxation times than the bath have been studied; cardiac signal with T_1 and T_2 values similar to those of the bathing solution will be missed or underrepresented with these techniques. This is one possible explanation as to why the magnitude of the signal from non-perfused heart tissue (obtained without nulling signal with a long T_1) was greater than the cardiac magnitude determined from perfused preparations. The fact that non-perfused relaxation times are somewhat longer than the corresponding perfused cardiac relaxation times is in accordance with this possibility.

Similarly, only the cardiac sodium which is NMR visible under these conditions has been studied. Since specific visibility experiments have not been conducted on cardiac sodium, the possibility of invisible sodium, namely sodium whose T_2 value is so short as to be undetectable with the parameters of this study, still exists.

With these facts in mind, the primary finding is that at least a component of the interstitial sodium signal possesses short relaxation

times for perfused hearts under control conditions. When fit to a biexponential T_2 decay, this includes one component of approximately 2 ms. Thus the interstitium contains sodium relaxation times which are similar to the relaxation times found for the intracellular sodium of perfused hearts. This indicates that it will be difficult to separate the intracellular and extracellular sodium signal on the basis of relaxation times under control conditions. Methods which rely, either directly or indirectly, on differences in relaxation times probably will not work.

7.2. The fast component of T_2 decay with global ischemia and interstitial edema

7.2.1. Global ischemia

One finding from the global ischemia study is that large increases in the magnitude of fast T_2 signal occur with this pathologic state. Also revealing was the fact that no trends in the time constant T_{2f} were observed with this intervention, indicating that the fast relaxation time constants are relatively stable in the presence of alterations in the sodium environment. Stability of sodium relaxation times in tissue has been noted before for intracellular sodium of frog hearts despite a five-fold increase in concentration due to the addition of ouabain (Burstein and Fossel, 1987a) and for intracellular sodium in chicken erythrocytes with seven-fold changes in concentration (Shinar and Navon, 1991).

A rough calculation as to whether the increases of M_f seen during ischemia could be due entirely to increases in intracellular sodium concentration would be informative. From control experiments where the M_f

arising from the entire heart and the M_f arising from the intracellular space alone was measured, the intracellular M_f was found to be 20-30% of total M_f (see Table 6-7). If we assume that the initial intracellular sodium concentration was 10 mM, that intracellular M_f comprised 25% of initial total M_f, that the ratio of intracellular M_f to M_s remains unchanged despite changes in sodium concentration (about 40:60, Table 6-3 and Table 6-7), and that the entire 230% increase in total M_f was due to increases in intracellular sodium concentration without changes in intracellular volume, then this would predict a final intracellular sodium concentration of 102 mM for the 3 ischemic hearts exhibiting large increases in M_f. Since 100 mM or a ten-fold increase is probably high for intracellular sodium, even under ischemic conditions (Balschi et. al., 1990, skeletal muscle), some of the increase in M_f is likely to be due to the interstitial sodium.

The possibility that M_f remains unchanged immediately after the onset of ischemia and then increases after about 30 minutes should be studied with multiple observations on a single heart to confirm the observation. Parallel observation with ^{31}P spectroscopy may indicate correlations between the energetic state of the heart and the changes in this M_f parameter. Another interesting study would be to compare M_f with the function and/or viability of the heart during global ischemia and during reperfusion. Preliminary observations on one perfused heart, however, revealed that M_f following global ischemia and reperfusion was significantly elevated from pre-ischemia levels despite recovery of the majority of function as determined by pressure monitoring.

7.2.2. Interstitial edema

M_f was found to increase in the presence of interstitial edema while the amount of intracellular sodium was shown to remain constant. The implication of this is that increases in M_f cannot be ascribed to a particular compartment, since they occur with both intracellular (Burstein and Fossel, 1987a; Shinar and Navon, 1991) and extracellular pathologic increases in sodium content. This inability to quantify the compartmental origin of altered sodium signals will limit the use of relaxation-based contrast for identifying pathologic lesions.

The results of the edema experiments indicate that the increase in magnitude of signal with a fast T_2 component was greater in those hearts where shift reagent perfusion and normal buffer perfusion was alternated than when shift reagent perfusion was not used. It is unclear why this occurred. During the shift reagent perfusion portion of an alternating normal and shift reagent perfusion experiment, the intracellular sodium levels were stable. Following reperfusion with normal Krebs Henseleit, the heart's function recovered. One possibility was that during perfusion with shift reagent, the low free calcium concentration of the shift reagent buffer led to physiologic changes, such as interstitial edema, which led to increases in M_f even after resumption of perfusion with a normal buffer. The experiment where a low calcium buffer was substituted for the shift reagent buffer and perfusion with this low calcium buffer was alternated with normal buffer perfusion indicates that this is not the factor which leads to large increases in M_f following perfusion with shift reagent buffer.

Another possibility is that the shift reagent precipitated in the interstitial space, which might lead to increased M_f values due to the interaction of sodium ions with the precipitant. Sodium ions of the interstitial space which formerly had slow T_2 time constants might experience increased interactions with the precipitant and relax with a faster T_2 time constant. Also, M_f may be increased due to interstitial edema as a result of osmotic pressure of the precipitants. Note that it is impossible to distinguish between these two possibilities in the perfused heart system due to similarity of the long component of myocardial T_2 decay with bath T_2 decay, thereby making quantification of total myocardial sodium impossible. Although the method of perfusion with a low calcium buffer for brief periods of time between perfusion with alternating normal Krebs and shift reagent buffers appeared to solve the problem of a decreasing flow rate (presumably caused by shift reagent precipitation in the perfusion lines and the capillaries), it is possible that the interaction of $Dy(PPP)_2^{-7}$ with residual calcium in the interstitium led to precipitants which could not be washed out of the interstitium during perfusion with normal Krebs.

The fact that larger increases in M_f were observed for global ischemia than for edema should be noted. The values were a 230% increase for global ischemia versus a 71% increase for edema when only a normal buffer was used. However further work is necessary to determine if such differences are significant, since they are likely to depend on the severity of the disorder. Note particularly the 381% increase in M_f when alternating normal and shift reagent buffers were used to monitor

interstitial edema. Although the shift reagent may have contributed to this large increase, interstitial edema *in vivo* may possess factors which lead to enhanced increases in fast T_2 relaxation, such as a high protein content (Perman et. al., 1986).

7.3. Sodium Imaging

The goals of the imaging studies were to monitor image intensity for several different pathologic interventions and to utilize the relaxation based contrast at the two echo times to draw conclusions about changes in relaxation times which occur with pathologic states. The first of these goals was achieved, as significant changes in image intensity were observed for many of the pathologic conditions. However, the pathologic contrast appears to be non-specific in perfused hearts, as most interventions resulted in a 20 to 90% increase in image intensity at short and long echo times. Coronary occlusion (and possibly global ischemia) results in a lower image intensity in the region which is not perfused. Mechanisms by which this might occur are discussed below.

The high standard deviation of intensities due to poor S/N within an image (Table 6-9) precluded the second imaging goal from being achieved. One example of a question which it had been hoped the relaxation based imaging could answer was raised by the spectroscopic and imaging data on ischemia in perfused hearts. In spectroscopy experiments presented above, M_f increased dramatically with global ischemia. A higher S/N on images before and during global ischemia (before reperfusion) might have revealed if this increased M_f was due to a shift of sodium signal from slow to fast

T_2 time constants, or was due to an increase in the total myocardial sodium content (increase in either myocardial volume or sodium concentration) with consequent increase in signal with a fast T_2.

The decrease in sodium image intensity for the locally occluded region of the heart deserves further speculation as to its mechanism, since ischemia is generally associated with increases of intracellular and/or interstitial sodium content (Elgavish, 1989; Jelicks and Gupta, 1989c), both of which should lead to an increased image intensity. Two possible explanations exist for this finding.

One is that the total concentration of sodium ions present within a voxel may have decreased. This can occur if the volume ratio of two compartments within a voxel shifts toward one with a lower sodium concentration. Specifically, for heart tissue with an occluded coronary, interstitial fluid might be expected to leave the tissue as a result of vascular collapse. Since interstitial fluid has a higher sodium concentration than intracellular fluid, the total sodium density would decrease in this instance. Note that this explanation assumes a total stoppage of flow to the heart or a region of the heart. If even a small flow exists or if reperfusion occurs, then this fluid flow constitutes a source of additional sodium which can enter damaged cells, or expand an altered interstitial space (Whalen et. al., 1974; Willerson et. al., 1977).

The second possibility is that the sodium density remains the same,

but that the sodium signal shifts from a slower T_2 time constant to a faster T_2 time constant, such that a significant amount of signal decays even before the echo time of 1.6 to 2.4 ms. Although changes in the sodium density or the amount of sodium signal with a fast T_2 time constant are not known for heart tissue with an occluded coronary artery, this mechanism may be partially responsible for the decrease observed in image intensity at the short echo time.

Since the image at a short echo time does not acquire all of the sodium signal with a fast T_2 time constant, an estimate of the difference between the total sodium density and the image intensity at an echo time of about 2 ms would be useful. To determine this difference, it is necessary to estimate the fraction of total sodium signal which has a fast T_2 time constant. If the non-perfused heart tissue data (Results, section 6.2.1.) is used as an estimate of the total sodium content of the myocardium, and if the difference between this magnitude and the lesser cardiac magnitude as determined with the IHE pulse sequence is assumed to be due to the presence of slow T_2 components in tissue (see Discussion above) then the magnitude of cardiac fast T_2 of Table 6-1 can be expressed as a fraction of total myocardial sodium signal. The fraction of total myocardial sodium with a fast T_2 time constant is thus estimated to be 19% for frog hearts and 15% for rat hearts. Since a 2 ms echo time results in loss of 63% of signal with a 2 ms T_2, the signal at a 2 ms echo time is estimated to detect 88% and 91% of the total myocardial signal for frog and rat hearts, respectively.

7.4. General comments / Future directions

The interstitial sodium observed in this study was fit to equations of a single T_1 time constant and two T_2 time constants because this adequately characterized the data. Less than two T2 time constants did not provide a good fit, and more time constants were not justified for the available S/N ratio. Note that this provides merely a characterization of the interstitial sodium relaxation and not a description of the distribution of time constants which may be physically present. The interstitial space is heterogeneous, with features that may produce a multitude of NMR interactions for the sodium nuclei.

The finding of short relaxation times in the interstitium increases the difficulty of separating the sodium NMR signal originating from the intracellular and extracellular spaces. Possibilities still exist, however, for obtaining this compartmental information using NMR. Multiple quantum spectroscopy with paramagnetic quenching of the extracellular signal (Jelicks and Gupta, 1989a,b,c), and future development of a non-toxic shift reagent with uniform *in vivo* distribution remain possibilities.

These studies demonstrated that it is possible to combine several imaging and spectroscopic studies in a single experiment. For example, the coronary occlusion experiment combined proton and sodium imaging with flow imaging to correlate the flow deficit with sodium intensities and with the lack of change on a proton image. Also ^{31}P spectroscopy was combined with proton and sodium imaging in a study of global ischemia to

reveal changes in the energetic state of the heart which supplemented the proton and sodium imaging data.

Large changes in sodium image intensity due to pathologic states in perfused hearts were demonstrated. However, based on spectroscopy results, while sodium images emphasizing a particular aspect of relaxation may exhibit a high contrast between pathologic and normal tissue, compartmental information cannot be quantified. The inability to quantify the compartmental origin of altered sodium signals will limit the use of image contrast based on relaxation times for the purpose of identifying pathologic lesions. Due to the difficulty of obtaining sodium images in terms of imaging times and hardware limitations on short echo times, it should be shown that this contrast cannot be obtained from other diagnostic modalities, or that the sodium image can contribute unique electrophysiologic information, in order to consider sodium MRI practical.

This study revealed that relaxation based discrimination is not likely to succeed in quantitatively separating the intracellular and interstitial sodium NMR signals under control or pathologic conditions. Combined with the limitations of shift reagents, no optimal method currently exists for obtaining this compartmental information. Several applications of sodium NMR, such as electrophysiologic studies and identification of pathologic lesions on images, are likely to be fully realized only when true intra- and extracellular sodium data are available in a quantitative and non-toxic manner.

REFERENCES

Abragam, A., The Principles of Nuclear Magnetism, Oxford University Press, New York, 1961.

Albert, M. S., Lee, J., Patlak, C. S., Fenstermacher, J, D., and Springer, C. S., "^{23}Na MRS of the Rat Brain *In Vivo* at 9.4 T: On the Permeability of the Blood-Brain Barrier to Shift Reagent", Proc. Soc. Magn. Reson. Med. p36, abstract, 1990.

Ammann, H., Boulanger, Y., and Vinay, P., "Variable NMR Visibility of Intracellular Sodium Induced by Na^+-Substrate Cotransport in Dog Cortical Tubules", Magn. Reson. Med. 16:368-379, 1990.

Anderson, S. E., Adorante, J. S., Cala, P. M., "Dynamic NMR Measurements of Volume Regulatory Changes in *Amphiuma* RBC Na^+ Content", Am. J. Physiol. 254:C466-C474, 1988.

Armstrong, W. M., Lurie, D., Burt, M. R., and High, J. R., "Extracellular Volume and Ionic Content of Frog Ventricle", Am. J. Physiol. 217:1230-1235, 1969.

Atkinson, D. J., Burstein, D., and Edelman, R. R., "First-pass Cardiac Perfusion: Evaluation with Ultrafast MR Imaging", Radiology 174:757-762, 1990.

Balschi, J. A., Bittl, J. A., Springer, C. S., Ingwall, J. S., "^{31}P and ^{23}Na NMR Spectroscopy of Normal and Ischemic Rat Skeletal Muscle. Use of a Shift Reagent *In Vivo*", NMR in Biomed. 2:47-58, 1990.

Barac-Nieto, M., Neiberger, R., Spitzer, A., Gupta, R. K., "NMR Measurements of Intra- and Extravesicular Sodium in Renal Microvilli", Biochem. Biophys. Acta. 968:359-366, 1988.

Berendsen, H. J. C., and Edzes, H. T., "The Observation and General Interpretation of Sodium Magnetic Resonance in Biological Material", Ann. N. Y. Acad. Sci. 204:459-485, 1973.

Bevington, P. R., Data Reduction and Error Analysis for the Physical Sciences, McGraw-Hill Book Co., New York, 1969.

Bishop, S. P., "Cardiovascular Research", in The Laboratory Rat, Vol. II, ed. by H. Baker et. al., Academic Press, 1980.

Boulanger, Y., Vinay, P., and Boulanger, M., "NMR Monitoring of Intracellular Sodium in Dog and Rabbit Kidney Tubules", Am. J. Physiol. 253:F904-F911, 1987.

Boulanger, Y., and Vinay, P., "Nuclear Magnetic Resonance Monitoring of Sodium in Biological Tissues", Can. J. Physiol. 67:820-828, 1989.

Brauer, M., Towner, R. A., and Foxall, D. L., "Sodium-23 and Proton Nuclear Magnetic Resonance Imaging Studies of Carbon Tetrachloride-Induced Liver Damage in the Rat", Magn. Reson. Imag. 8:459-465, 1990.

Brown, J. W., Cristian, D., and Paradise, R. R., "Histological Effects of Procedural and Environmental Factors on Isolated Rat Heart Preparations", Proc. Soc. Exp. Biol. Med. 129:455-462, 1968.

Brunner, P., and Ernst, R. R., "Sensitivity and Performance Time in NMR Imaging", J. Magn. Res. 33:83-106, 1979.

Burstein, D., and Fossel, E. T., "Intracellular Sodium and Lithium NMR Relaxation Times in a Perfused Frog Heart", Magn. Reson. Med. 4:261-273, 1987a.

Burstein, D., and Fossel, E. T., "Effects of Temperature, Buffer Osmolarity, and Shift Reagent Concentration on the Intracellular Sodium and Potassium Relaxation Times of Red Blood Cells", J. Magn. Reson. 73:150-158, 1987b.

Burstein, D., and Fossel, E. T., "Nuclear Magnetic Resonance Studies of Intracellular Ions in the Perfused Frog Heart", Am. J. Physiol. 252:H138-H146, 1987c.

Burstein, D., and Mattingly, M., "Magnetic Resonance Imaging of Intracellular Sodium", J. Magn. Reson. 83:197-204, 1989.

Cannon, P. J., Maudsley, A. A., Hilal, S. K., Simon, H. E., and Cassidy, F., "Sodium Nuclear Magnetic Resonance Imaging of Myocardial Tissue of Dogs after Coronary Artery Occlusion and Reperfusion", J. Am. Coll. Cardiol. 7:573-579, 1986.

Carr, H. Y., and Purcell, E. M., "Effects of Diffusion on Free Precession in Nuclear Magnetic Resonance Experiments", Phys. Rev. 94:630-638, 1954.

Chang, D. C., and Woessner, D. E., "Spin Echo Study of Na-23 Relaxation in Skeletal Muscle. Evidence of Sodium Ion Binding Inside a Biological Cell", J. Magn. Reson. 30:185-191, 1978.

Cheung, L. P., Fossel, E. T., and Burstein, D. B., "Sodium NMR Spectroscopy of Normal and Neoplastic Tissues", Proc. Soc. Magn. Reson. Med. p451, abstract, 1988.

Civan, M. M., Degani, H., Margalit, Y., and Shporer, M., "Observation of ^{23}Na in Frog Skin by NMR", Am. J. Physiol. 245:C213-C219, 1983.

Cockman, M. D., Jelinski, L. W., Katz, J., Sorce, D. J., Boxt, L. M., and Cannon, P. J., "Double-Quantum-Filtered Sodium Imaging", J. Magn. Reson. 90:9-18, 1990.

Cohen, I., and Kline, R., "K^+ Fluctuations in the Extracellular Spaces of Cardiac Muscle. Evidence from the Voltage Clamp and Extracellular K^+ Selective Microelectodes", Circ. Res. 50:1-16, 1982.

Cope, F. W., "NMR Evidence for Complexing of Na^+ in Muscle, Kidney, and Brain, and by Actomyosin. The Relation of Cellular Complexing of Na^+ to Water Structure and to Transport Kinetics", J. Gen. Physiol. 50:1353-1375, 1967.

Cope F. W., "Spin-Echo Nuclear Magnetic Resonance Evidence for Complexing of Sodium Ions in Muscle, Brain, and Kidney", Biophys. J. 10:843-858, 1970.

DeLayre, J. L., Ingwall, J. S., Malloy, C., and Fossel, E. T., "Gated Na-23 NMR Images of an Isolated Perfused Working Rat Heart", Science 212:935-936, 1981.

Eisenstadt, M., "NMR Hybrid Relaxation Methods of Studying Chemical, Physical, and Spin Exchange. II. Suppression Methods", J. Magn. Reson. 39:263-274, 1980.

Elgavish, G. A., "Shift-Reagent-Aided ^{23}Na NMR Spectroscopy", Invest. Radiol. 24:1028-1033, 1989.

Farrar, T. C., and Becker, E. D., Pulse and Fourier Transform NMR, Academic Press, New York, 1971.

Farrar, T. C., Introduction to Pulse NMR Spectroscopy, Farragut Press, Madison WI, 1989.

Feinberg, D. A., Crooks, L. A., Kaufman, L., Brant-Zawadzki, M., Posin, J. P., Arakawa, M., Watts, J. C., and Hoenninger, J., "Magnetic Resonance Imaging Performance: A Comparison of Sodium and Hydrogen", Radiology 156:133-138, 1985.

Fisher, R. B., and Young, D. A. B., "Direct Determination of Extracellular Fluid in the Rat Heart", J. Physiol. 158:50-58, 1961.

Frank, J. S., and Langer, G. A., "The Myocardial Interstitium: Its Structure and Its Role in Ionic Exchange", J. Cell Biol. 60:586-601, 1974.

Freeman, R., Kempsell, S. P., and Levitt, M. H., "Radiofrequency Pulse Sequences Which Compensate Their Own Imperfections", J. Magn. Reson. 38:453-479, 1980.

Fukishima, E., Roeder, S. B. W., Experimental Pulse NMR, Addison-Wesley Publishing Co., 1981.

Goldberg, M., and Gilboa, H., "Sodium Magnetic Resonance in Biological Systems. Interpretation of the Relaxation Curves", in Nuclear Magnetic Resonance Spectroscopy in Molecular Biology, ed. by B. Pullman, D. Reidel Publ. Co., Holland, 1978a.

Goldberg, M., and Gilboa, H., "Sodium Exchange Between Two Sites. The Binding of Sodium to Halotolerant Bacteria", Biochim. Biophys. Acta 538:268-283, 1978b.

Granot, J., "Sodium Imaging by Gradient Reversal", J. Magn. Reson. 68:575-581, 1986.

Granot, J., "Sodium Imaging of Human Body Organs and Extremities In Vivo", Radiology 167:547-550, 1988.

Griffey, R. H., Griffey, B. V., and Matwiyoff, N. A., "Triple-Quantum-Coherence-Filtered Imaging of Sodium Ions *in Vivo* at 4.7 Tesla", Magn. Reson. Med. 13:305-313, 1990.

Grodd, W., and Klose, U., "Sodium MR Imaging of the Brain: Initial Clinical Results", Neuroradiology 30:399-407, 1988.

Gullans, S. R., Avison, M. J., Ogino, T., Giebisch, G., and Shulman, R. G., "NMR Measurements of Intracellular Sodium in the Rabbit Proximal Tubule", Am. J. Physiol. 249:F160-F168, 1985.

Gupta, R. K., and Gupta, P., "Direct Observation of Resolved Resonances from Intra- and Extracellular Sodium^{-23} Ions in NMR Studies of Intact Cells and Tissues Using Dysprosium(III)-Tripolyphosphate as a Paramagnetic Shift Reagent", J. Magn. Reson. 47:344-350, 1982.

Gustavsson, H., Siegel, G., Lindman, B, and Fransson, L., "$^{23}Na^{+}$ NMR in Solutions of Mucopolysaccharides", FEBS Letters 86:127-130, 1978.

Guyton, A. C., Granger, H. J., and Taylor, A. E., "Interstitial Fluid Pressure", Physiol. Rev. 51:527-563, 1971.

Hahn, E. L., "Spin Echoes", Phys. Rev. 80:580-594, 1950.

Henkelman, R. M., "Measurement of Signal Intensities in the Presence of Noise in MR Images", Med. Phys. 12:232-233, 1985.

Hilal, S. K., Maudsley, A. A., Simon, H. E., Perman, W. H., Bonn, J., Mawad, M. E., Silver, A. J., Ganti, S. R., Sane, P., and Chien, I. C., "*In Vivo* NMR Imaging of Tissue Sodium in the Intact Cat Before and After Acute Cerebral Stroke", A. J. N. R. 4:245-249, 1983.

Hilal, S. K., Maudsley, A. A., Bonn, J., Simon, H. E., Cannon, P., and Perman, W. H., "NMR Imaging of Tissue Sodium, *In Vivo* and in Resected Organs", Magn. Reson. Med. 1:165-166, abstract, 1984.

Hilal, S. K., Maudsley, A. A., Ra, J. B., Simon, H. E., Roschmann, P., Wittekoek, S., Cho, Z. H., and Mun, S. K. "*In Vivo* NMR Imaging of Sodium-23 in the Human Head", J. Comput. Assist. Tomogr. 9:1-7, 1985.

Hilal, S. K., Ra, J. B., Oh, C. H., Mun, I. K., Einstein, S. G., and Roschmann, P., "Sodium Imaging", in Magnetic Resonance Imaging, ed. by D. D. Stark and W. G. Bradley, Jr., Mosby Co., St. Louis, 1988.

Hilal, S. K., Oh, C. H., Mun, I. K., and Johnson, G., "Grading of Gliomas by Sodium MRI", Proc. Soc. Magn. Reson. Med. p83, abstract, 1989.

Hubbard, P. S., "Nonexponential Nuclear Magnetic Relaxation by Quadrupole Interactions", J. Chem. Physiol. 53:985-987, 1970.

Jelicks, L. A., and Gupta, R. K., "Observation of Intracellular Sodium Ions by Double-Quantum-Filtered ^{23}Na NMR with Paramagnetic Quenching of Extracellular Coherence by Gadolinium Tripolyphosphate", J. Magn. Reson. 83:146-151, 1989a.

Jelicks, L. A., and Gupta, R. K., "Double-Quantum NMR of Sodium Ions in Cells and Tissues. Paramagnetic Quenching of Extracellular Coherence", J. Magn. Reson. 81:586-592, 1989b.

Jelicks, L. A., and Gupta, R. K., "Multinuclear NMR Studies of the Langendorff Perfused Rat Heart", J. Biol. Chem. 264:15230-15235, 1989c.

Joseph, P. M., and Summers, R. M., "The Flip-Angle Effect: A Method for Detection of Sodium-23 Quadrupole Splitting in Tissue", Magn. Reson. Med. 4:67-77, 1987.

Keenan, M. J., and Niedergerke, R., "Intracellular Sodium Concentration and Resting Sodium Fluxes of the Frog Heart Ventricle", J. Physiol. 188:235-260, 1967.

Kohler, S. J., Kolodny, N. H., D'Amico, D. J., Balasubramaniam, S., Mainardi, P., and Gragoudas, E. S., "Magnetic Resonance Imaging Determination of ^{23}Na Visibility and T_2^* in the Vitreous Body", J. Magn. Reson. 82:505-517, 1989.

Kohler, S. J., Ingwall, J. S., and Kolodny, N. H., "Evaluation of $TmDOTP^{5-}$ as a Shift Reagent for ^{23}Na Spectroscopy and ^{23}Na Chemical Shift Imaging", Proc. Soc. Magn. Reson. Med. p39, abstract, 1990.

Kohler, S. J., Perry, S. B., Stewart, L. C., Atkinson, D. E., Clarke, K., and Ingwall, J. S., "Analysis of ^{23}Na NMR Spectra from Isolated Perfused Hearts", Magn. Reson. Med. 18:15-27, 1991.

Kolodny, N. H., Gragoudas, E. S., D'Amico, D. J., and Albert, D. M., "Magnetic Resonance Imaging and Spectroscopy of Intraocular Tumors", Surv. Ophthalmol. 33:502-514, 1989.

Kramer, D. M., "Imaging of Elements Other than Hydrogen", in NMR Imaging in Medicine, ed. by L. Kaufman, L. E. Crooks, and A. R. Margulis, Igaku-Shoin, New York, 1981.

Kundel, H. L., Shetty, A., Joseph, P. M., Summers, R. M., Kassab, E. A., and Moore, B., "Sodium NMR Imaging of Lung Water in Rats", Magn. Reson. Med. 6:381-389, 1988.

Lerner L., and Torchia, D. A., "A Multinuclear NMR Study of the Interactions of Cations with Proteoglycans, Heparin, and Ficoll", J. Biol. Chem. 261:12706-12714, 1986.

Liebling, M. S., and Gupta, R. K., "A Comparison of Intracellular Sodium Ion Concentrations in Neoplastic and Non-Neoplastic Human Tissue Using ^{23}Na NMR Spectroscopy", Ann. N. Y. Acad. Sci. 508:149-161, 1986.

Maeda, M., Seo, Y., Murakami, M., Kuki, S., Watari, H., Iwasaki, S., and Uchida, H., "Sodium-23 MR Imaging of the Kidney in Guinea Pig at 2.1 T, Following Arterial, Venous, and Ureteral Ligation", Magn. Reson. Med. 16:361-367, 1990.

Marquardt, D. W., "An Algorithm for Least-Squares Estimation of Nonlinear Parameters", J. Soc. Ind. Appl. Math. 11:431-441, 1963.

Maudsley, A. A., and Hilal, S. K., "Biological Aspects of Sodium-23 Imaging", Br. Med. Bull. 40:165-166, 1984.

Meiboom, S., and Gill, D., "Modified Spin Echo Method for Measuring Nuclear Relaxation Times", Sci. Instrum. 29:688-691, 1958.

Monoi, H., "Nuclear Magnetic Resonance of Tissue Na-23: I.Na-23 Signal and Na^+ Activity in Homogenate", Biophys. J. 14:645-651, 1974a.

Monoi, H., "Nuclear Magnetic Resonance of Tissue Na-23: II.Theoretical Line Shape", Biophys. J. 14:653-659, 1974b.

Morris, P. G., Nuclear Magnetic Resonance Imaging in Medicine and Biology, Clarendon Press, Oxford, 1986.

Moseley, M. E., Chew, W. M., Nishimura, M. C., Richards, T. L., Murphy-Boesch, J., Young, G. B., Marschner, T. M., Pitts, L. H., and James, T. L., "*In Vivo* Sodium-23 Magnetic Resonance Surface Coil Imaging: Observing Experimental Cerebral Ischemia in the Rat", Magn. Reson. Imag. 3:383-387, 1985.

Nishimura, T., Sada, M., Sasaki, H., Yamada, N., Yamada, Y., Yutani, C., Amamiya, H., Fujita, T., Akutsu, T., and Manabe, H., "Sodium Nuclear Magnetic Resonance Imaging of Acute Cardiac Rejection in Heterotopic Heart Transplantation", Cardiov. Res. 23:561-566, 1989.

Norne, J., Gustavsson, H., Forsen, S., Chiancone, E., Kuiper, H. A., and Antonini, E., "Sodium and Calcium Binding to *Panulirus interruptus* Hemocyanin as Studied by ^{23}Na Nuclear Magnetic Resonance", Eur. J. Biochem. 98:591-595, 1979.

Page, E., and Page, E. G., "Distribution of Ions and Water Between Tissue Compartments in the Perfused Left Ventricle of the Rat Heart", Circ. Res. 22:435-446, 1968.

Page, S. G., and Niedergerke, R., "Structures of Physiological Interest in the Frog Heart Ventricle", J. Cell. Sci. II:179-203, 1972.

Patt, S. L., and Sykes, B. D., "Water Eliminated Fourier Transform NMR Spectroscopy", J. Chem. Phys. 56:3182-3184, 1972.

Payne, G. S., Seymour, A. L., Styles, P., and Radda, G. K., "Multiple Quantum Filtered ^{23}Na NMR Spectroscopy in the Perfused Heart", NMR in Biomed. 3:139-146, 1990.

Pekar, J., Multiple-Quantum Nuclear Magnetic Resonance Studies of Sodium-23 in Model and Biological Systems", Doctoral Thesis, Univ. of Penn., 1988.

Pekar, J., and Leigh, J. S., "Detection of Biexponential Relaxation in Sodium-23 Facilitated by Double-Quantum Filtering", J. Magn. Reson. 69:582-584, 1986.

Pekar, J., Renshaw, P. F., and Leigh, J. S., "Selective Detection of Intracellular Sodium by Coherance-Transfer NMR", J. Magn. Reson. 72:159-161, 1987.

Perman, W. H., Turski, P. A., Houston, L. W., Glover, G. H., and Hayes, C. E., "Methodology of *in Vivo* Human Sodium MR Imaging at 1.5 T", Radiology 160:811-820, 1986.

Perman, W. H., and Turski, P. A., "Multinuclear Magnetic Resonance Imaging", in Biomedical Magnetic Resonance Imaging, ed. by F. W. Wherli, D. Shaw, and J. B. Kneeland, VCH Publishing, New York, 1988.

Perman, W. H., Thomasson, D. M., Bernstein, M. A., and Turski, P. A., "Multiple Short-Echo (2.5-ms) Quantitation of *in Vivo* Sodium T2 Relaxation", Magn. Reson. Med. 9:153-160, 1989.

Pettegrew, J. W., Woessner, D. E., Minshew, N. J., and Glonek, T., "Sodium-23 NMR Analysis of Human Whole Blood, Erythrocytes, and Plasma. Chemical Shifts, Spin Relaxation, and Intracellular Sodium Concentration Studies", J. Magn. Reson. 57:185-196, 1984.

Pike, M. M., Frazer, J. C., Dedrich, D. F., Ingwall, J. S. Allen, P. D., Springer, C. S. Jr., and Smith, T. W., "^{23}Na and ^{39}K Nuclear Magnetic Resonance Studies of Perfused Rat Hearts. Discrimination of Intra- and Extracellular Ions Using a Shift Reagent", Biophys. J. 48:159-173, 1985.

Polimeni, P. I., "Extracellular Space and Ionic Distribution in Rat Ventricle", Am. J. Physiol. 227:676-683, 1974.

Ra, J. B., Hilal, S. K., and Cho, Z. H., "A Method for *in Vivo* MR Imaging of the Short T_2 Component of Sodium-23", Magn. Reson. Med. 3:296-302, 1986.

Ra, J. B., Hilal, S. K., Oh, C. H., and Mun, I. K., "*In Vivo* Magnetic Resonance Imaging of Sodium in the Human Body", Magn. Reson. Med. 7:11-22, 1988.

Ra, J. B., Hilal, S. K., and Oh, C. H., "An Algorithm for MR Imaging of the Short T2 Fraction of Sodium Using the FID Signal", J. Comput. Assist. Tomogr. 13:302-309, 1989.

Renshaw, P. F., Blum, H., and Leigh, J. S., "Applications of Dextran-Magnetite as a Sodium Relaxation Enhancer in Biological Systems", J. Magn. Reson. 69:523-526, 1986.

Robb, J. S., Comparative Basic Cardiology, Grune and Stratton, New York, 1965.

Seo, Y., Murakami, M., Matsumoto, T., Nishikawa, H., and Watari, H. "Applications of Aqueous Shift Reagent, Dy(TTHA), for ^{23}Na NMR Studies of Exocrine Glands. Viabilities of Organs Perfused with Shift Reagent", J. Magn. Reson. 72:341-346, 1987.

Shinar, H, and Navon, G., "NMR Relaxation Studies of Intracellular Na^+ in Red Blood Cells", Biophys. Chem. 20:275-283, 1984.

Shinar, H., and Navon, G., "Sodium-23 NMR Relaxation Times in Body Fluids", Magn. Reson. Med. 3:927-934, 1986.

Shinar, H., and Navon, G., "Sodium-23 NMR Relaxation Times in Nucleated Red Blood Cells and Suspensions of Nuclei", Biophys. J. 59:203-208, 1991.

Shporer, H., and Civan, M. M., "Nuclear Magnetic Resonance of Sodium-23 Linoleate Water: Basis for an Alternative Interpretation of Sodium-23 Spectra Within Cells", Biophys. J. 12:114-122, 1972.

Shporer, M., and Civan, M. M., "Effects of Temperature and Field Strength on the NMR Relaxation Times of Na-23 in Frog Striated Muscle", Biochim. Biophsic. Acta 354:291-304, 1974.

Slichter C. P., Principles of Magnetic Resonance, Springer-Verlag, New York, 1980.

Sutherland, T. M., and Young, D. A. B., "Increased Permeability of the Capillaries of the Rat Heart to Plasma Albumin With Asphyxiation and With Perfusion", J. Physiol. 183:112-122, 1966.

Turski, P. A., Perman, W. H., Hald, J. K., Houston, L. W., Strother, C. M., and Sackett, J. F., "Clinical and Experimental Vasogenic Edema: *In Vivo* Sodium MR Imaging", Radiology 160:821-825, 1986.

Turski, P. A., Houston, L. W., Perman, W. H., Hald, J. K., Turski, D., Strother, C. M., and Sackett, J. F., "Experimental and Human Brain Neoplasms: Detection with *in Vivo* Sodium MR Imaging", Radiology 163:245-249, 1987.

Whalen, D. A., Hamilton, D. G., Ganote, C. E., and Jennings, R. B., "Effect of a Transient Period of Ischemia on Myocardial Cells", Am. J. Path. 74:381-398, 1974.

Wiederhielm, C. A., "The Interstitial Space", in Biomechanics: Its Foundations and Objectives, ed. by Y. C. Fung, N. Perrone, and M. Anliker, Prentice-Hall, Englewood Cliffs N.J., 273-286, 1972.

Wiederhielm, C. A., "Dynamics of Capillary Fluid Exchange: A Nonlinear Computer Simulation", Microvasc. Res. 18:48-82, 1979.

Willerson, J. T., Scales, F. S., Mukherjee, A., Platt, M., Templeton, G. H., Fink, G. S., and Buja, L. M., "Abnormal Myocardial Fluid Retention as an Early Manifestation of Ischemic Injury", Am. J. Path. 87:159-188, 1977.

Winkler, S. S., Thomasson, D. M., Sherwood, K., and Perman, W. H., "Regional T2 and Sodium Concentration Estimates in the Normal Human Brain by Sodium-23 MR Imaging at 1.5 T", J. Comput. Assist. Tomagr. 13:561-566, 1989.

Wolff, S. D., Eng, C., and Balaban, R. S., "NMR Studies of Renal Phosphate Metabolites *in Vivo*: Effects of Hydration and Dehydration", Am. J. Phyiol. 255:F581-F589, 1988.

Wolff, S. D., Eng, J., Berkowitz, B. A., James, S., and Balaban, R. S., "Sodium-23 Nuclear Magnetic Resonance Imaging of the Rabbit Kidney *in Vivo*", Am. J. Physiol. 258:F1125-F1131, 1990.